



Remotely measuring and controlling specific parameters of photovoltaic modules via a radio frequency link

By

Ntombizanele Agnes Maqache

Dissertation submitted in fulfilment of the requirements for the degree:

Master of Engineering

in

Electrical Engineering

Department of Electrical, Electronic and Computer Engineering

Faculty of Engineering, Built Environment and Information Technology

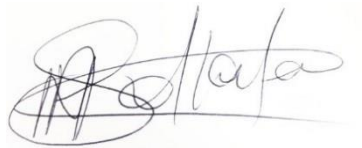
Central University of Technology, Free State

Supervisor: Prof. A.J Swart

March 2021

Declaration

I, Ntombizanele Agnes Maqache, student number _____, do hereby declare that this research project, which has been submitted to the Central University of Technology Free State, for the degree: Master of Engineering in Electrical Engineering, is my own independent work and complies with the Code of Academic Integrity, as well as other relevant policies, procedures, rules and regulations of the Central University of Technology, Free State. This project has not been submitted before by any person in fulfilment (or partial fulfilment) of the requirements for the attainment of any qualification.



NA Maqache

10 March 2021

Acknowledgements

I'm grateful to Yahweh, the Almighty Jehovah for bringing me thus far. In Him I draw strength, courage and inspiration.

A big thank you to Prof. Swart for his patience and wisdom that has led me through this study. I have learnt a lot from Prof. J and I appreciate the knowledge he has imparted to me.

To my colleagues, thank you for the technical support you selflessly gave when I needed you.

My parents, my sisters, thank you for all the babysitting you do when I need a break, I never have to ask.

To my husband, my soundboard, my number one supporter, thank you for unwavering support.

Dedication

This study is dedicated to my daughters, Kemelo, Kano and Kaboentle. Everything I do is informed by how I can be a better mother to you. I want to realize my full potential if only to inspire to go beyond yours. You always tell me “don’t give up mommy” in the simplest things and it drives me to want to achieve even bigger things. I want you to remember that you can achieve anything you set mind to. You are my inspiration, my force.

Abstract

Background: The efficiency of PV modules is affected by a number of factors, including installation parameters and the module surface temperature. Installation parameters of PV modules focus primarily on the tilt and orientation angles, which have to be considered for optimum output power. Furthermore, the operating temperature of a PV module must be kept within certain limits, in order to obtain optimum electrical energy efficiency, depending on the module used. Controlling these parameters of a remote PV module can prove challenging. **Purpose:** The purpose of this study was to measure the instantaneous surface temperature, voltage and current of a remote PV module that can be used to control some of these parameters in order to maintain a high output power. **Methodology:** An energy monitoring system was developed that received measurement data and sent control signals over an RF link. The PC transceiver of the system featured a CC1101 RF transceiver connected to the PC via an Arduino UNO, using a USB cable. The PV transceiver featured an Arduino Mega 2560, connected to a CC1101 RF transceiver to make the slave transceiver board, which harboured all the sensors of the system. In addition, the graphical user interface was developed for sending and receiving measurements and control signals between the PC transceiver and the PV transceiver. **Results:** The PV module voltage and current data was verified using a Fluke 115 DMM. The results showed a 4.9% error percentage for voltage measurements and a 3.9% error percentage for current measurements. Furthermore, a 29-day period of data showed the surface temperature to rise significantly higher than the ambient temperature during the day, indicating that there was considerable heating of the PV Module when there was solar radiation. Whereas for low temperatures measured at night, the surface temperature and the ambient temperature were fairly similar. In addition, PV module current measurements were obtained for a sunny and cloudy day of September that showed 2.32 A and 1.98 A at 11:00 am respectively. Control signals were sent using the graphical user interface from the PC transceiver that were used to activate an actuator that can adjust the orientation angle. A single click of the “Move Left” button in the interface provided an extension of 3 cm of the actuator while a single click of the “Move Right” button resulted in the actuator being retracted by 4 cm. The difference in the displacement of the actuator for the “Move Left” and “Move Right” commands was for demonstration purposes only.

Control signals from the PC transceiver to activate a water sprayer (to cool the PV module) were confirmed by switching on and off a LED at the PV module transceiver. The cooling method used is but only an example, the review and selection of a cooling method did not form part of this study. **Recommendations:** The work presented here could be extended by modifying the graphical user interface to form part of a smart city where the adjustment to the actuator and activation of the water sprayer could be automated. Incorporating cloud storage for monitoring of the output power and surface temperature from any location at any time could also be considered.

Table of Contents

List of Figures	ix
List of Tables	xi
List of Annexures.....	xii
Glossary of Abbreviations and Symbols.....	xiii
Chapter 1 Introduction	1
1.1 Background	1
1.2 Problem statement.....	2
1.3 Research objectives.....	2
1.4 Important definitions.....	3
1.5 Value of the research	4
1.6 Outline of the research and the research methodology	5
1.7 Delimitations.....	6
1.8 Summary	6
Chapter 2 Literature review	7
2.1 Introduction.....	7
2.2 The effect of high temperature on the output power of a PV module	7
2.2.1 Temperature measuring techniques.....	8
2.3 The effect of orientation angle on the output power of a PV module.....	14
2.3.1 Orientation measuring techniques	16
2.4 Power measurements	19
2.5 The use of microcontrollers in data processing	25
2.6 The use of wireless technologies in data transfer	27
2.7 Summary	29
Chapter 3 Methodology	31
3.1 Introduction.....	31
3.2 System design	31
3.2.1 Master transceiver board	32
3.2.2 Slave transceiver board	34
3.2.2.1 Slave transceiver sensors	35

3.2.2.2	PV parameter control.....	39
3.2.3	User interface and programming.....	40
3.3	Practical setup.....	43
3.4	Summary.....	44
Chapter 4 Test and results.....		46
4.1	Introduction.....	46
4.2	Graphical User Interface (GUI).....	46
4.3	Experimental measurements and controls.....	51
4.3.1	PV Module voltage and current measurements verified by DMM.....	52
4.3.2	Practical setup measurements of PV voltage and current over seven days...54	
4.3.3	Battery charge and discharge data.....	57
4.3.4	PV module surface temperature verified by DMM.....	58
4.3.5	Practical setup measurement of PV surface temperature over 29 days.....	59
4.4	Water sprayer control.....	61
4.5	PV module orientation angle control.....	62
4.6	Summary.....	63
Chapter 5 Conclusions and recommendations.....		65
5.1	Introduction.....	65
5.2	Chapter overview.....	65
5.3	Research objectives met.....	66
5.4	Solution to the problem statement.....	69
5.4.1	Remotely measuring parameters.....	69
5.4.2	Remotely controlling parameters.....	70
5.5	Recommendations for future work.....	70
Bibliography.....		71

List of Figures

Figure 1: Practical setup.....	3
Figure 2: Ambient temperature	8
Figure 3: Thermocouple operating principle (Elprocus, 2016)	10
Figure 4: Resistance thermometer's operating principle (JMS SE, 2016)	11
Figure 5: Radiation thermometer operating principle (Machinery Equipment Online, 2015)	13
Figure 6: Semiconductor thermometers (Elprocus, 2016).....	14
Figure 7: Orientation and tilt angles of a PV module	15
Figure 8: Sun position for different orientations.....	16
Figure 9: Optical encoder disk (Engineer on a Disk, 2016)	18
Figure 10: Magnetic rotatory sensor operation (StackExchange, 2016).....	18
Figure 11: Potentiometer schematic symbol (Engineer on a Disk, 2016)	19
Figure 12: Potentiometer used for measuring angles (Engineer on a Disk, 2016)	19
Figure 13: Voltage divider	21
Figure 14: Opto-Isolator (Wikipedia, 2018)	22
Figure 15: Shunt resistor	24
Figure 16: Hall Effect (Dangerous prototypes, 2012)	25
Figure 17: Block diagram of the practical set-up.....	31
Figure 18: Arduino and master transceiver.....	32
Figure 19: Master transceiver station.....	33
Figure 20: Send and receive code at PC	33
Figure 21: Slave transceiver board	34
Figure 22: Transmitting station.....	35
Figure 23: Slave transceiver board with sensors.....	35
Figure 24: Arduino Mega 2560 showing sensor pins	36
Figure 25: Voltage and current sensing circuit diagram	37
Figure 26: Voltage sensors.....	37
Figure 27: Voltage and current code.....	38
Figure 28: ACS712 current sensors	39
Figure 29: Control orientation angle and water sprayer	40
Figure 30: Relay for actuator	40

Figure 31: GUI flow chart.....	41
Figure 32: User interface	43
Figure 33: Block diagram of practical setup.....	44
Figure 34: Tab 1 of the GUI: settings	47
Figure 35: Tab 2 of the GUI: live table.....	47
Figure 36: Tab 3 of the GUI: PV charts.....	48
Figure 37: Tab 4 of the GUI: battery charts.....	49
Figure 38: Tab 5 of the GUI: load charts	49
Figure 39: Excel document where data from GUI is saved	50
Figure 40: Directory where data is periodically saved	51
Figure 41: Block diagram of the acquired measurements	51
Figure 42: PV voltage and current measurements verified using a DMM	53
Figure 43: PV voltage and current DMM reading	53
Figure 44: Hourly maximum of PV current for 27 September 2019 (Sunny day)	54
Figure 45: Hourly maximum of PV current for 29 September 2019 (Cloudy day).....	54
Figure 46: Hourly maximum of PV voltage from 24 to 30 September 2019	56
Figure 47: Hourly maximum of PV current from 24 to 30 September 2019.....	56
Figure 48: Hourly maximum battery voltage for 30 September 2019.....	57
Figure 49: Hourly maximum battery current for 30 September 2019	57
Figure 50: PV Module surface temperature measurements verified by DMM	58
Figure 51: PV Module surface temperature DMM reading.....	58
Figure 52: Hourly maximum of PV Module surface temperature for 29 September 2019	59
Figure 53: Hourly maximum of PV Module surface temperature for 27 September 2019	59
Figure 54: Sprayer on command to activate the water sprayer.....	61
Figure 55: LED is turned on and off representing the water sprayer.....	61
Figure 56: Actuator's initial position.....	62
Figure 57: GUI: Move left command to get back to the initial position.....	63
Figure 58: Actuator retracted and extended to achieve 20 degrees	63

List of Tables

Table 1: A comparison of types of temperature sensors	9
Table 2: A comparison of types of position sensors	17
Table 3: A comparison of different methods of measuring voltage	20
Table 4: A comparison of methods of measuring current.....	23
Table 5: A comparison of different development boards	26
Table 6: A comparison of different wireless technologies	28
Table 7: PV module parameters.....	52
Table 8: Maximum measurements when the load is switched on and off	55
Table 9: 29-day temperature data	60

List of Annexures

Annexure A: GUI Program	81
Annexure B: PV Transceiver Program	93
Annexure C: PC Transceiver Program	98
Annexure D: <i>TPV</i> 29-day data	102

Glossary of Abbreviations and Symbols

D

DMM – Digital Multimeter

I

I - Current

V – Voltage

P

PV – Photovoltaic

R

RF – Radio Frequency

T

T_a – Ambient Temperature

T_{PV} – PV Module Surface Temperature

Chapter 1 Introduction

1.1 Background

Reddy states that electrical energy is currently primarily produced worldwide by burning fossil fuels, such as coal, oil or gas (Reddy, 2012). Moreover, the author states that electrical energy demands continue to increase globally as the population increases, especially in developing countries. In addition, the increasing demand will possibly not be met by fossil fuels, which are limited resources that contribute significantly to greenhouse emissions, which impact negatively on the environment. President Jacob Zuma, the former president of South Africa, told the World Economic Forum in Davos-Klosters, Switzerland on Wednesday 21 January 2015 that, “Our electricity infrastructure was never designed to serve an expanded citizenry. This extension of electricity to more households that had been excluded in the past, coupled with a growing economy, has sharply put pressure on the infrastructure, which needs improved maintenance and expansion.” Moreover, South Africa is currently experiencing load-shedding periods, which are exerting a negative impact on the socio-economic development of the country. These, and other factors, have become the driving force behind many organisations venturing into alternative energy sources that are low-cost, sustainable and clean.

For example, such clean energy sources include wind, water and solar energy, which are renewable and ecologically friendly. In fact, solar energy is one of the fastest growing clean energy sources in the world and may continue to do so, due to the declining cost of solar cells. In addition, sunlight is the most abundant energy source on the planet. Photovoltaic (PV) modules are devices that convert this solar energy directly into electrical energy without requiring mechanical energy and without producing greenhouse emissions. However, the efficiency of PV modules is affected by a number of factors, including installation parameters and module surface temperature.

Installation parameters of PV modules focus primarily on the tilt and orientation angles, which have to be considered for optimum output power. Many studies and experiments have been conducted to determine the best tilt and orientation angles for specific climate

conditions (Asowata, Swart & Pienaar, 2012; Ehrlich, 2013; Fuchs & Masoum, 2011; Lalia, Dalila & Ahmed, 2013; Prashanthini et al., 2011; Reddy, 2012; Swart, Schoeman & Pienaar, 2011). The tilt angle refers to the horizontal angle of a PV module, which is often equal to the latitude of the site of installation, while the orientation angle refers to the angular distance between due north and the projection of the line of sight to the sun on the ground in the southern hemisphere (Suri et al., 2012). A variable orientation angle enables a PV module to be directly aligned with the rays of the sun as it moves across the sky (Clini, Musu & Gullino, 2008), thereby enabling a higher output power of a module.

Furthermore, the operating temperature of a PV module must be kept within a certain range in order to obtain optimum electrical energy efficiency, depending on the module used (Messenger & Ventre, 2010). Another study found that the operating temperature plays a key role in the process of PV conversion (Swapnil, Jatin Narotam & Bharath, 2013). In addition, the aforementioned authors concluded that there is a linear dependence of electrical efficiency, and thus output power, of a PV module with regard to the operating temperature of a module.

1.2 Problem statement

The output voltage, and subsequently output power, of a PV module reduces significantly with an increase in its surface temperature and with the misalignment of its orientation angle. Remotely measuring and controlling these two parameters in a cost-effective way, proves challenging.

1.3 Research objectives

The primary objective of this research was to be able to remotely measure specific data, which can be used to make decisions regarding the cooling and orientation of a given PV module. This necessitates the following sub-objectives:

- Identifying a suitable microcontroller that will form the core of the data acquisition (DAQ) and control and the programming thereof.
- Determining which temperature and orientation angle sensors will best suit the primary objective.

- Incorporating commands into the graphical user interface to control a 12V actuator (controller) that could be used to vary the orientation angle for regulating the direct exposure of a PV module to the sun.
- Incorporating commands into the graphical user interface to control a 12V water solenoid valve (controller), which could decrease the surface temperature of a PV module.
- Developing a suitable data logging interface circuit for voltage conditioning between all sensors, controllers and the microcontroller.
- Establishing which RF transceiver will be used for wireless communication between the remote DAQ and the monitoring PC.

The synthesis of all these components could very well lead to optimal PV module operating conditions with regard to surface temperature and orientation angles, producing maximum output power for different climate conditions on an identified site in South Africa.

1.4 Important definitions

Orientation angle: the angular distance between due north and the projection of the line of sight to the sun on the ground in the southern hemisphere, as shown in Figure 1.

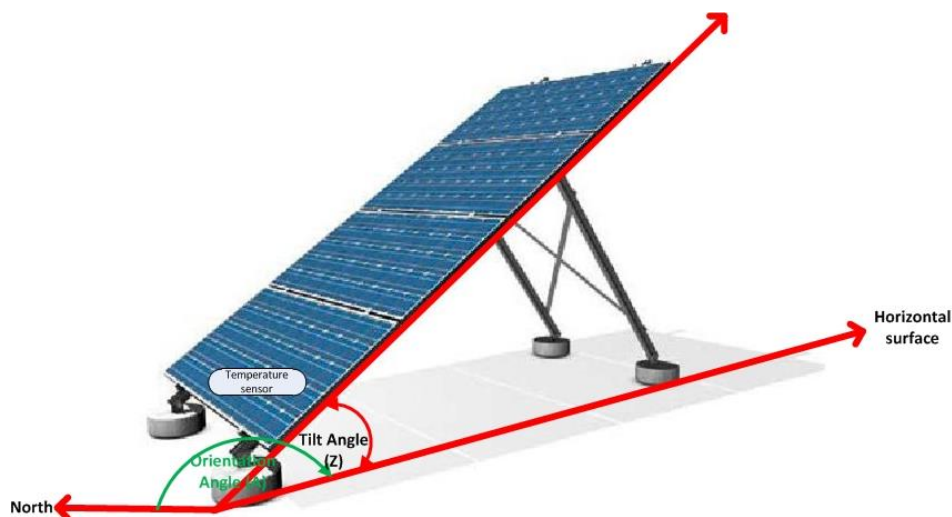


Figure 1: Practical setup

Tilt angle: the horizontal angle of a PV module, which is often equal to the latitude of the site of installation.

Photovoltaic module: a device that converts solar energy directly into electrical energy without requiring mechanical energy and without producing greenhouse emissions.

Actuator: A type of a motor that will be used to move the PV module, in order to change its angle of orientation.

Solenoid valve: a water release valve that is controlled by an electric current through an electromagnet to switch the water flow on and off.

1.5 Value of the research

The purpose of this research was to design and develop a cost-effective measuring and control system that will record the surface temperature and output power of a remote PV module via a RF link. Measuring the instantaneous surface temperature, voltage and current of a PV module will enable the effective control of these parameters in order to maintain a high output power.

The identified area of location for the research is the Central University of Technology in Bloemfontein. To date, there is little documented research providing specific data of the effect that the surface temperature and orientation angle of a PV module exerts on its output power for this specific geographical site.

The South African Government has invested millions of rands in PV system projects that provide electricity to rural communities that would otherwise not have access to electrical power. Such systems' maintenance is costly due to the fact that these communities are often isolated from the mainstream economy.

50% of the overall power consumption in the Information and Communication Technology (ICT) field is dedicated to telecommunication networks (Koutitas & Demestichas, 2010). In fact, research has shown that an average mobile base station uses approximately 35 MWh per year. The study included a sample of 100 mobile base stations around Italy, over a 1000-day period (Lubritto et al., 2008).

The 2014 Telkom SA Report reflects 656 669 130 kWh electricity consumption by the telecommunications giant (Telkom, 2014). Apart from this, Telkom SA uses solar energy to power some of its remote installations. In addition, a significant increase in the energy consumption of telecommunication networks is expected over the next 10 years (Lange et al., 2011). Therefore, the success of this research stands to benefit the Telecommunications Industry, as optimum operation of PV modules in remote locations may be maintained at all times without having personnel on site, and therefore contributing to a reduction in overall power consumption and maintenance costs, associated with PV systems.

1.6 Outline of the research and the research methodology

Chapter 1 gives the introduction of the research; it substantiates the research with a detailed background of the problem it aims to resolve. This chapter also presents the research objectives and an overview of the dissertation.

Chapter 2 reviews the literature available, in regard to the research. It will consider at length the effect of the surface temperature and the orientation angle of a PV module on its output power, and hence, its efficiency. A comparison of different methods of acquiring temperature and orientation angle measurements will be investigated along with the use of Radio Frequency Transceivers and microcontrollers for remote data acquisition.

Chapter 3 discusses the design and analysis of the practical setup. This part will detail what to measure, as well as how to interpret the measurements. Furthermore, voltage and current sensors will also be required to ensure effective monitoring of the output power. A data logging interface circuit must therefore be designed and developed to successfully interface a PV module with the microcontroller. The programming of the microcontroller will also form part of his chapter.

Chapter 4 is where results are acquired, analysed and interpreted. This will mainly involve photographs and sketches of the operational system.

Chapter 5 discusses the conclusions, as well as how the problem was solved. Succinct recommendations will be made.

1.7 Delimitations

The research did not focus on the different types of PV modules, actuators or solenoid valves. The inclusion of an energy regulator and storage system also did not form part of the research. In addition, the incorporation of the mechanical mechanism to adjust the orientation angle was not considered. Lastly, only the relay of the signals for modifying the temperature and orientation angles of a PV module were considered, as their impact on the performance of a PV module have already been established.

1.8 Summary

This research aimed to contribute to optimizing PV modules efficiency as sustainable alternative energy harnessers for a given geographical area. Two of the many parameters that affect the output power of a PV module were introduced in this chapter. The first parameter is a module's surface temperature that is directly proportional to the output power. The second parameter of interest that has an influence on the output power of a PV module, is the angle of orientation. The monitoring and ultimate control of these two parameters will hypothetically result in optimizing the output power of a given PV module.

The next chapter focuses on previous studies that have been conducted on how surface temperature and orientation angles affect the output power and ultimately the efficiency of a given PV module. In addition, different methods of acquiring and controlling these parameters are discussed. The effective use of RF technology as a means of communication between the remote site and the controlling PC, will be substantiated.

Chapter 2 Literature review

2.1 Introduction

The previous chapter gave a preamble of the study. It gave the research objectives and the problem statement. The outline of how the objectives would be met was given and why such a study is important. Delimitations were also given to describe what would not form part of the research. This chapter reviews firstly, research regarding the effect that high ambient temperatures exert on the output power of a photovoltaic (PV) module. It further explores different temperature measuring techniques. Secondly, a review of literature relating to the effect that the orientation angle exerts on a PV module's output power is presented. In addition, the chapter covers the use of different microcontrollers and wireless technologies that are used in data acquisition (DAQ) systems.

2.2 The effect of high temperature on the output power of a PV module

PV's only convert 4-17% of the solar energy to electrical energy, the rest is converted to heat energy that is not used (Bai et al., 2016). Ambient temperature (T_a) is defined as the temperature of the air around the PV module, as demonstrated in Figure 2 (Bhattacharya, Chakraborty & Pal, 2014; Liu et al., 2015). This temperature, together with solar radiation and other weather parameters, have an effect on a PV module's operating temperature, and as such on its cell temperature (T_c) (Al-Sabounchi, 1998; Skoplaki & Palyvos, 2009; Swapnil, Jatin Narotam & Bharath, 2013). Kaldellis, Kapsali and Kavadias (2014) used the following equation for calculating a PV cell temperature:

$$T_c = T_a + k \cdot G_T \quad 1$$

where " G_T " is the solar irradiance and " k " represents the Ross coefficient that is normally between 0.02 and 0.05 $^{\circ}Km^2/W$, which depends on the type of PV module, the way it is mounted and the wind speed at the area of operation. This suggests that the cell temperature is strongly affected by increased ambient temperatures in high ambient temperature climates. Researchers found that the ambient temperature plays a key role in the process of PV conversion (Al-Sabounchi, 1998; Mattei et al., 2006;

Skoplaki & Palyvos, 2009; Swapnil et al., 2013). They concluded that there is a linear dependence of electrical efficiency and thus power output of a PV module with regard to the cell temperature of the module. The cell temperature of a PV module must therefore be kept within a certain range in order to obtain optimum electrical energy efficiency, depending on the module used (Messenger & Ventre, 2010). The agreement across board is that the open-circuit voltage decreases considerably (about 2.3 mV/C), while the short circuit current only decreases somewhat with increased PV module temperature (Bai et al., 2016; Schwingshackl et al., 2013). Another study conducted over a 15-week period in South Africa found that a PV module without cooling had the average of 30.59 V in output voltage at average surface temperatures of 49.1°C, as compared to a PV module that had water cooling and averaged the output voltage of 31.3 V at average surface temperatures of 39.2°C, which translates to a decrease of 71.7 mV/°C (Ozemoya, Swart, & Pienaar, 2014).

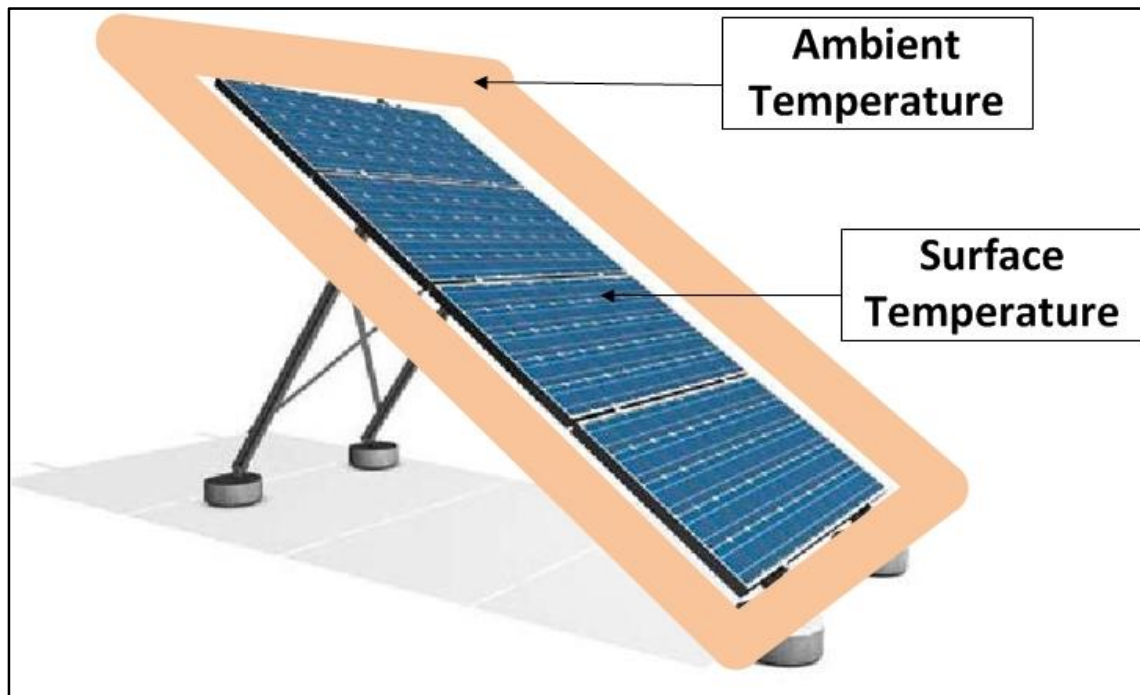


Figure 2: Ambient temperature

2.2.1 Temperature measuring techniques

There are many ways to measure temperature, as well as many factors that can affect an accurate measurement. It is therefore important to establish which method is best

suited for the system under study. Instruments used to measure temperature can be divided into 10 separate classes, according to the physical principles on which they behave. These principles include: thermoelectric effect, resistance change, sensitivity of semiconductor devices, radiative heat emission, thermography, thermal expansion, resonant frequency change, sensitivity of fibre-optic devices, colour change and change of the state of material (Morris & Langari, 2012). Five of the principles most suited for application within this study are compared by the range of temperature they are able to measure, their accuracy and advantages, as shown in Table 1.

Table 1: A comparison of types of temperature sensors

Type	Operating Temperature	Accuracy	Advantage	Disadvantage
Thermocouples	-250 to +1200°C	0.75%	Inexpensive	Efficiency deteriorates with age
Resistance thermometers (RTD)	-270 to +800°C	0.5%	Stable	Poor thermal sensitivity
Thermistors	-65 to +290°C	0.5%	Low cost	Non-linear
Radiation thermometers	-100 to +10 000°C	0.05%	No contact required	Expensive
Semiconductor devices	-50 to +150°C	3%	Linearity	Require external power

Thermoelectric effect sensors (**thermocouples**) are inexpensive, but their efficiency deteriorates with age; principle shown in Figure 3. The operating principle is based on the generation of an e.m.f at the junction of two different metals when they are connected together; this e.m.f is a function of temperature. Thermocouples are formed by connecting wires of these metals together at the one end known as the hot junction, and on the other end to form a closed circuit and thus a flow of current (Elprocus, 2016). The cold junction is the junction at the known temperature, or the reference and the hot junction is exposed to the measured temperature. A voltage is generated when there is

a difference in the temperatures at the two junctions. This is the most widely used method of acquiring temperature measurements in the industry. They need to be enclosed to protect them from being affected by the working environment, but this could lead to slow responses to temperature changes. These types of instruments are prone to noise, making them unsuitable to measure small temperature changes. Their accuracy is approximately 0.75% with a temperature range from -250°C to $+1200^{\circ}\text{C}$ (Morris & Langari, 2012). Thermocouples were used at the National University of Singapore in an experimental setup that investigated how temperature affects the output, and hence the efficiency, of a PV module during operation (Teo, Lee & Hawlader, 2011). After completing the experiment, the authors concluded that there was a decline in the electrical efficiency of a PV module with an increase in its temperature.

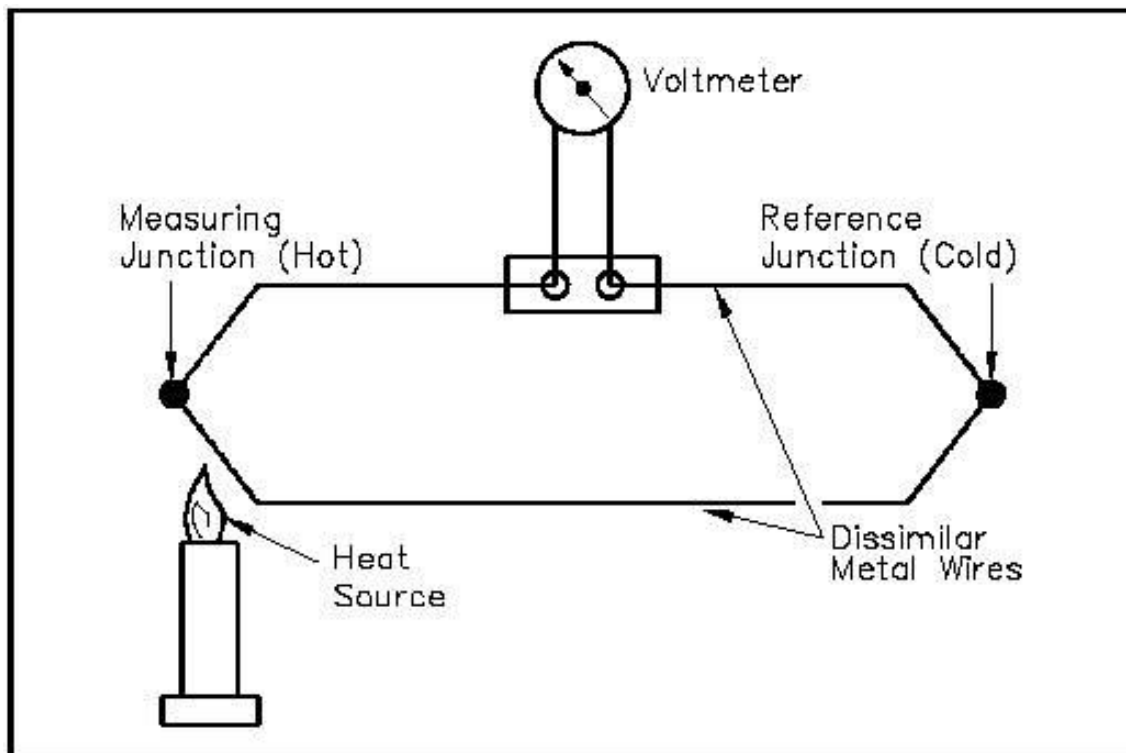


Figure 3: Thermocouple operating principle (Elprocus, 2016)

Thermocouples may be used to design digital thermometers. These comprise of a thermocouple, a battery-powered digital voltmeter to measure the output of the thermocouple and digital display, and offers good response for temperature differences as small as 0.1°C . A unique digital thermometer was used in the development of a data

acquisition system to obtain temperature readings for PV module characterization (Belmili et al., 2010). This thermometer, DS18B20 manufactured by DALLAS, communicates with a microcontroller using one wire with the ability to connect several sensors to one port, as each sensor has a unique serial code (Semiconductor, 2007).

Resistance thermometers (see Figure 4), also known as resistance temperature detectors (RTDs), can measure temperatures ranging from -270°C to $+800^{\circ}\text{C}$ with an accuracy of 0.5%. They rely on the principle that a material's electrical resistance changes with temperature. The resistance of a platinum wire, for an example, is measured by passing current through it and measuring the voltage by means of a suitable bridge or voltmeter, where after the voltage is then converted to temperature, using a calibration equation. These types are more stable than thermocouples and can measure small temperature changes (Morris & Langari, 2012).

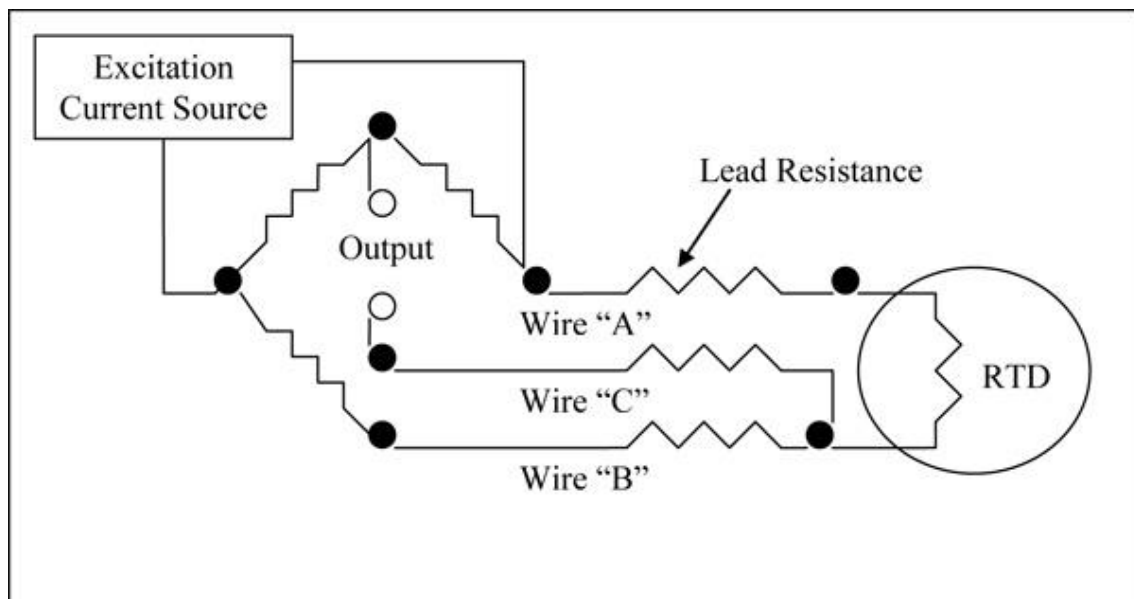


Figure 4: Resistance thermometer's operating principle (JMS SE, 2016)

RTDs were used in a Rotronic MP100A sensor in the development of an integrated data acquisition system for monitoring renewable energy systems (Koutroulis & Kalaitzakis, 2003). In another study, researchers used PT100 sensors - a type of RTD - to obtain PV cell temperature measurements when investigating the effect of wind on a PV module's temperature (Schwingssackl et al., 2013). Researchers found that the effect of wind-cooling plays a key role in lowering a PV module's temperature. RTD's have been used

in PV performance research for a number of years to acquire data for diagnostics and improvement in the efficiency of PV systems (Benghanem & Maafi, 1998). A thermistor bridge for sensing temperature was developed in another study that was able to convert the sensed signals into a 0-5 V range that can be processed by a microcontroller, which had an average error of $\pm 0.5\%$ (Moghavvemi et al., 2005)

Thermistors use the same principle as RTD's, but are made from certain metal oxides whose resistance decrease with increasing temperature. They are preferable over RTD's and thermocouples that are more expensive with applications where temperatures do not exceed 290°C (Morris & Langari, 2012). They have been used in PV performance research for a number of years to acquire data for diagnostics and improvement in the efficiency of PV systems (Benghanem & Maafi, 1998). A thermistor bridge for sensing temperature was developed in another study that was able to convert the sensed signals into a 0-5 V range that can be processed by a microcontroller, which had an average error of $\pm 0.5\%$ (Moghavvemi et al., 2005).

Radiation thermometers measure the electromagnetic radiation given out by an object and present this as a temperature value. When radiation changes, temperature also changes, allowing the temperature of the body to be calculated, using that which is emitted from the body. The radiation from the hot body (see Figure 5), passes through the lens and is directed on to the filament lamp and the current is adjusted according to that radiation. This is where filament matching takes place, if the radiation from the hot body is equal to that of the filament lamp, then the filament nears disappearing. The current through the filament is a measure of the temperature of the hot body. The different types of radiation thermometers can measure temperatures between -100°C and $+10\ 000^{\circ}\text{C}$ with accuracies as high as 0.05% and are expensive.

What makes radiation thermometers more attractive when measuring high temperatures, is the fact that there is no contact required with the hot body while its temperature is being measured (Morris & Langari, 2012). A non-contact infrared radiation thermometer was implemented to acquire the temperature of a concentrator V-trough PV module in a study that found that lower temperatures, due to good heat dissipation in these modules, result in higher open circuit voltage of the module, and hence higher output performances (Solanki et al., 2008). Radiation thermometers are

used in many industries for different applications, such as those used in thermal cameras. (Muhammad et al., 2017)

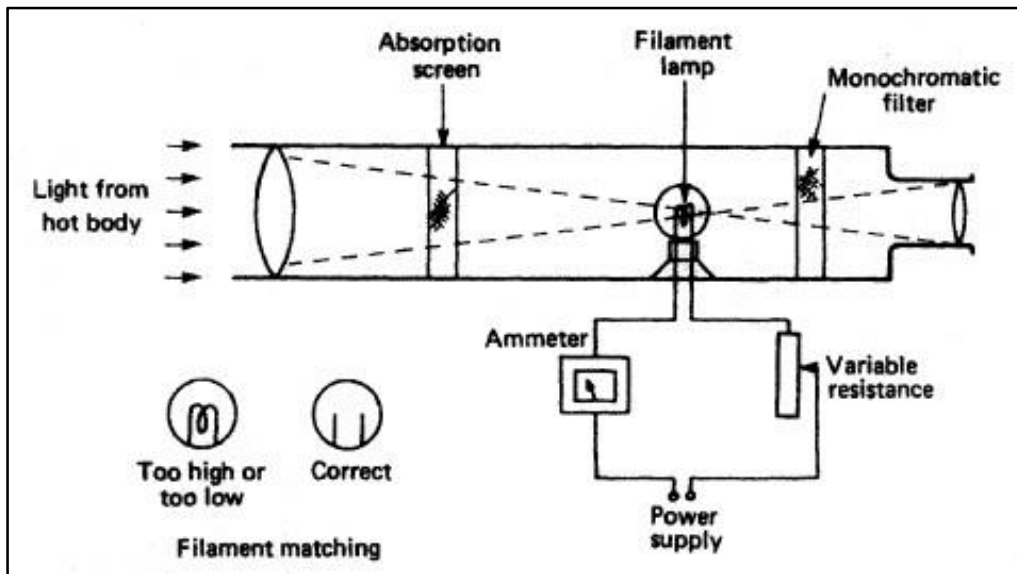


Figure 5: Radiation thermometer operating principle (Machinery Equipment Online, 2015)

Semiconductor devices (see Figure 6) are made up of diodes or integrated circuit transistors. These are inexpensive and offer better linearity than thermocouples and resistance thermometers. One difficulty with these devices is that they require an external power supply. They offer a temperature measurement range between -50°C to $+150^{\circ}\text{C}$ with an accuracy of around 3% (Morris & Langari, 2012). Their operation emanates from the fact that semiconductor materials have temperature-sensitive voltage vs. current characteristics. When two similar transistors are operated at a consistent ratio of collector current, the resulting difference in base-emitter voltages is directly proportional to the absolute temperature. The LM35 is an example of an integrated circuit sensor that is widely used in acquiring temperature measurements. It was used in the remote monitoring of a PV powered refrigerator, which detected operation problems that affected the reliability of a PV power supply (Tina & Grasso 2014).

The DHT 11 humidity and temperature sensor is another example of a semiconductor thermometer device that is made up of a resistive type humidity measurement component and an NTC (negative temperature coefficient) temperature measurement component. It connects to a microcontroller for excellent quality, fast response, anti-

interference ability and cost-effectiveness (D-Robotics 2010). This digital sensor was used to develop a humidity and temperature remote-sensing system that was cost-effective and fast for real-time operations (Randhir, Karhe 2015). It can measure temperatures of up to 50°C with the accuracy of $\pm 2^\circ\text{C}$.

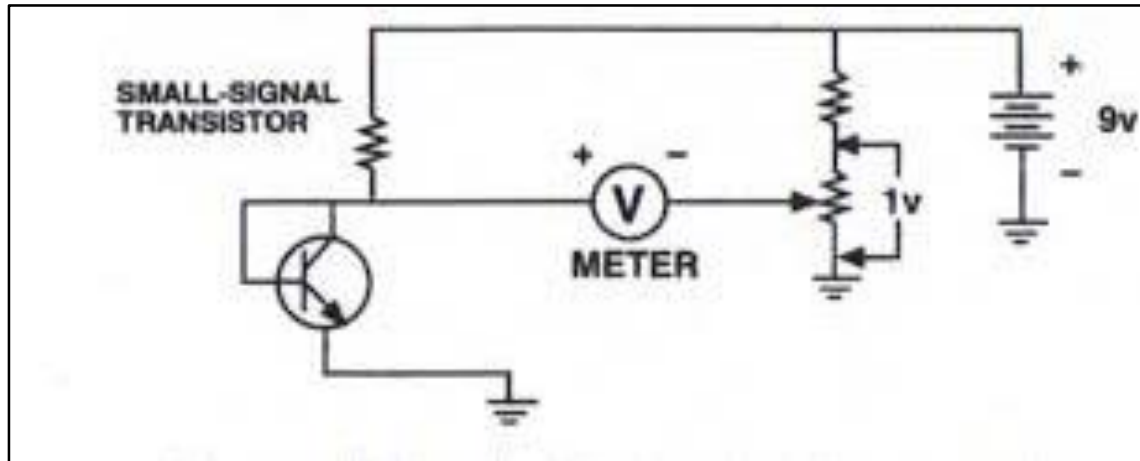


Figure 6: Semiconductor thermometers (Elprocus, 2016)

Semiconductor thermometers have been identified as the most suitable sensors for this study, due to their linear nature that provides fast responses for real-time operations. Their digital output can be connected to a microcontroller without complex circuitry, which contributes to the overall cost of the setup. Furthermore, a study done in South Africa showed PV module temperatures of around 50°C for a 200 W module (Ozemoya et al., 2014), which may readily be measured with this type of sensor.

2.3 The effect of orientation angle on the output power of a PV module

There are two angles of inclination to take into account when installing a PV module, as indicated in Figure 7, for optimum output power. First, there's the tilt angle (Z), which refers to the angle measured between the horizontal surface and the PV module, which is often equal to the latitude of the site of installation. Secondly, the orientation angle (A) is measured clockwise from the geographical north for regions in the Southern Hemisphere; also known as the Azimuth (Asowata, Swart & Pienaar, 2012a; Asowata, Swart & Pienaar, 2012b; Clini, Musu & Gullino, 2008; Dike et al., 2012; Suri et al., 2012).

The orientation angle ensures that the PV module has maximum sunlight exposure where it can utilise the direct beam radiation of the sun (Wenham et al., 2011). Ascertaining the best orientation angle for optimum efficiency depends on the position of the sun as the earth orbits it throughout the year. Figure 8 shows the position of the sun in different seasons for the city of Bloemfontein in South Africa - for a north-facing PV module - taken between 2017 and 2018. Different sunrise and sunset times are observed for different seasons, resulting in different noon positions for three of the four seasons. According to Sun Calculator (2018), the sun azimuth for 1 January 2018, 1 April 2018 and 1 July 2018 was 94.23° , 63.37° and 48.05° respectively for 9 am. Whereas the azimuth for noon for the same dates was 35.87° , 8.61° and 5.58° , indicating that the summer days are longer with the noon reaching a higher zenith point as compared to the winter noon. The orientation angle under study will always be between 0° and 180° , as informed by Figure 8.

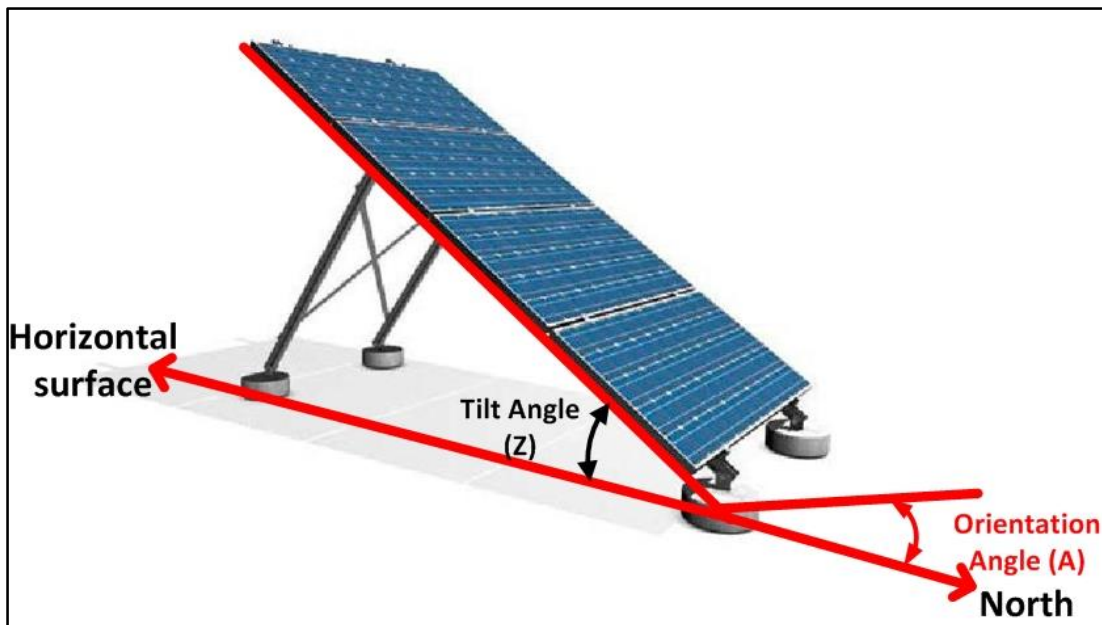


Figure 7: Orientation and tilt angles of a PV module

Many studies and experiments have been conducted to ascertain the best tilt and orientation angles for specific climate conditions (Asowata et al., 2012b; Lalia, Dalila & Ahmed, 2013; Prashanthini et al., 2011; Swart, Schoeman & Pienaar, 2011). One study considered the optimum tilt and orientation angles for PV modules in the Vaal Triangle in South Africa and found that tilt angles between 16 and 26, yielded optimum

output power in winter months (Asowata et al., 2012a). Another study from South Africa showed that a DCVRLA battery remained charged for longer (2.8 hours) when a PV module was orientated due north (0° N), as compared to a $+15^{\circ}$ orientation angle (2.3 h) or a -15° orientation angle (1.9 h) (Asowata, Swart & Pienaar, 2014). Furthermore, other researchers in South Africa found that a one-axis tracker typically provides gains of between 15% and 35% over fixed mounted modules (Suri et al., 2012). This one-axis tracker can either be for the tilt angle, or for the orientation angle. This study focused on the effects of the orientation angle of a PV module on its output power. As such, different techniques of acquiring angles electronically have to be explored, in order to determine the best suited technique for the current application.

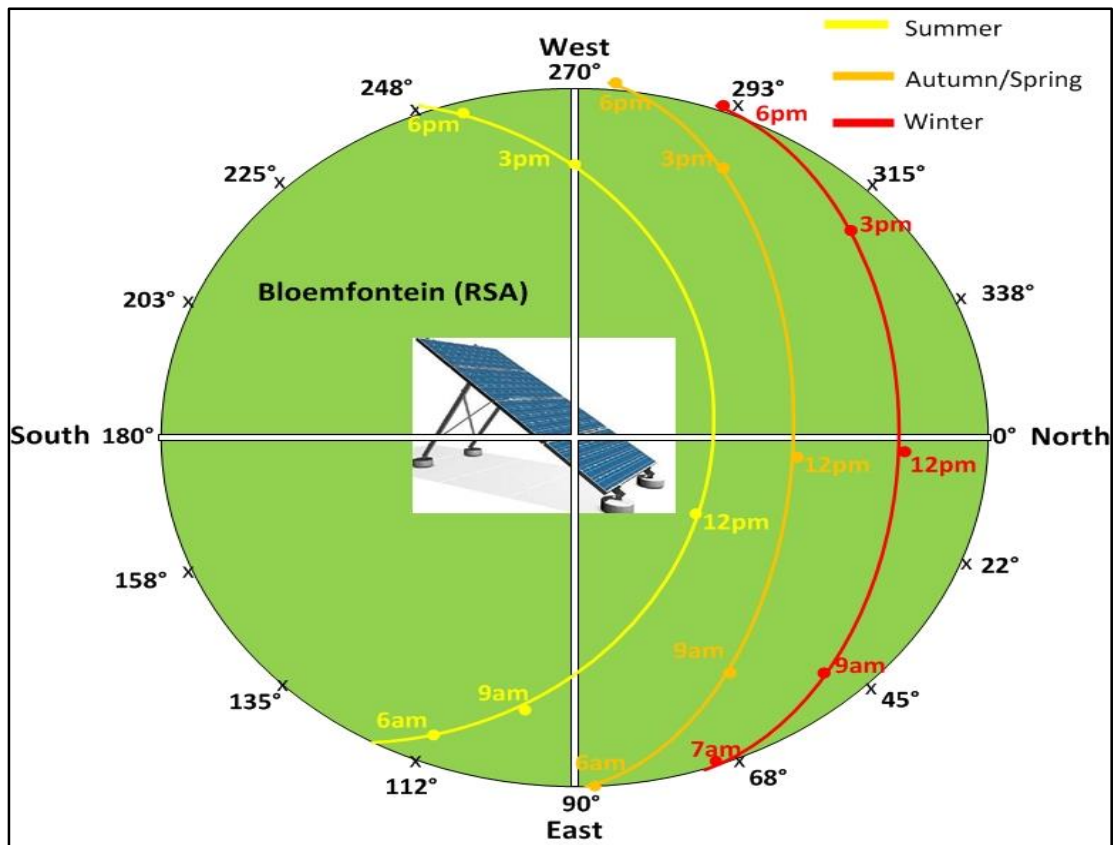


Figure 8: Sun position for different orientations

2.3.1 Orientation measuring techniques

Position sensors are used in various applications for detecting the position of an object; these can detect either angular or linear positions. There are five main principles that can be employed in sensors that measure angles electronically. This study considered

three, namely optical, magnetic and resistance (Sinclair, 2000; Zettlex, 2017). The first two technologies require no contact with the moving part of the application. The different types of sensor technologies are compared in Table 2, according to their operating temperature, rotation life and rotation angle.

Table 2: A comparison of types of position sensors

Type	Operating temperature	Rotational life	Angle rotation
Optical	-10°C to 70°C	30 000 cycles	0° to 360°
Magnetic	-40°C to 125°C	50 000 000 cycles	0° to 360°
Resistance	-25°C to 70°C	10 000 cycles	20° to 220°

Optical sensors can either be absolute or incremental encoders whose output is an analog or digital code. They have photo detectors that measure light by scanning a high-resolution disk with code patterns as it rotates. Figure 9 shows a horizontal shaft, which can also be oriented vertically (Sinclair, 2000; Zettlex, 2017). It then gives out a stream of binary output pulses, which are processed further to give the actual angular position of the shaft (0° to 360°) that is installed vertically. Incremental encoders have two outputs whose sequence determines the direction of the shaft when there is a change in position. Absolute encoders however, are more complex with a four-bit coded output indicating both position and direction whether stationary or moving (Tian, 2012). These types can operate in temperatures up to 70°C with the rotational life of about 30 000 cycles.

Magnetic sensors are also referred to as the Hall Effect sensors as they make use of the Hall Effect to detect position and are fairly expensive (Zettlex, 2017). These types are made of a shaft, Hall element and a magnet, as shown in Figure 10. They have a longer rotational life than optical sensors and can operate in extreme temperatures. The magnet is mounted to the shaft and it uses the Hall element to determine the angle of the magnet. It varies its output voltage in response to a magnetic field; this voltage is directly proportional to the angle of the shaft (Fraden, 2010).

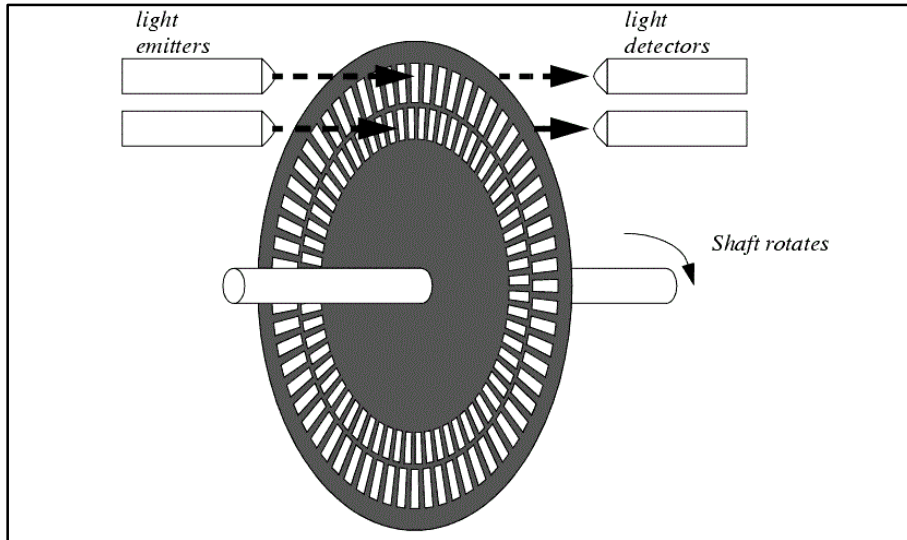


Figure 9: Optical encoder disk (Engineer on a Disk, 2016)

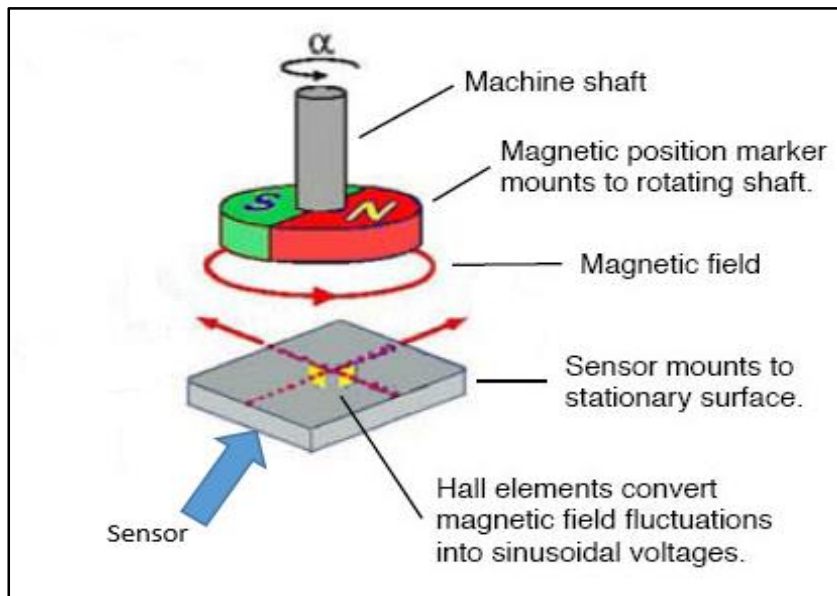


Figure 10: Magnetic rotatory sensor operation (StackExchange, 2016)

Resistance sensors take the form of a rotatory potentiometer (see Figure 11) that has a circular track with its wiper attached to the rotating shaft that is installed vertically. When the orientation angle changes, the wiper rotates, and the resistance between it and the end of the track changes (Zettlex, 2017). The voltage produced at the output is directly proportional to the angle of the shaft as shown in Figure 12. This form of sensing is inexpensive and easy to use. They can operate in temperatures between -25°C and 70°C with each potentiometer giving about 10 000 rotational cycles that can

detect angles between 20° and 220°. These characteristics make the potentiometer suitable for application to this study, given that the area of installation does not experience extreme temperatures and the orientation angles will be limited to between 0° and 180°.

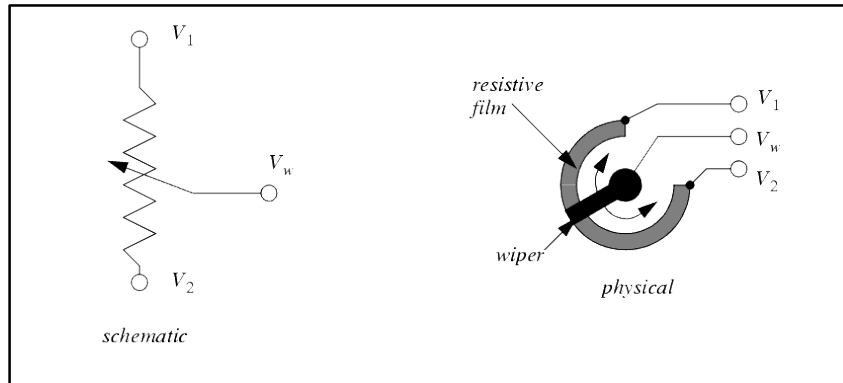


Figure 11: Potentiometer schematic symbol (Engineer on a Disk, 2016)

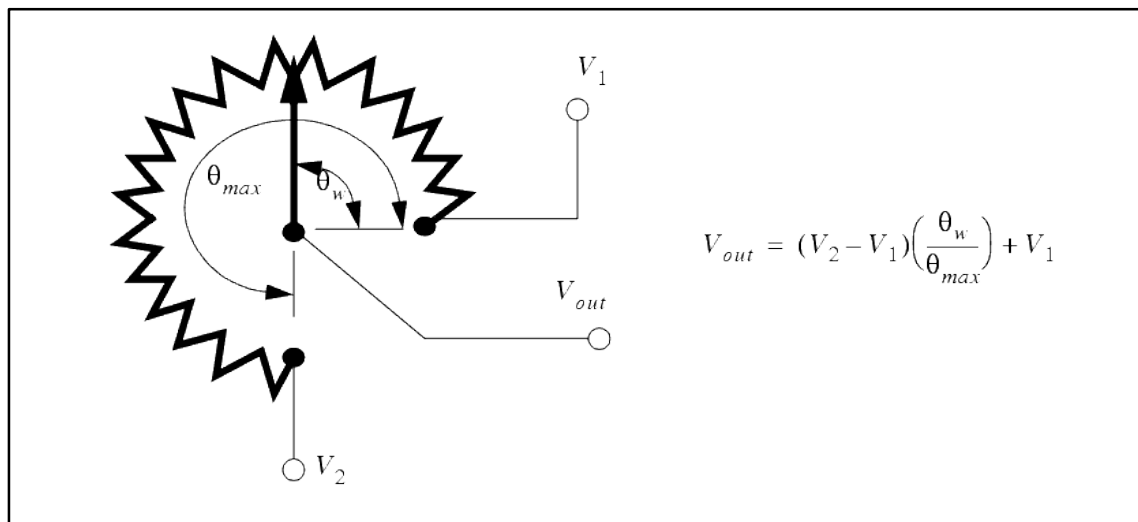


Figure 12: Potentiometer used for measuring angles (Engineer on a Disk, 2016)

2.4 Power measurements

PV modules undergo performance characterization in Standard Test Conditions (STC); PV cell temperature of 25°C, irradiance of 1000 W/m² and air mass AM = 1.5; by primarily measuring its voltage-current (*I-V*) curve (Schwingshacklel et al., 2013). The output power of a PV module is the product of its current and voltage, hence the importance of the *I-V* curve (these parameters are the short circuit current (*I_{sc}*) and the

open-circuit voltage (V_{oc})). The output power is given by:

$$P = V_{oc} \times I_{sc} \quad 2$$

Light-generated current (I_{sc}) is the current in a solar cell that is due to the generation and collection of light-generated carriers (PV Education, 2018). Therefore, I_{sc} is almost proportional to the incident solar irradiance, while the V_{oc} increases only a little with an increase in solar irradiance. When it comes to PV module temperature, however, the V_{oc} decreases with ambient temperature increase, leading to a decrease in the overall output power, despite a small increase in the I_{sc} (due primarily to thermally excited electrons that dominate the electrical properties of the semiconductor) (Mattei et al., 2006; Skoplaki & Palyvos, 2009). As such, field measurements of the voltage and current of a PV module, allow more accurate data to be collected for practical operating conditions that differ slightly from the STC, in order to optimise the overall system performance. Table 3 presents non-isolated and isolated methods that can be employed to acquire voltage measurements with their accuracies, pros and cons.

Table 3: A comparison of different methods of measuring voltage

	Non-isolated		Isolated secondary side	
Type	Direct connection	Voltage divider	Voltage transducer	Opto-isolator
Accuracy	High	Medium to high	High	High
Price	Low	Low	High	Medium
Advantage	Low cost	Simple, inexpensive	Linearity	Accurate
Disadvantage	Low voltages	Over-voltage possibilities may occur	Complex	Requires additional isolated supply voltage

Directly connecting the voltage to an analog-to-digital converter of a microcontroller can detect a voltage of 3.3 V or 5.5 V maximum; connecting anything more will damage

the microcontroller. For instance, the microchip PIC18F24Q10 microcontroller has an operating voltage range from 1.8 V to 5.5 V DC (Microchip, 2018). This method is limited to applications with low voltages.

The voltage divider, shown in Figure 13, is one way to obtain higher voltage measurements that is non-complex and inexpensive, and is commonly used in PV data acquisition (Belmili et al., 2010; Koutroulis & Kalaitzakis, 2003; Leite & Chenlo, 2010; Ranhotigamage & Mukhopadhyay, 2011; Tina & Grasso, 2014). The voltage divider is designed such that its output (V_{OUT}) is proportional to the input voltage (V_{IN}) and small enough to be processed by a microprocessor as in the equation below:

$$V_{OUT} = \frac{R_2}{R_1 + R_2} V_{IN} \quad 3$$

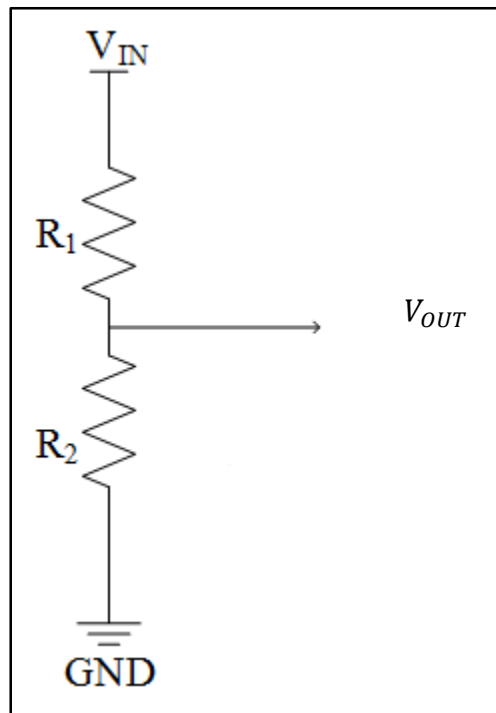


Figure 13: Voltage divider

The major drawback is that it is vulnerable to resistor variation with a change in temperature. Metal film resistors can be used to mitigate this drawback, in that they have a low temperature coefficient and low tolerance, which contributes to more accurate resistance readings. The typical tolerance availability for metal film resistors is $\pm 0.1\%$, $\pm 0.25\%$, $\pm 0.5\%$, $\pm 1\%$, $\pm 2\%$, with the temperature coefficient of ± 50 to $> \pm 100$

ppm/°C (KOA Speer Electronics inc., 2017b; TT Electronics, 2018; Yageo Corporation, 2019b), compared to tolerance availability of $\pm 2\%$, $\pm 5\%$, $\pm 10\%$, $\pm 20\%$ and temperature coefficient ranging from ± 350 to $> \pm 1500$ ppm/°C of carbon film resistors (KOA Speer Electronics inc., 2017a; Vishay Day, 2016; Yageo Corporation, 2019a). This form of detection is well suited for the current research study for dropping the sensed voltage to a value low enough to be connected to the microcontroller with the added benefit of its simplicity and low cost.

Voltage Transducers measure either AC or DC voltage and convert it to an analog output signal, which is directly related to the measured input. These transducers provide an output which is load-independent and isolated from the input and are mainly used to drop high voltages to low signals, safe for electronic components (Meco, 2018; NK Technologies, 2018).

With the **opto-isolator** the input voltage is scaled according to the isolation amplifier. The input voltage is converted into light and is detected from one side to the other through an optical connection (see Figure 14). The optical output is received on the output side and converted to a voltage signal (Broadcom, 2018). This method of detecting voltage is more expensive than the voltage divider, but offers accurate and isolated voltage detection.

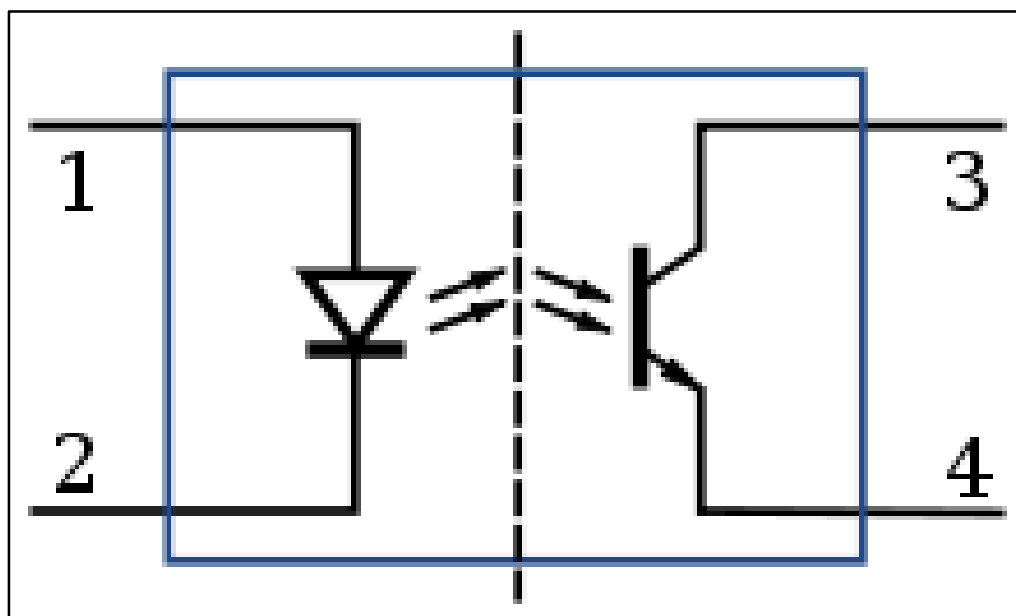


Figure 14: Opto-Isolator (Wikipedia, 2018)

Table 4 presents three ways of detecting DC current, comparing their accuracies, advantages and disadvantages. First, a simple, low-cost way to obtain current measurements is a low value **shunt resistor** that has proved effective in small scale PV applications (Leite & Chenlo, 2010). A low value resistor (shunt resistor) is connected in a series with the point to be measured as in Figure 15, then the voltage across the shunt resistor is used to obtain the current at that point. Current flowing through a small resistance means that an insignificant voltage drop will occur, which will be proportional to the current flowing as in the equation below.

$$I = \frac{V}{R} \quad 4$$

Table 4: A comparison of methods of measuring current

	Non-isolated	Isolated secondary side	
Type	Shunt resistor	Fluxgate	Hall Effect
Accuracy	Medium	High	High
Price	Low	High	Medium
Advantage	Most linear	Low noise	High operating temperature
Disadvantage	Power dissipation	Complex	Noisy

The challenge with this method is that the resistance will be affected by high temperatures. As such, manufacturers have developed two or four terminal power resistors of sub-ohmic resistance values that exhibit high current capacity. These shunt resistors have a maximum current rating, tolerance, temperature coefficient of resistance and power rating, depending on the material used. The resistance value is given by the voltage drop at the maximum current rating. For example, a shunt resistor rated at 100 A and 50 mV has a resistance of $50 / 100 = 0.5$ mOhm. The power rating shows the amount of electric power that the resistor can dissipate at a given ambient temperature without damaging the resistor.

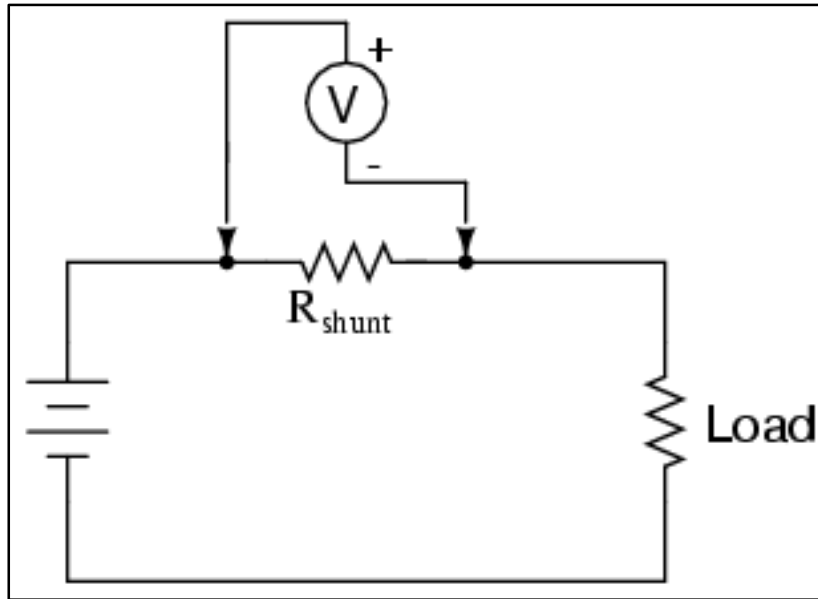


Figure 15: Shunt resistor

Secondly, a **fluxgate current sensor** has basically the same structure as a current sensor with a magnetic stability system, except that it has a magnetic probe coil instead of a Hall element (Ziegler et al., 2009). The fundamental fluxgate principle uses the non-linear relation between the magnetic field and magnetic flux density in a magnetic material. The measurable current is within a range from 6 to 600 A with its implementation being complex leading to high costs, which is why it is not widely used.

Lastly, **Hall Effect current transducers** (LEM LA100-P, LA55p, Honeywell Microswitch CSLA1CF) have been used to measure current for more complex PV applications (Belmili et al., 2010; Tina & Grasso, 2014). It comprises a precise, low-offset, linear Hall sensor circuit with a Hall element, as shown in Figure 16 **Error! Reference source not found.** An applied current flowing through this Hall element generates a magnetic field, which is detected by the integrated Hall IC that provides a proportional voltage. Device accuracy is improved through the close proximity of the magnetic signal to the Hall transducer. A precise, proportional voltage is provided by the low-offset, chopper-stabilized BiCMOS Hall IC, which is programmed for accuracy after packaging (Allegro Microsystems, 2006). This type is applicable for the current research study, due to its accuracy and its insensitivity to temperature change.

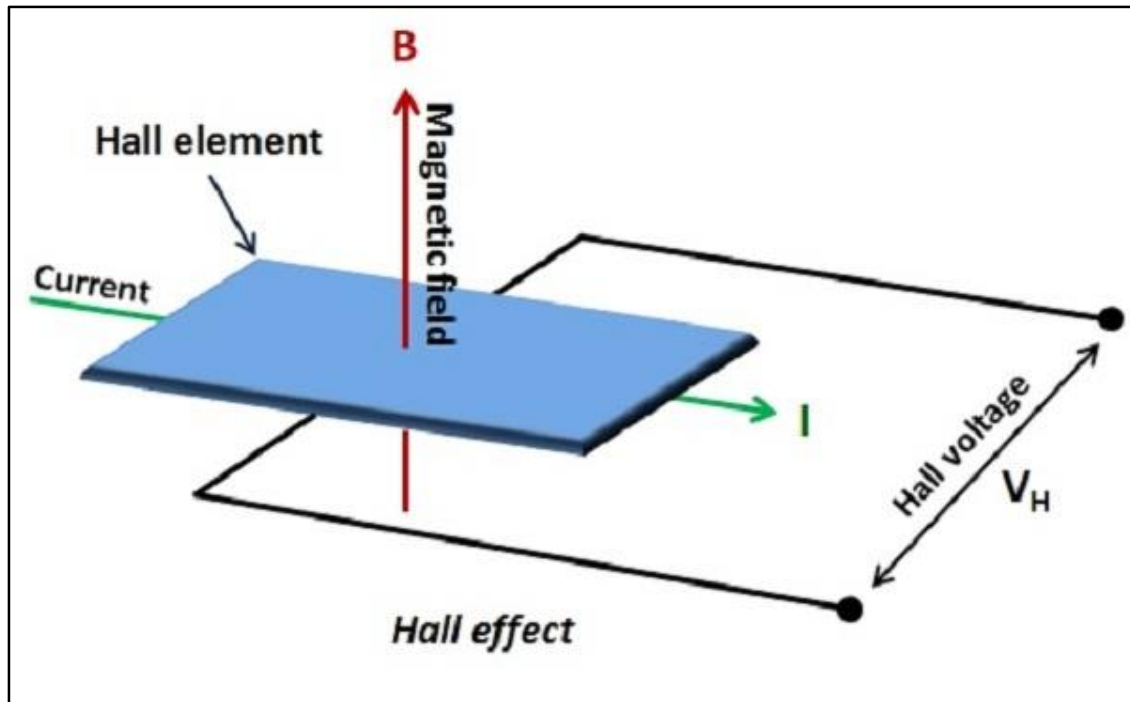


Figure 16: Hall Effect (Dangerous prototypes, 2012)

2.5 The use of microcontrollers in data processing

Once measurements are acquired from the PV module, there needs to be a method of processing and saving the data for monitoring or analysis. A microcontroller provides such a method. Microcontrollers have been used in data acquisition systems in many spheres of renewable energy and environmental monitoring and control (Forero, Hernandez & Gordillo, 2006; Gagliarducci, Lampasi & Podesta, 2007; Koutroulis & Kalaitzakis, 2003; Mukaro & Carelse, 1999; Papadakis, Koutroulis & Kalaitzakis, 2005; Papageorgas et al., 2013; Rosiek & Batlles, 2008).

A microcontroller often plays a central role when developing a data acquisition system (DAC) for characterization of PV modules, in that it is responsible for converting the acquired analog data to digital, facilitating data transfer, between the designed system and the computer (Belmili et al., 2010). A development board is a printed circuit board that has a microcontroller and its required circuitry that allows different peripheral connections, depending on what the microcontroller allows. Popularity of a particular board depends on the amount of technical support available on the internet and its associated costs. Table 5 compares popular development boards available in the market.

Table 5: A comparison of different development boards

Development board	Microcontroller	Operating speed	RAM	Input voltage	Analog
Arduino UNO	Atmel ATmega328P	16 MHz	2 kb	7 - 12 V	6 pins 10-bit ADC, PWM
Arduino Mega 2560	Atmel ATmega2560	16 MHz	8 kb	7 - 12 V	16 pins 10-bit ADC, PWM
Raspberry Pi 3 model B+	Broadcom BCM2837B0	1.4 GHz	1 Gb	5 V	No
BeagleBone Black	TI Sitara AM3358	1 GHz	512 Mb	5 V	6 pins 12-bit ADC
Intel Galileo Gen 2	Intel Quark X1000	400 MHz	256 Mb	7 – 15 V	6 pins 12-bit ADC, PWM

The Arduino Uno is based on the ATmega328 microcontroller, has 16 digital input / output pins, six analog inputs and a USB connection. It was chosen for designing a data logger for a PV system for its simplicity and modularity, in comparison with other boards (Arduino, 2018; Fuentes et al., 2014). The **Arduino Mega 2560** uses the Atmel ATmega2560, which has the same processing speed as the Arduino Uno with more RAM (8 Kb) and I/O (54) pins allowing more data to be processed in and out by the microcontroller (Arduino, 2018). The Uno's cheapest selling price is R181.09 at the Bot Shop, whereas the Mega goes for R317.76. The Arduino platforms allow for easy learning and adaptation, because it is open ware, as such there are modules and libraries readily available on the internet. In addition, there is an on-board analog-to-digital conversion (ADC) via selected I/O pins with pulse-width-modulation (PWM) capabilities.

Raspberry Pi 3 model B+ is the latest release in the Raspberry Pi 3 range that makes use of the Broadcom BCM2837B0 processor with 1.4 GHz operating speed. Although a RAM of 1Gb makes it attractive, the drawback is that this board requires an external

ADC, which will contribute to the cost and complexity of the design (Raspberry Pi, 2018). This board is currently selling for R629.00 at Makro. The **BeagleBone Black** incorporates the TI Sitara AM3358 processor at the operating speed of 1GHz and 512Mb of RAM with six analog input pins (Beagleboard, 2018). The board is selling for R730.41 at RS components. **Intel Galileo Gen 2** is not as widely available in South Africa as the other boards. It is based on the Intel Quark X1000 processor with 400 MHz processing speed and 256Mb of RAM (Intel, 2017). This is the most expensive, selling for R926.00 online from Importitall.

The Arduino Uno and Mega 2560 are ideal for the current application, the Uno for the wireless communication and the Mega 2560 for data sensing and processing. The Arduino platform offers high modularity, guaranteeing a wide range of modules to interconnect with, in order to meet many requirements for a data acquisition system. The Mega 2560 boasts 54 I/O pins, which meets the demand of the parameters to be detected. The two microcontrollers are the least expensive, they also have extensive support on the internet, providing programming libraries and examples.

2.6 The use of wireless technologies in data transfer

Wireless technology is used to transfer information between two or more points that are not physically connected to form wireless communication. Wireless technologies prove useful when it comes to accessing data from a remote site that is without electricity or telephone lines. Wireless communication can be achieved through either radio frequency, microwave or infrared. There are four popular wireless technologies that make use of radio frequency in remote communication, namely Bluetooth, RF, Zigbee and Wi-Fi. Range, data transfer rate, frequency band and power usage are some of the factors to consider when choosing a wireless device relevant to the application. Table 6 presents a comparison between different wireless technologies in terms of their range, data rate, frequency band and power usage.

Bluetooth is a short-range technology, initially intended to eliminate cables when connecting portable devices. It operates in the 2.4 GHz frequency band with devices that are within 50 meters of each other at a rate of up to 3 MBps (Chhabra, 2013). The BGM113 Bluetooth module has receiver sensitivities as low as -93 dBm and

transmission output power as high as +3 dBm with current consumption of 8.8mA (Edimax Technology Co. Ltd, 2014).

Table 6: A comparison of different wireless technologies

Type	Range	Data rate	Frequency band	RX sensitivity	TX Output Power	Power usage
BGM113 blue Gecko Bluetooth	50 m	3 Mbps	2.4 GHz	-93 dBm	+3 dBm	RX: 8.7 mA TX: 8.8 mA
CC1101 RF Transceiver	300-500 m	600 kbps	433 MHz	-116 dBm	+10 dBm	RX: 15.7 mA TX: 16 mA
XBee	30-90 m	250 kbps	2.4 GHz	-92 dBm	0 dBm	RX: 50 mA TX: 45 mA
AC600 Wi-Fi	100 m	150 Mbps or 433 Mbps	2.4 GHz or 5 GHz	4 dBi or 6 dBi	17 dBm or 14 dBm	RX: 180 mA TX: 220 mA

An **RF transceiver module** is an integrated circuit that transmits and receives radio signals on a given (433 MHz as an example) carrier frequency. An example is the CC1101 that operates at 433 MHz. It has different communication modes that can be changed by command. Of these, there are four modes responsible for sending and receiving data with low idle currents of 80 μ A, 3.5 mA and 22 mA, depending on which mode is chosen. It can achieve transmission output power as high as +10 dBm and reception sensitivity as low as -116 dBm with current consumption of 16 mA (Texas Instruments, 2018). In addition, it can transmit over distances of up to 500 m in open-air line of sight without any obstacles to absorb radio signals at a rate of about 600 kbps (Texas Instruments, 2018). The usefulness of RF modules in remote-sensing and control is widely accepted in many industries. Yuce used RF technology to implement a system for wireless body area networks for the healthcare environment (Yuce, 2010). This type of wireless linking was also used in monitoring various room environment parameters, including temperature, humidity and flying dust (Chung & Oh, 2006). In addition, a popular application in the healthcare industry for RF wireless

communication, is for systems that monitor the health status of elderly persons at home (Inada & Horio, 1992; Virone et al., 2003). In wireless communication, power consumption is increased with bigger communication distances. It is therefore required for wireless communication to consume minimal power for remote sites. This is why RF modules are also widely used in renewable energy system monitoring, as they have very low power consumption and also for their low-cost and wide open-air range capabilities (Benghanem, 2010; Koutroulis & Kalaitzakis, 2003; Papadakis et al., 2005).

XBee is a specification of an assembly of high-level communication protocols, utilizing small, low-power radios to present mesh networking to personal area networks. It is more complex to implement than RF, but is also widely used in studies that involve monitoring the performance of PV systems (Andreoni Lopez, Galdeano Mantinan & Molina, 2012; Ranhotigamage & Mukhopadhyay, 2011; Shariff, Rahim & Hew, 2015). Communication is possible for distances of up to 90 meters at a rate of 250 kbps for the 2.4 GHz frequency band (Abinayaa & Jayan, 2014; Digi International Inc., 2008).

Wireless Fidelity (Wi-Fi) refers to the IEEE 802.11 communication standard for wireless local area networks (WLANs), where devices can connect to other devices or the internet wirelessly. A centralized router is used to connect devices and the Wi-Fi signal is shared amongst the connected devices for high speed data transfer (up to 6 Gbps) on the designated frequency band (Chhabra, 2013). The AC600 Wi-Fi module operates on the 2.4 and 5 GHz frequency band with the data rate of 150 and 433 Mbps respectively.

The features of the CC1101 highlighted in this section, make these RF transceivers ideal tools of communication for the current research study. These include the open-air range of up to 500 m, coupled with high receiver sensitivity and high transmitter output power with minimal power consumption. CC1101 transceivers were used to develop an early flood detection system at the Indonesian Hasanuddin University (Katu et al., 2016).

2.7 Summary

A summary of relevant literature was presented in this chapter, in order to make an informed decision, regarding which components to use for the monitoring and control

of a remote PV module. Focus was first directed to the importance of temperature and the orientation angle of a PV module, and how to measure them. The DHT11 digital temperature sensor was selected for detecting temperature for its ability to connect directly to a microcontroller with no need for complex circuitry. A potentiometer would be used as an angle sensor to sense the orientation of the PV module between 0° and 180° . Power measurements are equally important and methods of obtaining them were given. To obtain these, the ACS712 current sensor and the voltage divider would be used for current and voltage measurements. Different microcontrollers for the processing of obtained data and wireless technologies for data transfer were also compared. It was concluded to make use of the Arduino microcontroller development boards for sensor connections and the CC1101 RF transceiver for wireless transmission purposes. The following chapter outlines the practical setup of the proposed system, the data that are required, as well as how to interpret it. The programming of the different components will also be presented.

Chapter 3 Methodology

3.1 Introduction

The previous chapter discussed literature on the effect that temperature and orientation angle exert on the output power of a PV module. The different measuring techniques were discussed, and relevant technologies selected. The design and implementation of the PV monitoring and control system is presented in the sections below. Details of how the different sensors are linked to the transceivers for remote transmission are elaborated upon. Furthermore, pictures of the practical setup are presented to explain the functionality of the system. The design of the user interface that organises and saves the data is also offered, together with its programming.

3.2 System design

The block diagram contained in Figure 17 shows the overall setup of the system design for remotely measuring current, voltage, temperature and the orientation angle for the purpose of controlling the temperature and orientation angle, in order to improve the PV efficiency. Block 1 is the PC transceiver side where the user can see the real-time sensor data displayed on the PC that is sent from block 2, which is the PV module transceiver side responsible for collecting data, using the microcontroller. Block 3 shows all the parameters of the PV module that are collected by the microcontroller. Block 4 harbours the control mechanisms for the two important parameters of the PV module, temperature and orientation angle.

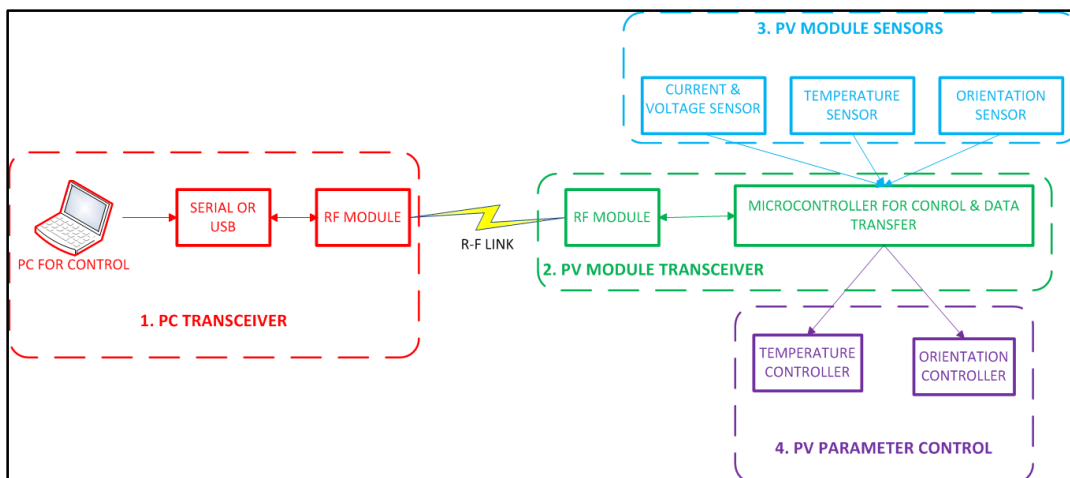


Figure 17: Block diagram of the practical set-up

A research approach mainly used in computer systems is Design Science Research (DSR). Baskerville explains DSR as typically involving the creation of an artefact and/or design theory as a means to improve the current state of practice as well as existing research knowledge (Baskerville, Baiyere, Gregor, et al. 2018). “Research can be very generally defined as an activity that contributes to the understanding of a phenomenon. In the case of design science research, all or part of the phenomenon may be created as opposed to naturally occurring” (Vaishnavi, Kuechler and Petter, 2019). This method of research was not suited to the current study in that it involves a synthesis of pre-existing components to answer a research problem rather than creating an artefact. Added to that, the phenomenon under study is a naturally occurring one and not a created one.

3.2.1 Master transceiver board

This part of the system is responsible for receiving measurements and sending commands over the RF-link, as well as saving it on the PC. The master transceiver board in Figure 18 is designed to plug into the Arduino UNO board that connects to the PC, using the USB port as in Figure 19. The master transceiver board has three LED’s that indicate the mode of the transceiver module (red), receive data (green) and transmit data (yellow). The transceiver is a CC1101 module, as discussed in chapter 2.

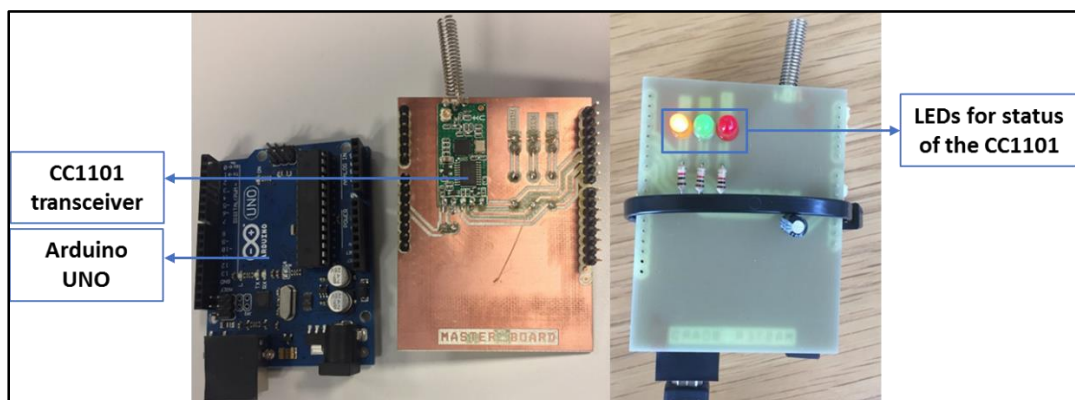


Figure 18: Arduino and master transceiver

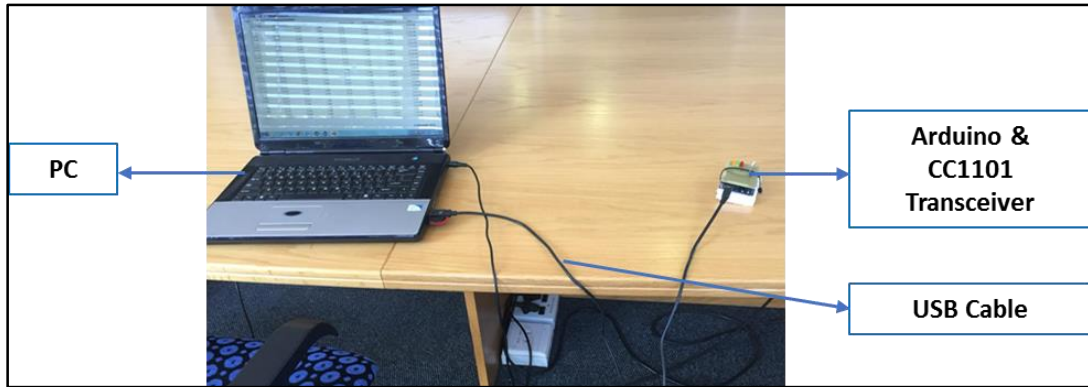


Figure 19: Master transceiver station

In this instance, the software serial port of the Arduino UNO has been utilized to connect the PC to the CC1101 transceiver for wireless reception of the sensor measurements and transmission of the commands from the user interface. As such, the TX and RX pins of the CC1101 RF transceiver have been connected to pins 5 and 6 of the Arduino UNO respectively and the pins declared in the program (Annexure C) as communication pins as can be seen in Figure 20 (third line from the top). As long as there are data received by the CC1101 transceiver (loop), it will be sent to the serial port that is linked to the PC, therefore receiving data via the RF link and saving it on the PC.

```
include <SoftwareSerial.h>

const int CMD = 4;
softwareSerial HC12(5, 6); // HC-12 TX Pin, HC-12 RX Pin

void setup() {
  pinMode(CMD, OUTPUT);
  digitalWrite(CMD, LOW);
  Serial.begin(9600);           // Serial port to computer
  HC12.begin(9600);           // Serial port to HC12
}

void loop() {
  while (HC12.available()) {   // If HC-12 has data
    Serial.write(HC12.read()); // Send the data to Serial monitor
  }
  while (Serial.available()) { // If Serial monitor has data
    HC12.write(Serial.read()); // Send that data to HC-12
  }
}
```

Figure 20: Send and receive code at PC

3.2.2 Slave transceiver board

The slave transceiver board that harbours the CC1101 and the sensors (sensor board) on the PV module side, is connected to the Arduino Mega 2560 (Figure 21) and the Arduino is powered by the battery. This transceiver board connects the voltage, current and temperature sensors to the Arduino Mega 2560 that obtain data from the PV module, battery and the load seen in Figure 22. This data is transmitted to the PC Arduino UNO device at 100 seconds intervals.

The measurements from the sensors are sent to the serial port of the Arduino Mega 2560. The transmitting device, CC1101 transceiver RX and TX pins are connected to this Arduino's serial port 0 at pin 0 and 1 respectively. This means that the measurements that are sent to the serial port of the Arduino Mega 2560 are then transmitted by the CC1101 transceiver. When the Arduino Mega 2560 is connected to a PC using a USB cable, terminal software can be used to display these measurements on the serial port of the PC through the USB port. This feature might be used in environments that are not remote and do not require wireless transmission.

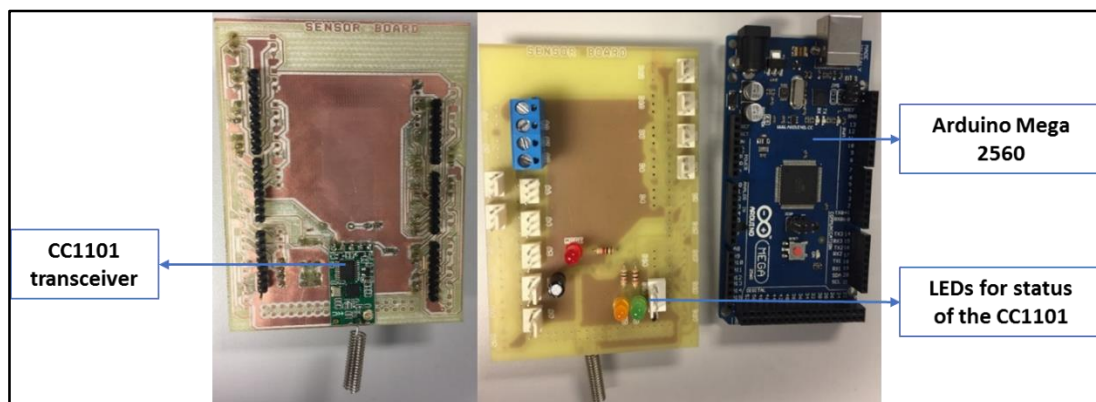


Figure 21: Slave transceiver board

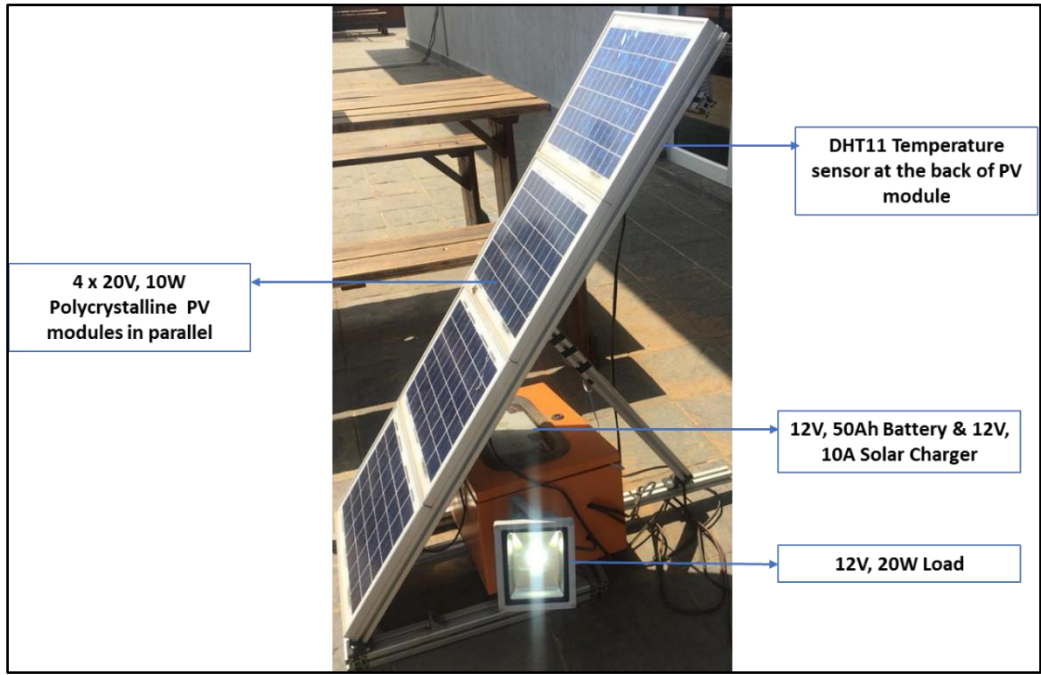


Figure 22: Transmitting station

3.2.2.1 Slave transceiver sensors

Measurements are obtained using sensors connected on the slave transceiver board; designed to fit on to the Arduino Mega 2560, which processes the signals.

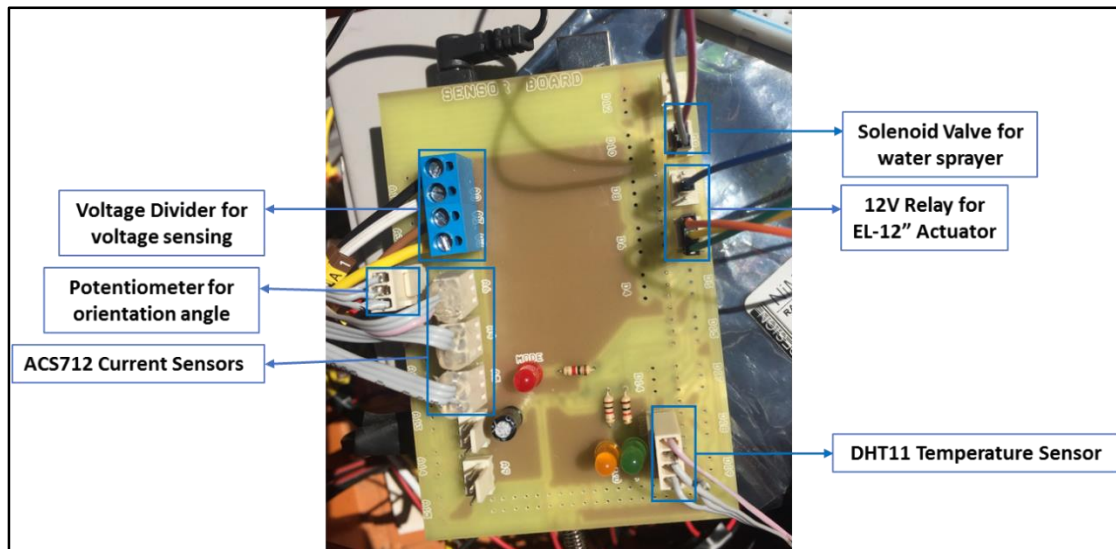


Figure 23 shows where the sensors plug into the slave transceiver board, while Figure 24 demonstrates the dedicated sensor pins on the Arduino Mega 2560.

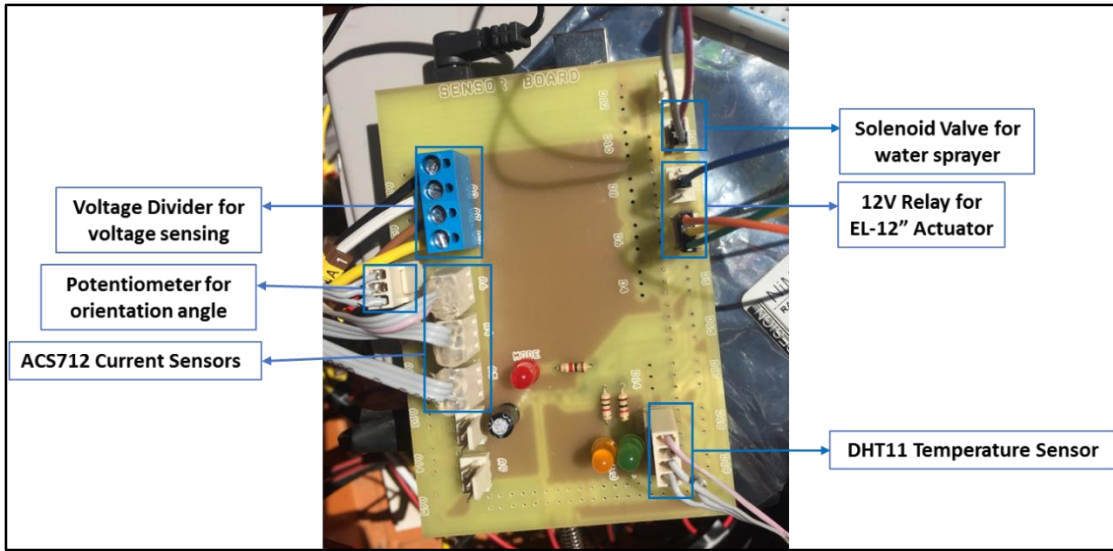


Figure 23: Slave transceiver board with sensors

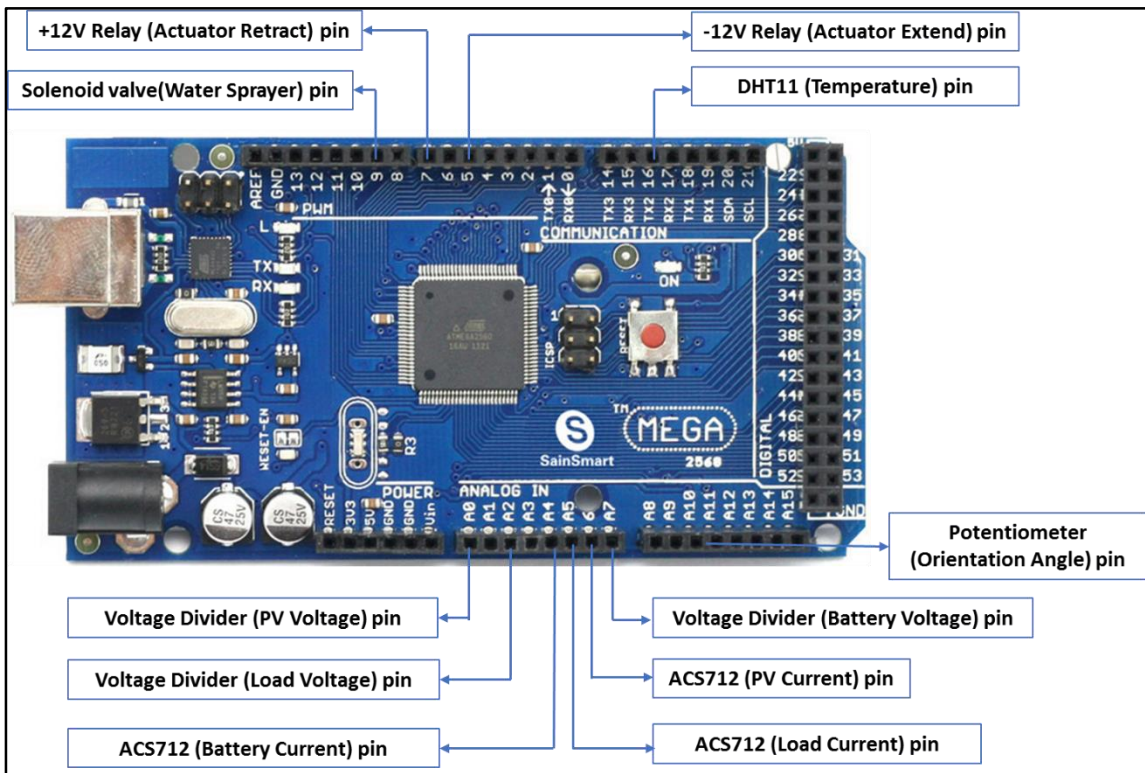


Figure 24: Arduino Mega 2560 showing sensor pins

A circuit diagram of the voltage divider for voltage-sensing and ACS712 for current-sensing is provided in

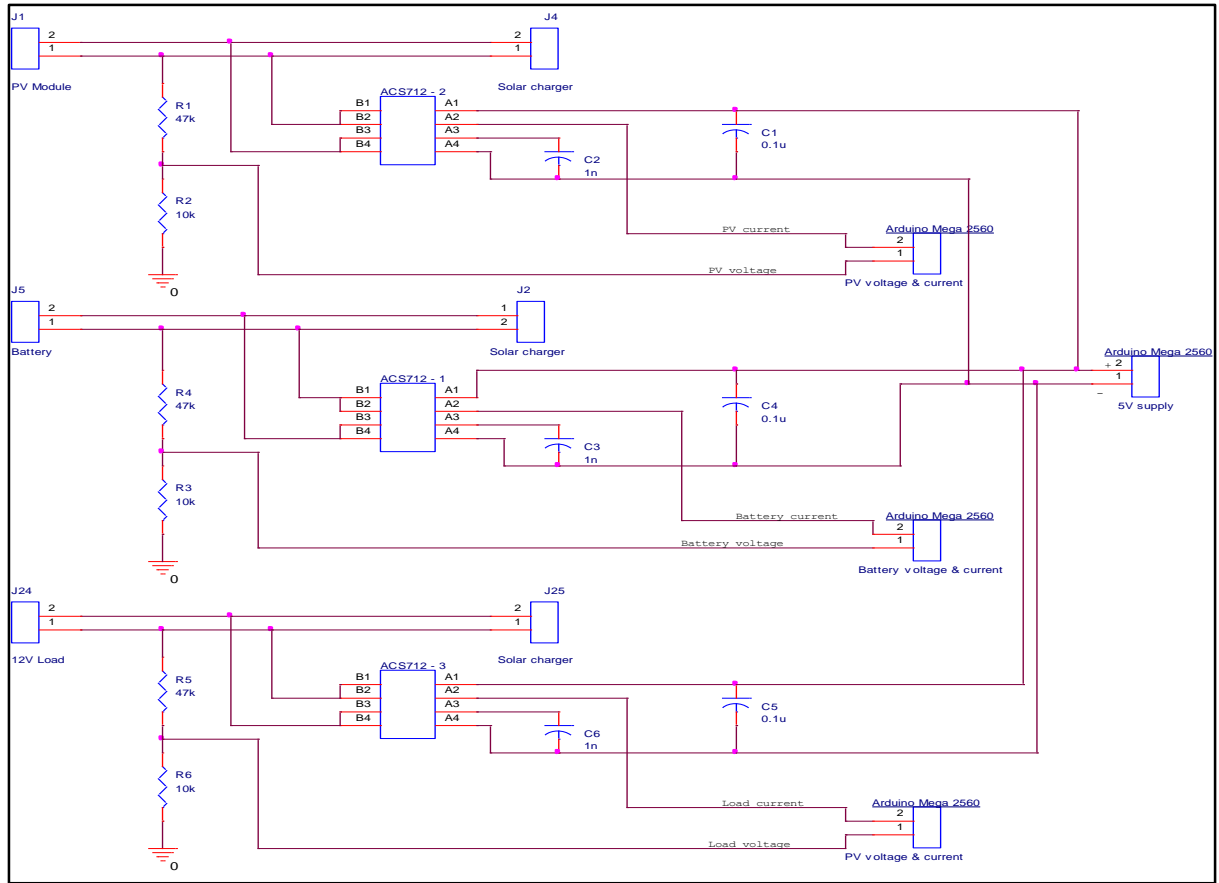


Figure 25. The output of the voltage divider is calculated by:

$$V_{out} = \left(\frac{10\text{ K}\Omega}{47\text{ K}\Omega + 10\text{ K}\Omega} \right) \times V_{PV} \quad 5$$

where V_{PV} is the voltage from the PV modules (4 x SD ECO PLUS 10W PV modules connected in parallel). The open circuit voltage (V_{OC}) for these is 20.8 V and the short circuit current (I_{SC}) is 0.78 A. The Arduino Mega 2560 analog input pins can measure voltages from ground to 5 V; supplying these pins with anything more will damage them. As such, voltage dividers are used to sense the voltages of the PV module, battery and load, while fuses (see Figure 26) are used to protect the circuitry against any unwanted currents.

V_{out} from these sensors is connected to the three analog pins of the Arduino Mega 2560 respectively. The microcontroller then uses a programmed algorithm (Annexure B) to process the voltage divider output and convert it to a relative voltage. Figure 27 displays how the signal sensed at the Arduino Mega 2560 pin is converted to the actual voltage sensed, by multiplying it with the ADC reference voltage and dividing it by the

10-bit resolution 1023.

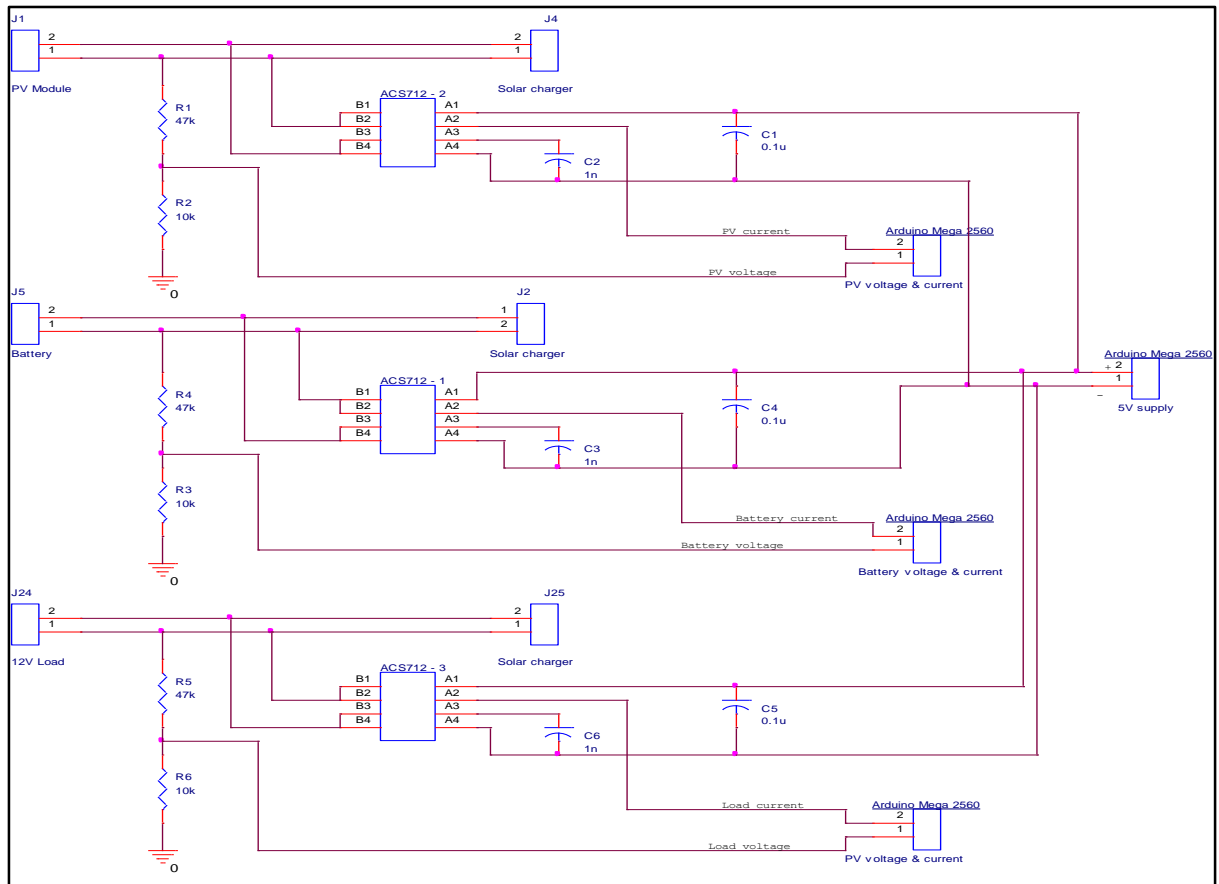


Figure 25: Voltage and current sensing circuit diagram

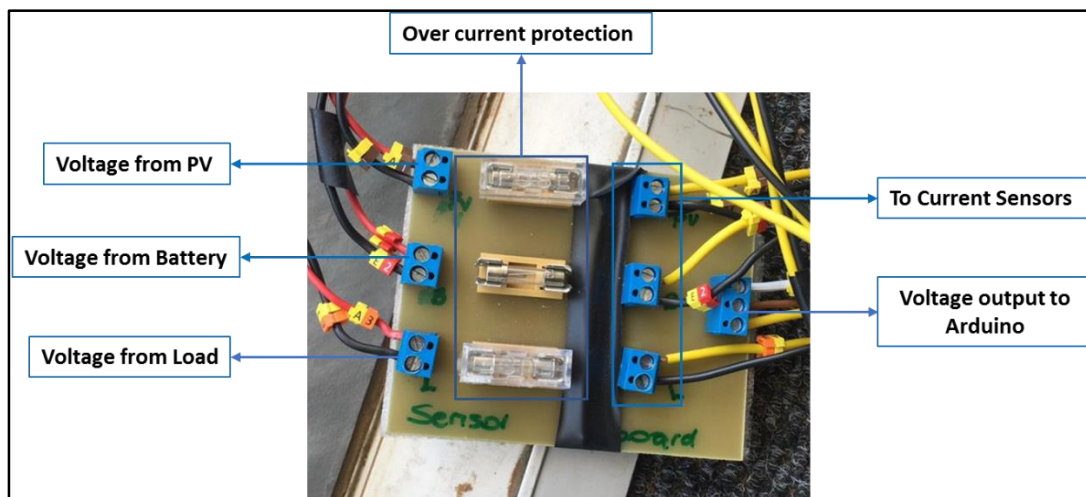


Figure 26: Voltage sensors

A closer look of the current sensors is seen in Figure 28, where the inputs are from the PV modules, battery and load. The output of these sensors is plugged into the slave transceiver board. The current through the PV module, battery and the load are sensed, using three Allegro ACS712 sensors, which give analog outputs proportional to the current sensed and are connected to the relative three analog pins of the Arduino Mega 2560. The proportional output of the sensors is processed by the microcontroller to give an actual current reading in Amperes (Figure 27).

```

//Voltage measurements
PinRead = analogRead(PV_VPin); //Read analog data
PV_Vin = (((PinRead * 5.0) / 1023) / 0.175); //Convert to actual voltage
delay(100);
PinRead = analogRead(BT_VPin); //Read analog data
BT_Vin = (((PinRead * 5.0) / 1023) / 0.175); //Convert to actual voltage
delay(100);
PinRead = analogRead(LD_VPin); //Read analog data
LD_Vin = (((PinRead * 5.0) / 1023) / 0.175); //Convert to actual voltage
delay(100);

//Current measurements
PinRead = analogRead(PV_IPin); //Read analog value
PV_Iin = (((PinRead / 1023.0) * 5000) - 2500) / 100; //Convert to actual current
PinRead = analogRead(BT_IPin); //Read analog value
BT_Iin = (((PinRead / 1023.0) * 5000) - 2500) / 100; //Convert to actual current
PinRead = analogRead(LD_IPin); //Read analog value
LD_Iin = (((PinRead / 1023.0) * 5000) - 2500) / 100; //Convert to actual current

```

Figure 27: Voltage and current code

The analog input of the Arduino is used in the formula below, in order to arrive at the current reading:

$$I = \frac{\left(\frac{PinRead}{1023} \times 5000\right) - 2500}{100} \quad 6$$

PinRead is the analog input, the 1023 is the 10-bit resolution of the ADC and the 5000 is the reference voltage in milli-Volts of the same. Because the offset of the current sensor is 2500 mV, it must be subtracted to arrive to the actual current in milli-amperes (mA). This is divided by 100 to convert to Amperes (A).

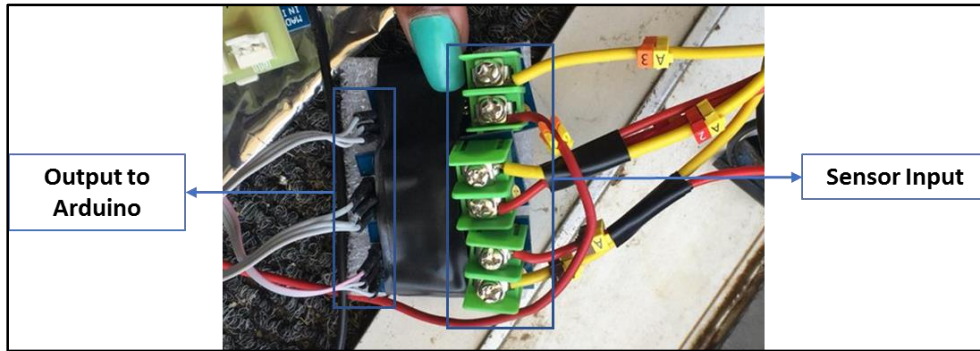


Figure 28: ACS712 current sensors

The temperature sensor also connects to the slave transceiver board and gives real-time temperature of the PV module's surface in Degrees Celsius ($^{\circ}\text{C}$). As established in the previous chapters, the surface temperature of the PV module is important to its efficiency. As such, the DHT11 temperature sensor is attached to the back of the PV module, in order to obtain real-time temperature measurements. This sensor's digital output is connected to the digital pin of the Arduino Mega 2560 where it is processed through an Arduino IDE library that returns the actual temperature in $^{\circ}\text{C}$.

3.2.2.2 PV parameter control

The Arduino Mega 2560 connected to the slave transceiver board is programmed to test if there are commands sent from the user interface to either adjust the orientation angle or to switch the water sprayer on or off (for temperature control of the PV module). It receives commands via the CC1101 transceiver through the serial port (Figure 29). If command "R" is received, the pin linked to -12V of the actuator is activated for 8 100 milliseconds (ms), which extends the actuator to achieve an angle shift of 10° . This combination adjusts the orientation 10° to the right. When command "L" is received, the pin linked to +12V of the actuator is activated for 8 100 ms, which retracts the actuator to achieve an adjustment of 10° to the left. Should "N" be the command that is received by the Arduino Mega 2560, the water sprayer pin will be high for five seconds. This switches the water sprayer on for five seconds, in order to cool off the PV module. The 12 V relay (Figure 30) is connected between the Arduino and the actuator, in order to provide sufficient current and the correct polarity required to extend or retract the actuator for the left and right motions. When a mechanism is installed to change the orientation angle of the PV module or the water prayer was installed, sensors would

then be used to confirm the position of the structure after the employment of the commands.

```

if(Serial.available()) // check if UART receive data
{
  rx_data = Serial.read(); //store data received
  if(rx_data==0x52) //turn right
  {
    Serial.println("Right");
    digitalWrite(forwardPin, HIGH);
    delay(8100);
    digitalWrite(forwardPin, LOW);
  }
  else if(rx_data==0x4C) //turn left
  {
    Serial.println("Left");
    digitalWrite(backwardPin, HIGH);
    delay(8100);
    digitalWrite(backwardPin, LOW);
  }
  else if(rx_data==0x4E) //spray on
  {
    Serial.println("On");
    digitalWrite(Spray_Pin, HIGH);
    delay(5000);
    digitalWrite(Spray_Pin, LOW);
  }
}

```

Figure 29: Control orientation angle and water sprayer

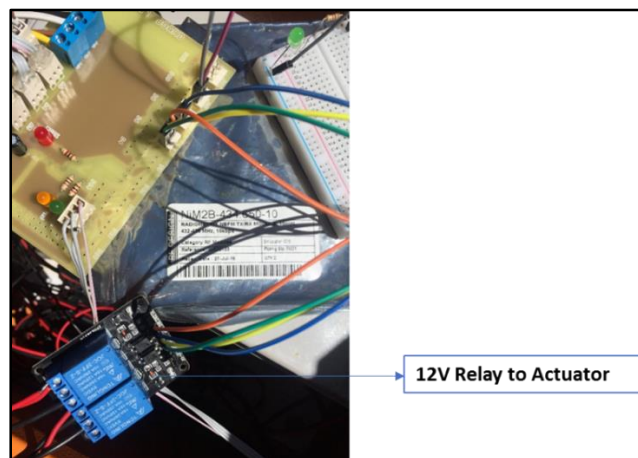


Figure 30: Relay for actuator

3.2.3 User interface and programming

The flow chart of the graphical user interface (GUI) is shown in Figure 31 where the user can initiate serial communication and observe the data being received with the option of sending relevant commands to the PV module. The user first has to set parameters of the serial port, in order to initialize communication with the Arduino Mega 2560. The parameters that have to be set are namely the “port name” set to the

relative port, “baud rate” set to 9600, “parity” set to none, “stop bits” set to one and “handshake” set to none. Clicking on the “Start Serial Com” button then initiates the serial port with the selected parameters and starts the read method that reads the data received by the Arduino UNO, if there are any data received.

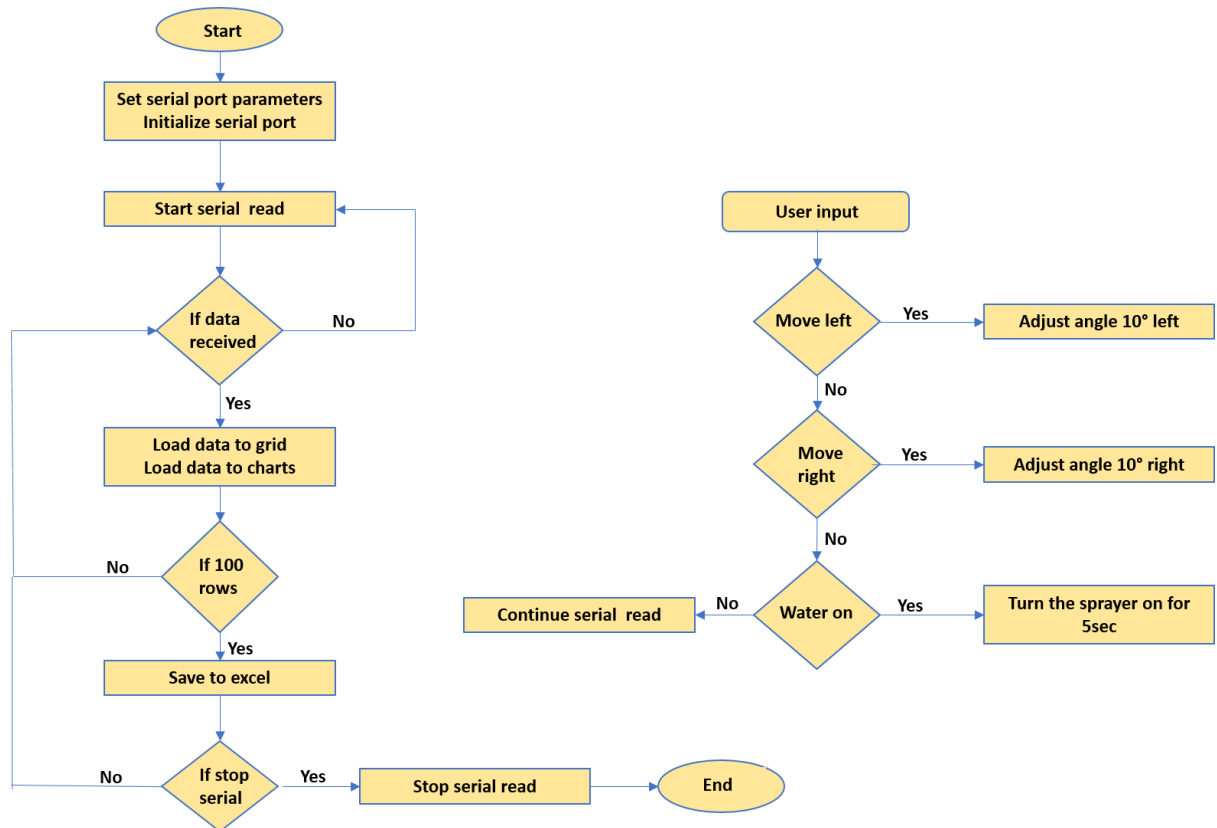


Figure 31: GUI flow chart

The data are then loaded on to the data grid that is displayed on the GUI and also on to the different graphs. When 100 rows have been loaded on to the grid, the GUI automatically exports the measurements to an Excel sheet with a pre-set file name in a pre-determined location. This process is repeated for as long as the serial connection is maintained. The user can send commands at any point of the communication by using the set buttons to adjust either the orientation angle or switch on the water sprayer.

The GUI is designed using Visual Studio C# (Annexure A) with its purpose being for the end user of the system to visually see the data being sent from the PV module or to interact with the system. Figure 32 shows the GUI with numbered items that are used to illustrate its functionality. The numbered items of the GUI are presented below with

their functionality explained:

1. Serial port settings to be selected by the user.

The serial port settings are obtained from combo boxes where the user selects the appropriate port name, baud rate, parity, stop bits and handshake.

2. Tabs that can be selected to view different data representations.

The data grid sorts the data received into the seven relative columns with the last column being the time the measurements are received. The columns are named after the measurement reading they collect, namely PV voltage, battery voltage, load voltage, PV current, battery current, load current and temperature. The data grid is displayed in the second tab of the GUI that is named live table. The third tab displays the chart representation of all the PV measurements, this being the PV voltage vs time, PV current vs time, temperature vs time and power vs time. Tab four and five show the same charts (except for temperature) for the battery and the load.

3. The button used to turn on the water sprayer for five seconds at the PV module.
4. Buttons used to move the PV module either left or right by 10° to adjust the orientation angle.
5. Displays the real time measurements as they are received from the PV module CC1101 transceiver. Measurements received by the PC Arduino UNO from the PV Arduino Mega 2560 are displayed in this text box.
6. Displays commands that are sent to the PV Arduino Mega 2560 when buttons are clicked.
7. The button that is used to send data to an Excel sheet and save as a predetermined file name.

The export to Excel method is called after every 100 rows and when the user clicks the button. When this is done, an Excel file is created, named "ExportedFromDatGrid". The file is saved to the path specified that includes

the day's date and binary time format, which ensures a unique file name each time.

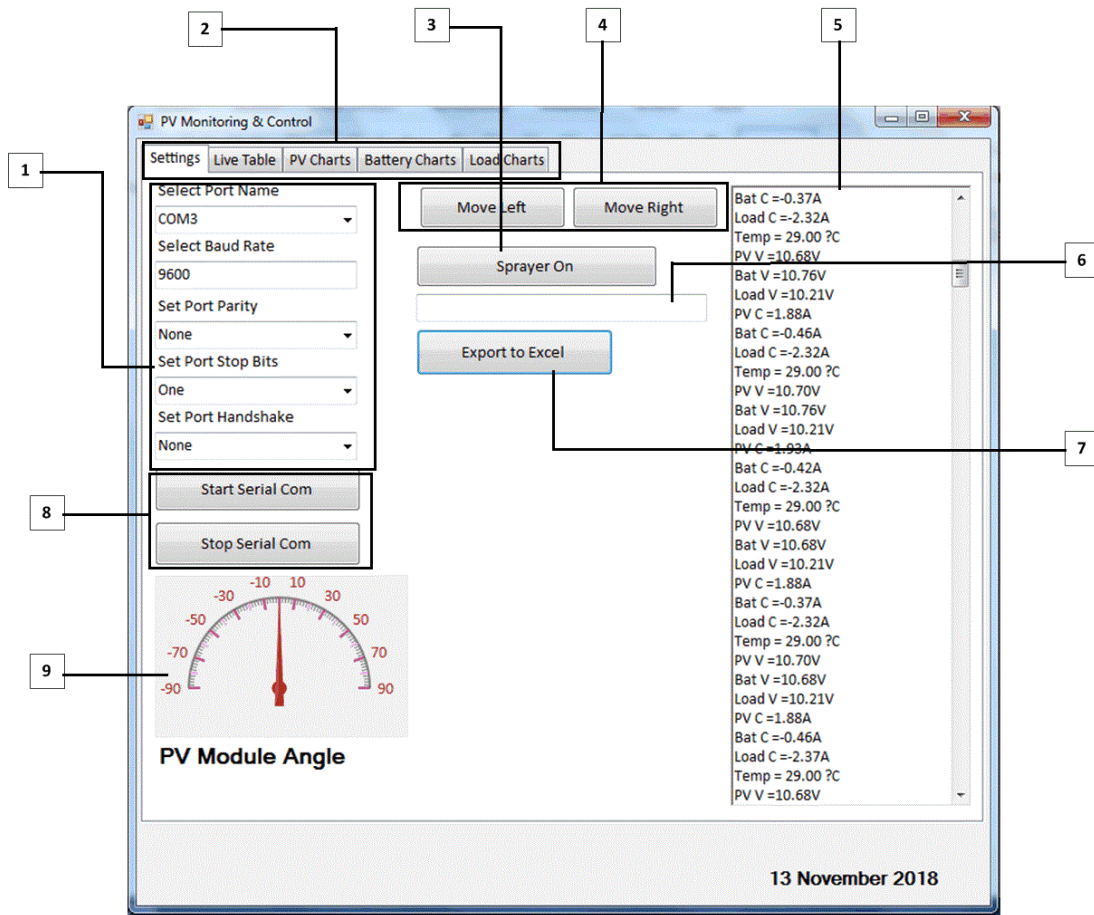


Figure 32: User interface

8. Buttons used to either start or stop serial communication between the PC Arduino UNO and the PV Arduino Mega 2560.
9. Displays the real time orientation angle of the PV module. This is programmed to adjust and display the orientation angle as the actuator adjusts. When a mechanism to move the PV Module is included, sensors that measure the angle can be included and feedback to the gauge. An error detection method can then be developed to detect any accumulated errors.

3.3 Practical setup

Having presented the various parts of the system and how they all fit together in the

previous sections, a visual representation of how they link is given in the form of the block diagram in Figure 33. Block 1 is the PC transceiver of the system where the CC1101 RF transceiver is connected to the PC via the Arduino UNO, using the USB cable. Block 2 is the PV transceiver where the Arduino Mega 2560 connects the CC1101 RF transceiver, block 3 and block 4 to make the slave transceiver board.

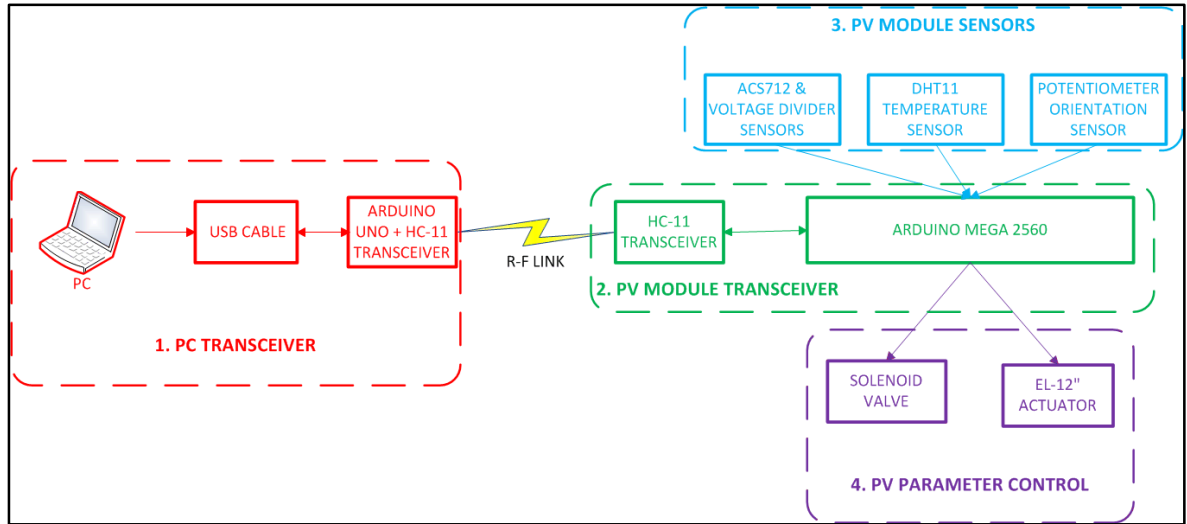


Figure 33: Block diagram of practical set-up

Block 3 shows how the PV parameters are obtained with the different sensors. The ACS712 current sensors are used to obtain the current through the PV module, the battery and the load. Voltage dividers are used to sense the voltage across the PV module, battery and load. For the temperature measurements, the DHT11 is used and the potentiometer is used to obtain the orientation angle. Block 4 is where the solenoid valve activates the water sprayer and the EL-12” actuator is used to adjust the orientation angle of the PV module. Block 2 sends the measurements from the sensors through the CC1101 transceiver and it also receives commands from block 1 to control the water sprayer and the actuator.

3.4 Summary

A method of measuring data from the PV module using sensors was presented for the purpose of controlling the temperature and orientation angle of a PV module. The Arduino UNO and Arduino Mega 2560 were linked and programmed to the sensors and CC1101 transceivers were used to establish the remote communication. This wireless

data transfer was implemented for transmitting data to and from the remote system, using a tailor-made user interface, designed using C-Sharp. A combination of these technologies and designs enabled a fully operational system that measures and controls specific PV parameters for remote PV systems, using a RF link. The next chapter gives the analysis and discussion of the results.

Chapter 4 Test and results

4.1 Introduction

The design and implementation of a PV monitoring and control system were discussed in the previous chapter. In addition, pictures of the practical setup were presented to elaborate on the operation of the system and how the sensors are used to collect the relevant data. The sections that follows present experimental results collected, using the practical setup coupled with the interpretation thereof. The Graphical User Interface used to interact with the PC transceiver, will be shown with its different functions. Following which, the PV module voltage and current measurements for cloudy and non-cloudy days will be presented. The PV module surface temperature is also one of the parameters that were recorded that will be shown in this chapter. In addition, evidence of electronic control of the water sprayer and orientation angle will be presented, which excludes their impact on the performance of the PV module. Lastly, the battery profile showing the voltage and current of the battery in the practical setup, will be shown.

4.2 Graphical User Interface (GUI)

The Graphical User Interface (GUI) forms part of block 1 of the practical setup that was presented in Figure 33 of chapter 3. The GUI, named PV monitoring and control, was designed to initiate communication between the master transceiver board on the user / computer side (PC transceiver) and slave transceiver board on the PV module side (PV module transceiver) where the sensors collect data. The PV module transceiver is powered by the battery on site. Visual Studio's C# platform was used to create the GUI and for communication between the two RF transceivers. Figure 34 shows the serial port settings required to establish connection for transmitting and receiving data. These are the user selected port name, the pre-set baud rate, the user selected port parity, stop bits and handshake. In addition, the instantaneous orientation angle of the PV module and measurements of the different parameters of the PV module, battery and the load can be observed once communication has been established. Figure 35 shows how the measurements are placed in the live table with headers as they are received.

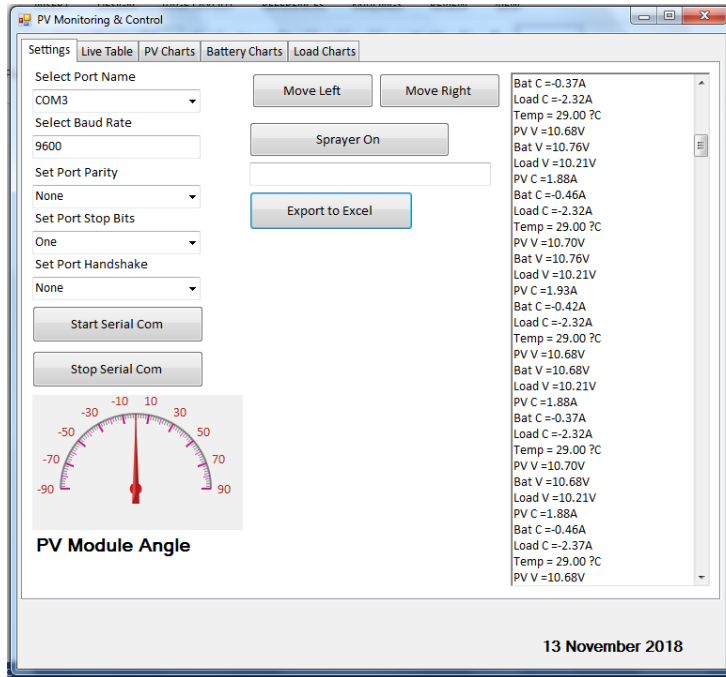
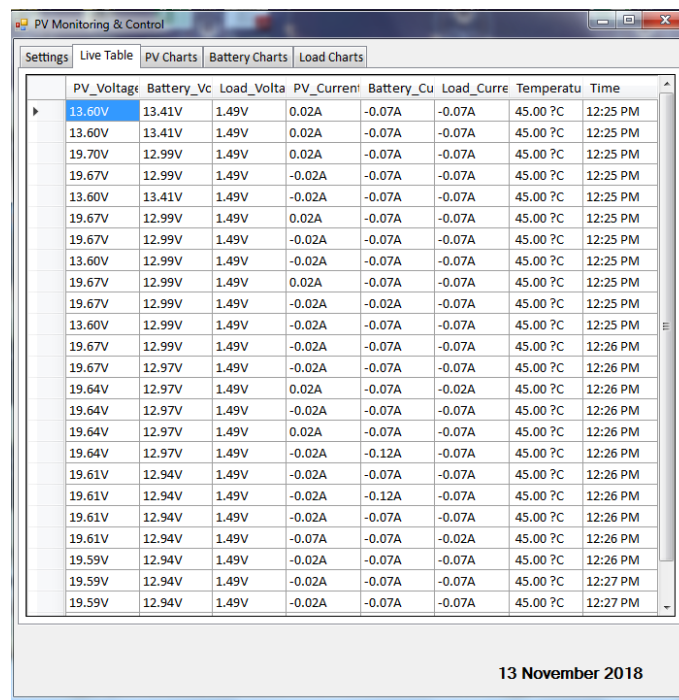


Figure 34: Tab 1 of the GUI: settings



	PV_Voltage	Battery_Vc	Load_Volts	PV_Current	Battery_Cu	Load_Curre	Temperatu	Time
▶	13.60V	13.41V	1.49V	0.02A	-0.07A	-0.07A	45.00 °C	12:25 PM
	13.60V	13.41V	1.49V	0.02A	-0.07A	-0.07A	45.00 °C	12:25 PM
	19.70V	12.99V	1.49V	0.02A	-0.07A	-0.07A	45.00 °C	12:25 PM
	19.67V	12.99V	1.49V	-0.02A	-0.07A	-0.07A	45.00 °C	12:25 PM
	13.60V	13.41V	1.49V	-0.02A	-0.07A	-0.07A	45.00 °C	12:25 PM
	19.67V	12.99V	1.49V	0.02A	-0.07A	-0.07A	45.00 °C	12:25 PM
	19.67V	12.99V	1.49V	-0.02A	-0.07A	-0.07A	45.00 °C	12:25 PM
	13.60V	12.99V	1.49V	-0.02A	-0.07A	-0.07A	45.00 °C	12:25 PM
	19.67V	12.99V	1.49V	0.02A	-0.07A	-0.07A	45.00 °C	12:25 PM
	19.67V	12.99V	1.49V	-0.02A	-0.07A	-0.07A	45.00 °C	12:25 PM
	13.60V	12.99V	1.49V	-0.02A	-0.07A	-0.07A	45.00 °C	12:25 PM
	19.67V	12.99V	1.49V	-0.02A	-0.07A	-0.07A	45.00 °C	12:26 PM
	19.67V	12.97V	1.49V	-0.02A	-0.07A	-0.07A	45.00 °C	12:26 PM
	19.64V	12.97V	1.49V	0.02A	-0.07A	-0.02A	45.00 °C	12:26 PM
	19.64V	12.97V	1.49V	-0.02A	-0.07A	-0.07A	45.00 °C	12:26 PM
	19.64V	12.97V	1.49V	0.02A	-0.07A	-0.07A	45.00 °C	12:26 PM
	19.61V	12.94V	1.49V	-0.02A	-0.07A	-0.07A	45.00 °C	12:26 PM
	19.61V	12.94V	1.49V	-0.02A	-0.12A	-0.07A	45.00 °C	12:26 PM
	19.61V	12.94V	1.49V	-0.02A	-0.07A	-0.07A	45.00 °C	12:26 PM
	19.61V	12.94V	1.49V	-0.07A	-0.07A	-0.02A	45.00 °C	12:26 PM
	19.59V	12.94V	1.49V	-0.02A	-0.07A	-0.07A	45.00 °C	12:26 PM
	19.59V	12.94V	1.49V	-0.02A	-0.07A	-0.07A	45.00 °C	12:27 PM
	19.59V	12.94V	1.49V	-0.02A	-0.07A	-0.07A	45.00 °C	12:27 PM

13 November 2018

Figure 35: Tab 2 of the GUI: live table

The measurements received by the PC transceiver from the PV module transceiver via the RF link are recorded in the live table according to these categories: PV voltage, battery voltage, load voltage, PV current, battery current, load current, temperature and

the time of receipt. These measurements received are also instantaneously displayed in graphical form in the GUI as seen in Figure 36, Figure 37 and Figure 38 for PV module, battery and load parameters respectively. The load connected to the system is a 12 V, 20 W LED flood light. The PV charts tab of Figure 36 displays the measurement in four graphs as they are received namely, PV voltage vs time, PV current vs time, PV surface temperature vs time.

PV power is also calculated and plotted vs time. PV voltage can be observed to be 10.70 V at 10:17 am with the PV current being 1.88 A, in turn producing 20.11 W of power when the load is switched on as seen in the PV power chart. The surface temperature of the PV module is recorded as 29°C at the same time and could be seen going up to 30°C at 10:19 am.

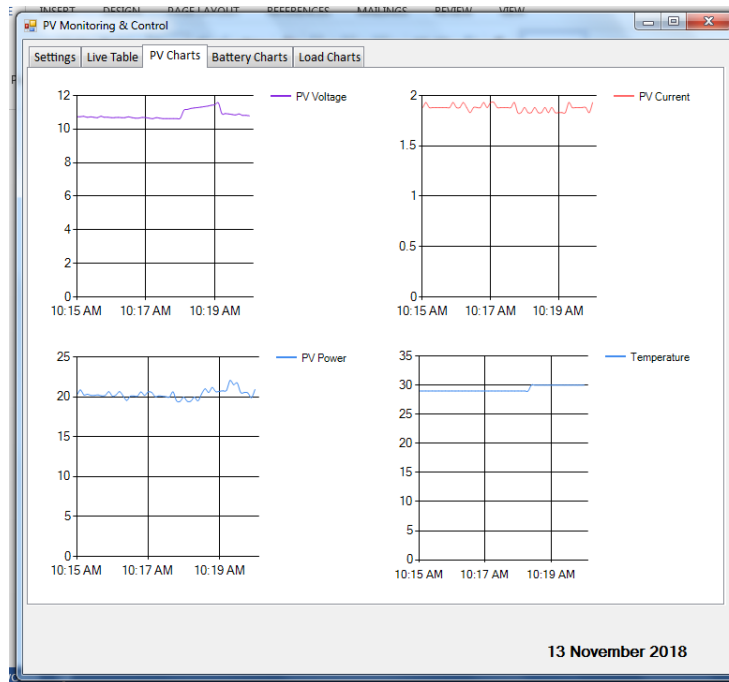


Figure 36: Tab 3 of the GUI: PV charts

The battery instantaneous profile can be seen in Figure 37 where the tab for battery charts is presented. The measurements of the battery parameters are plotted into three graphs as they are received; battery voltage vs time, battery current vs time; then the battery power is calculated and plotted. The battery voltage is measured as 11.23 V and battery current as 1.74 A for 10:18 am. The last tab seen in Figure 38 of the GUI shows the load charts.

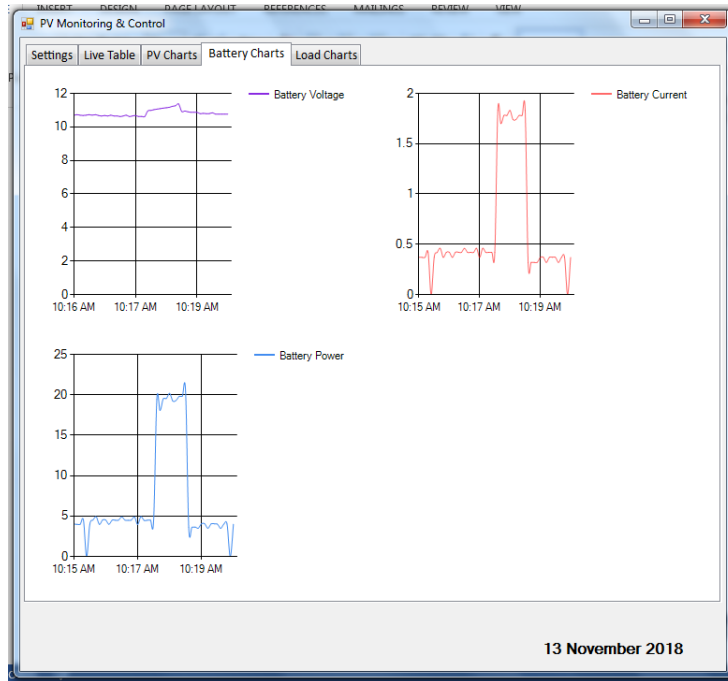


Figure 37: Tab 4 of the GUI: battery charts

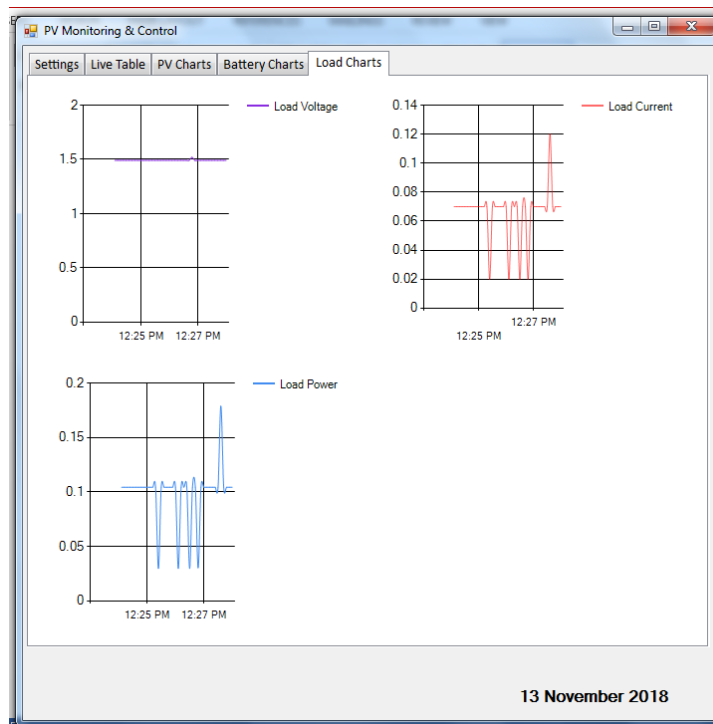


Figure 38: Tab 5 of the GUI: load charts

Load voltage vs time, load current vs time and the calculated load power can be viewed in this tab. In this instance, the load is switched off as can be seen in Figure 38 where

the instantaneous load charts are shown. The load is switched off automatically at pre-set conditions of the solar charge regulator. When the load is switched off during the day, the load voltage indicates 1.49 V and the load current indicates 0.07 A at 12:25. These measurements at load off are negligible and not really significant and can be attributed to the self-consumption current of the regulator (6 mA), the noise sensed and the percentage error that is calculated in the following sections. The measured PV voltage is 19.67 V and PV current is 0.02 A. There is no current conducting path for the PV module and as such the PV Voltage is almost equal to the rated open circuit voltage of the PV module that is indicated in Table 7. This condition means that there is no significant power generated by the PV module. The table is then exported to an MS Excel document (as shown in Figure 39) and saved to a specific directory (as shown in Figure 40).

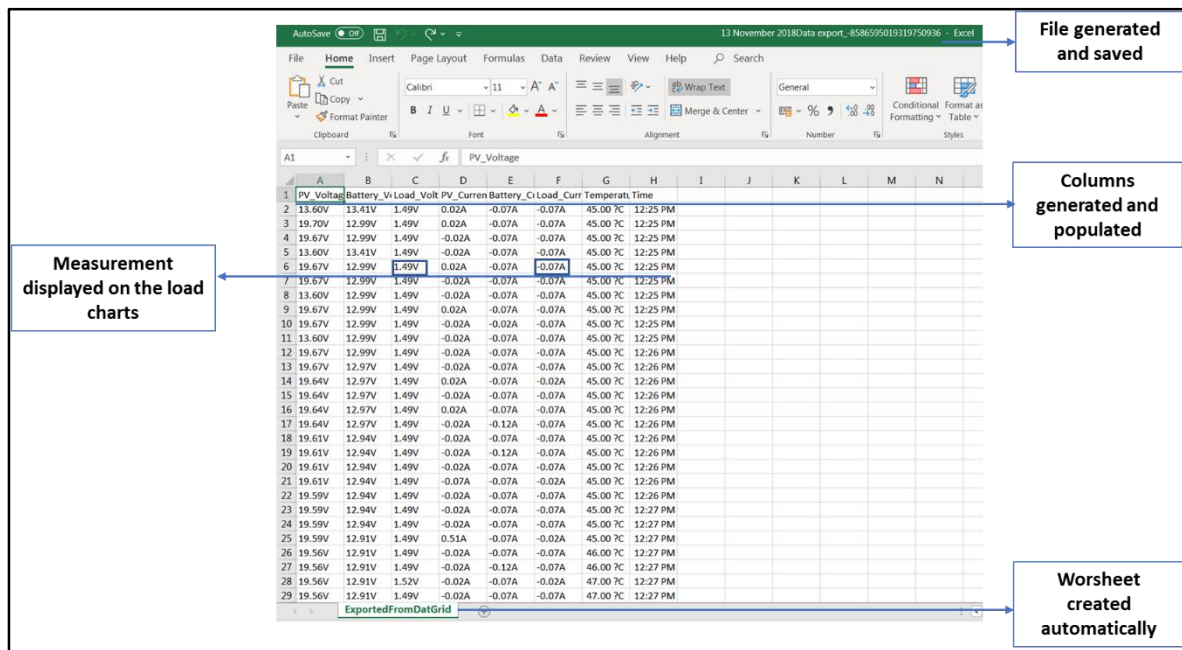


Figure 39: Excel document where data from GUI is saved

The live table is exported to an MS Excel workbook that is automatically created and saved in a pre-set location on the PC after every 100 records or the user can click the “Export to Excel” button at any point to save immediate measurements. The file name includes the date of the recordings and the time saved in binary to ensure that no file name duplications exist.

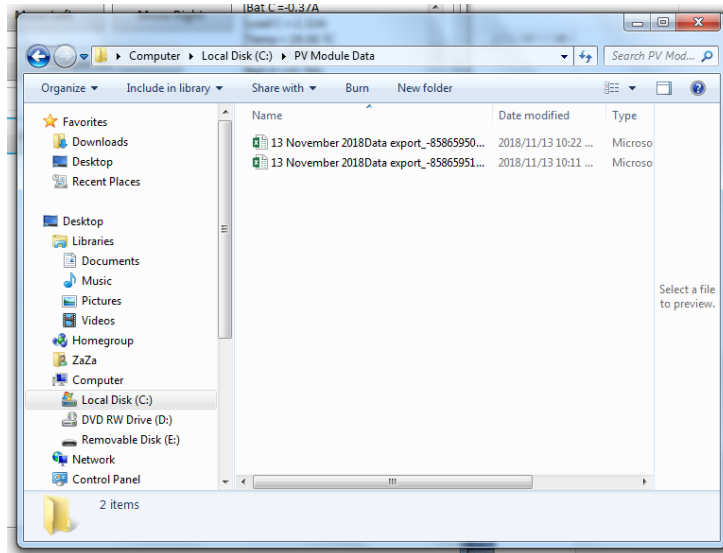


Figure 40: Directory where data is periodically saved

4.3 Experimental measurements and controls

A block diagram of where the measurements were acquired on the practical setup is shown in Figure 41. The PV module, battery and 12 V LED flood light were connected to the programmable solar charge controller. The PV voltage and current were measured between the charge controller and the PV module. The battery voltage and current measurements were acquired between the battery and the charge controller.

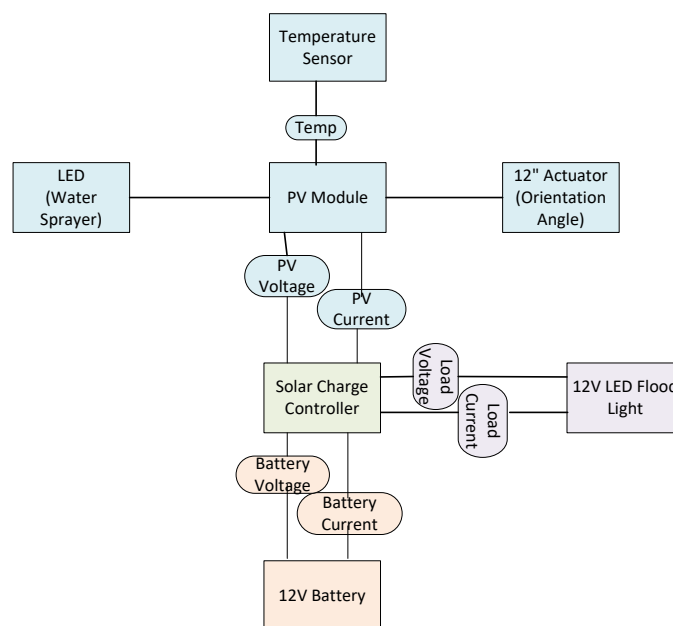


Figure 41: Block diagram of the acquired measurements

The load voltage and current measurements were taken between the LED flood light and the charge controller. The temperature (Temp) is a measurement of the PV module surface temperature and was obtained from the sensor that was attached to the back of the PV module. The switching on and off of the LED was used to demonstrate the control of the water sprayer that might be used to spray water on to the PV module in order to cool it off. In addition, the actuator was used to demonstrate the control of the orientation angle by means of extending or retracting the actuator. The mechanical structure used to adjust the orientation angle of the PV module and the measurement of the orientation angle did not form part of this research study.

4.3.1 PV module voltage and current measurements verified by DMM

Experimental results are presented here for different weather conditions with the load connected. The SD eco plus 10 W PV module was used with the rated parameters shown in Table 7 that are obtained under Standard Testing Conditions (STC). Four of these modules were connected in parallel, giving the expected parameters of Table 7.

Table 7: PV module parameters

STC parameters for one PV module	STC parameters for four PV modules in parallel
I_{mp} (maximum power current) = 0.61 A	$I_{mp} = 2.44$ A
V_{mp} (maximum power voltage) = 16.5 V	$V_{mp} = 16.5$ V
I_{sc} (short circuit current) = 0.78 A	$I_{sc} = 3.12$ A
V_{oc} (open circuit voltage) = 20.8 V	$V_{oc} = 20.8$ V
Peak Power = 10 W	Peak Power = 40 W

A Fluke 115 digital multimeter (DMM) was used to verify the voltage and current measurements from the voltage divider and ACS712 sensors on the PV module transceiver. In

	D	F	H	I	J	K	L	M	N
1	Date	Time	PV V	Bat V	Load V	PV C	Bat C	Load C	Temp
419	27 Sep	12:55:41 PM	13.71	12.76	0.47	1.54	1.25	-0.17	41
420	27 Sep	12:57:21 PM	13.69	12.76	0.47	1.54	1.25	-0.17	41
421	27 Sep	01:00:42 PM	13.69	12.76	3.85	1.44	1.2	-0.12	38
422	27 Sep	01:02:23 PM	13.69	12.71	3.8	1.44	1.2	-0.12	38
423	27 Sep	01:04:03 PM	13.66	12.76	3.66	1.44	1.25	-0.12	37
424	27 Sep	01:05:44 PM	13.69	12.76	3.41	1.44	1.25	-0.12	37
425	27 Sep	01:07:24 PM	13.69	12.74	3.1	1.44	1.25	-0.17	37
426	27 Sep	01:09:05 PM	13.71	12.76	2.63	1.44	1.2	-0.12	35
427	27 Sep	01:10:46 PM	13.71	12.76	3.32	1.44	1.2	-0.17	34
428	27 Sep	01:12:26 PM	13.69	12.74	3.57	1.39	1.2	-0.17	34
429	27 Sep	01:14:07 PM	13.57	12.68	3.49	1.3	1.05	-0.17	34
430	27 Sep	01:17:28 PM	13.35	12.6	2.93	1.15	0.9	-0.42	33
431	27 Sep	01:19:08 PM	13.29	12.57	2.51	1.05	0.81	-0.12	34
432	27 Sep	01:20:49 PM	13.29	12.57	2.51	1.05	0.81	-0.12	34
433	27 Sep	01:22:29 PM	13.27	12.51	1.98	1	0.76	-0.12	33
434	27 Sep	01:24:10 PM	13.24	12.54	2.4	0.95	0.81	-0.12	32
435	27 Sep	01:25:50 PM	13.24	12.51	3.66	0.95	0.81	-0.12	32
436	27 Sep	01:27:31 PM	13.24	12.51	3.77	0.95	0.81	-0.17	32
437	27 Sep	01:29:11 PM	13.24	12.51	3.04	0.9	0.76	-0.07	32
438	27 Sep	01:30:52 PM	13.24	12.51	3.04	0.9	0.76	-0.07	32
439	27 Sep	01:32:32 PM	13.18	12.51	2.18	1	0.81	-0.07	32
440	27 Sep	01:34:13 PM	13.21	12.54	3.07	0.95	0.76	-0.17	32
441	27 Sep	01:35:53 PM	13.24	12.51	3.66	0.95	0.76	-0.12	32
442	27 Sep	01:39:14 PM	13.21	12.51	3.66	0.95	0.76	-0.12	32
443	27 Sep	01:40:55 PM	13.21	12.51	3.32	0.95	0.76	-0.12	32
444	27 Sep	01:45:56 PM	13.18	12.51	3.8	0.95	0.76	-0.12	32
445	27 Sep	01:47:37 PM	13.21	12.51	2.09	0.95	0.76	-0.12	32
446	27 Sep	01:50:58 PM	13.18	12.51	0.34	0.9	0.61	-0.07	31

Figure 42, a spreadsheet of sensor measurements obtained from the PV module transceiver for 27 September 2019 is observed, where a voltage and current reading was compared to a DMM voltage reading in and a DMM current reading in Figure 43.

	D	F	H	I	J	K	L	M	N
1	Date	Time	PV V	Bat V	Load V	PV C	Bat C	Load C	Temp
419	27 Sep	12:55:41 PM	13.71	12.76	0.47	1.54	1.25	-0.17	41
420	27 Sep	12:57:21 PM	13.69	12.76	0.47	1.54	1.25	-0.17	41
421	27 Sep	01:00:42 PM	13.69	12.76	3.85	1.44	1.2	-0.12	38
422	27 Sep	01:02:23 PM	13.69	12.71	3.8	1.44	1.2	-0.12	38
423	27 Sep	01:04:03 PM	13.66	12.76	3.66	1.44	1.25	-0.12	37
424	27 Sep	01:05:44 PM	13.69	12.76	3.41	1.44	1.25	-0.12	37
425	27 Sep	01:07:24 PM	13.69	12.74	3.1	1.44	1.25	-0.17	37
426	27 Sep	01:09:05 PM	13.71	12.76	2.63	1.44	1.2	-0.12	35
427	27 Sep	01:10:46 PM	13.71	12.76	3.32	1.44	1.2	-0.17	34
428	27 Sep	01:12:26 PM	13.69	12.74	3.57	1.39	1.2	-0.17	34
429	27 Sep	01:14:07 PM	13.57	12.68	3.49	1.3	1.05	-0.17	34
430	27 Sep	01:17:28 PM	13.35	12.6	2.93	1.15	0.9	-0.42	33
431	27 Sep	01:19:08 PM	13.29	12.57	2.51	1.05	0.81	-0.12	34
432	27 Sep	01:20:49 PM	13.29	12.57	2.51	1.05	0.81	-0.12	34
433	27 Sep	01:22:29 PM	13.27	12.51	1.98	1	0.76	-0.12	33
434	27 Sep	01:24:10 PM	13.24	12.54	2.4	0.95	0.81	-0.12	32
435	27 Sep	01:25:50 PM	13.24	12.51	3.66	0.95	0.81	-0.12	32
436	27 Sep	01:27:31 PM	13.24	12.51	3.77	0.95	0.81	-0.17	32
437	27 Sep	01:29:11 PM	13.24	12.51	3.04	0.9	0.76	-0.07	32
438	27 Sep	01:30:52 PM	13.24	12.51	3.04	0.9	0.76	-0.07	32
439	27 Sep	01:32:32 PM	13.18	12.51	2.18	1	0.81	-0.07	32
440	27 Sep	01:34:13 PM	13.21	12.54	3.07	0.95	0.76	-0.17	32
441	27 Sep	01:35:53 PM	13.24	12.51	3.66	0.95	0.76	-0.12	32
442	27 Sep	01:39:14 PM	13.21	12.51	3.66	0.95	0.76	-0.12	32
443	27 Sep	01:40:55 PM	13.21	12.51	3.32	0.95	0.76	-0.12	32
444	27 Sep	01:45:56 PM	13.18	12.51	3.8	0.95	0.76	-0.12	32
445	27 Sep	01:47:37 PM	13.21	12.51	2.09	0.95	0.76	-0.12	32
446	27 Sep	01:50:58 PM	13.18	12.51	0.34	0.9	0.61	-0.07	31

Figure 42: PV voltage and current measurements verified using a DMM

The accuracy of the voltage and current sensor measurements was evaluated by calculating the percentage error between the sensor measurements and the DMM readings as follows:

$$\% \text{ error} = \frac{\text{sensor reading} - \text{DMM reading}}{\text{DMM reading}} \times 100 \quad 7$$

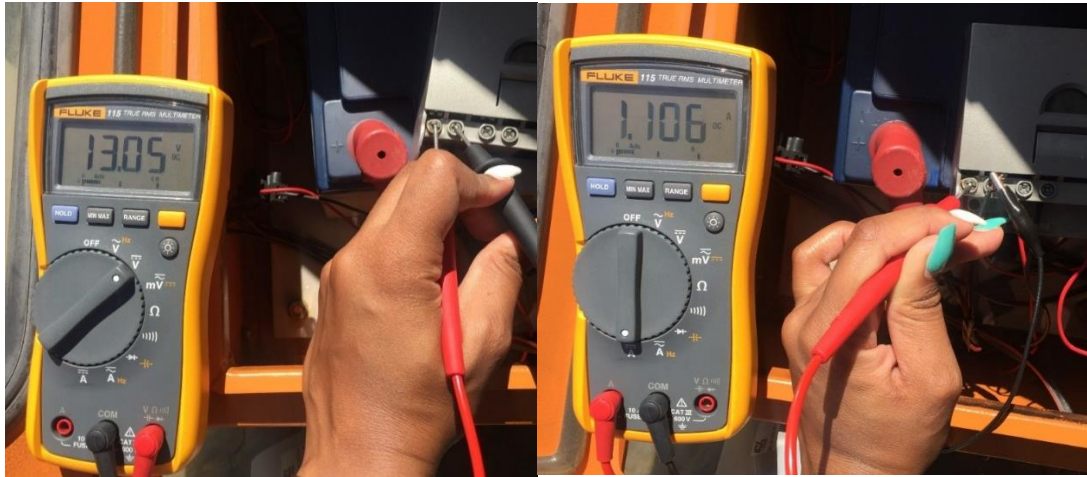


Figure 43: PV voltage and current DMM reading

The PV voltage of 13.69 V from the PV module transceiver and 13.05 V from the DMM were used in equation 7 to give an error percentage of 4.9%. In addition, the error percentage for the current reading was calculated using the PV current of 1.15 A from the PV module transceiver and 1.106 A from the DMM, giving a value of 3.9%. A percentage error of between -10% and +10% has been found to be acceptable for these type of measurements (Ertekin & Yaldiz, 2000).

4.3.2 Practical setup measurements of PV voltage and current over seven days

Measurement data was acquired every 100 seconds from the PV module transceiver via RF using the PC transceiver continually for a period of seven days. The data stored by the GUI was processed using pivot tables and summarized to hourly maximums. A closer look at the daily performance shows hourly maximum PV currents for a sunny day on site (Figure 44) and for a cloudy day (Figure 45). The measurements reflect the maximum current drawn from the PV module as 2.32 A at 11 am for the sunny day.

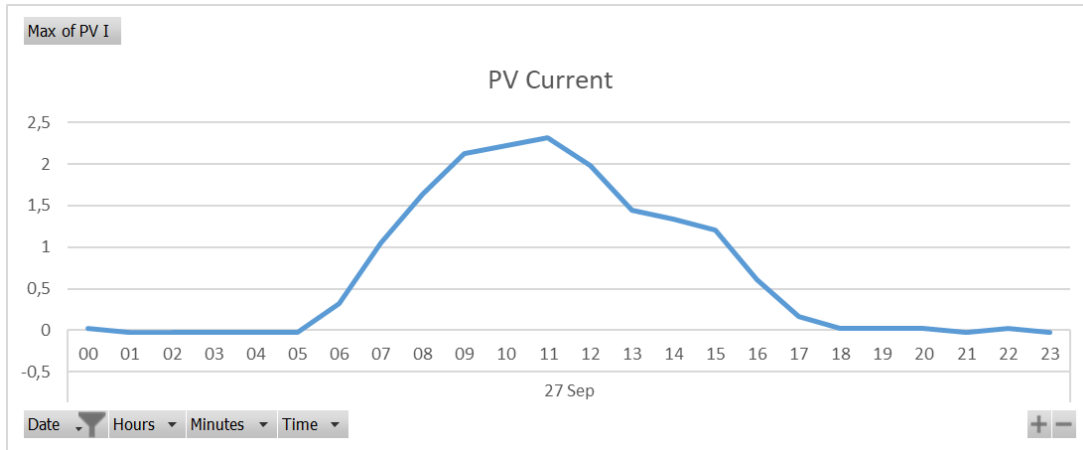


Figure 44: Hourly maximum of PV current for 27 September 2019 (Sunny day)

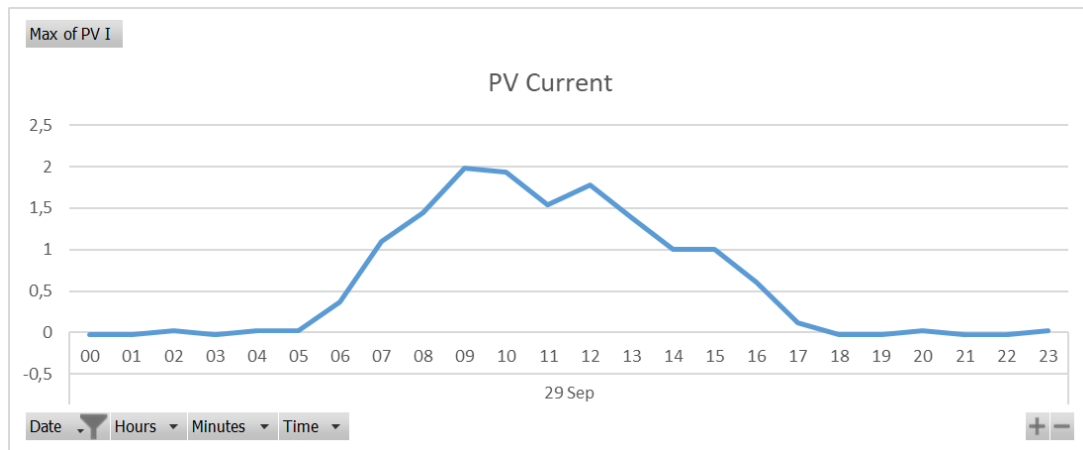


Figure 45: Hourly maximum of PV current for 29 September 2019 (Cloudy day)

Figure 45 shows hourly maximum PV currents for a cloudy day on site where the measurements reflect the maximum current drawn from the PV module as 1.98 A at 11 am. Both currents are less than $I_{mp} = 2.44$ A, suggesting that the measurement process is satisfactory.

Voltage and current daily maximum measurements of the PV module and the battery from 24 September to 30 September are shown in Table 8. The load was switched on between 24 and 28 September and manually switched off on 29 and 30 September. The solar charge controller’s Low Voltage Disconnect function (LVD) mode 3 was also used, where it disconnects at a battery voltage of 11.0 to 12.2 V, depending on the load and previous charging cycles.

Table 8: Maximum measurements when the load is switched on and off

Day	Max of PV V	Max of PV I	Max of PV Power	Max of Bat V	Max of Bat I	Max of Load V	Max of Load I
24 Sep	12,76	2,42	21,66	12,23	2,03	11,51	2,42
25 Sep	12,96	2,42	21,58	12,4	1,74	11,48	2,42
26 Sep	13,32	2,27	23,52	12,76	1,93	11,73	2,52
27 Sep	13,8	2,32	27,07	12,96	2,37	12,01	2,42
28 Sep	13,6	2,43	24,52	12,74	2,13	11,98	2,57
29 Sep	14,63	1,98	28,65	13,32	1,78	1,06	0,17
30 Sep	15,44	2,27	28,81	13,94	2,08	1,76	0,22

The daily PV voltage curve for the period above is presented in Figure 46 where the voltage can be observed to be higher for the days where the load is switched off. The PV module terminal voltage reaches 13.8 V when the load is on. When the load is switched off by the solar charge controller, the battery then acts as a load and draws current from the PV module. The terminal voltage the PV module, in this case, reaches 15.44 V when the LED load is switched off and the battery is charging. Both values of PV voltage are less than the rated V_{mp} of 16.5 V, which indicates that the process of measuring is satisfactory. In addition, the rated peak power for these modules is 40 W, which is supported by the data of Table 8 where the daily maximum power generated does not exceed 40 W. The highest PV power recorded for 29 September was 28.65 W, for which the load was off and the battery was charging. The highest PV power for 24 September is 21.66 W where the load was switched on.

Hourly maximum measurements of PV voltage for 24 September show a maximum of 12.76 V at 12 pm. Hourly maximum PV voltage for 27 September show a maximum of 13.8 V at 10 am. The maximum terminal voltage of the PV module is less than the rated $V_{mp} = 16.5$ V throughout the presented period.

Daily maximum PV current is presented in Figure 47 from 24 to 30 September. The diagram shows that the maximum current recorded was less than the rated $I_{mp} = 2.44$ A

for the said period. The highest maximum PV current is 2.43 A on 28 September and the lowest recorded maximum PV current 1.98 A on 29 September.

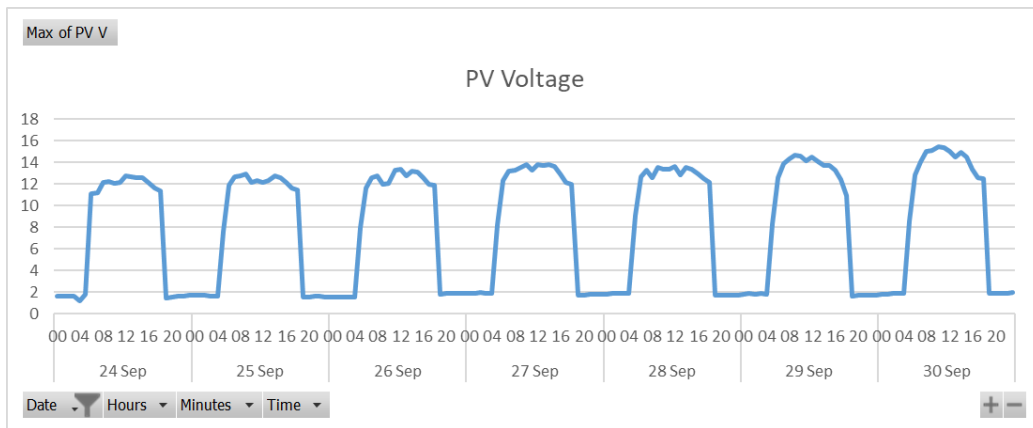


Figure 46: Hourly maximum of PV voltage from 24 to 30 September 2019

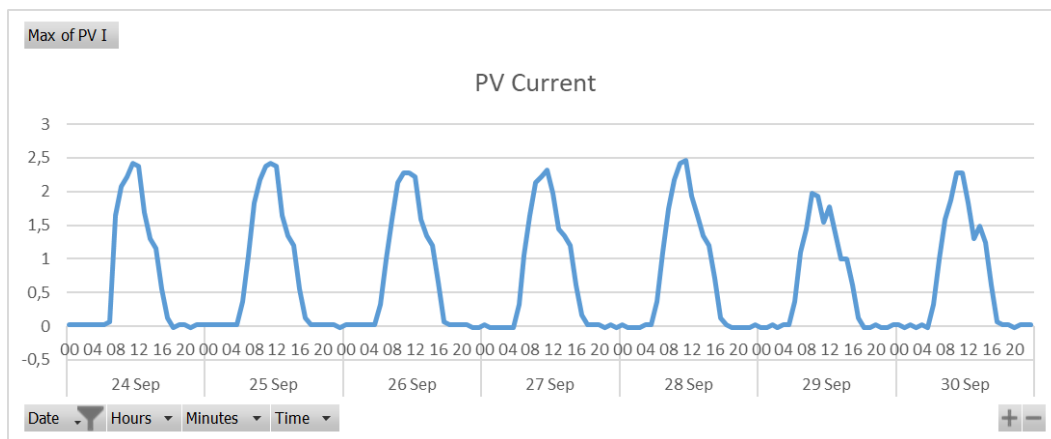


Figure 47: Hourly maximum of PV current from 24 to 30 September 2019

4.3.3 Battery charge and discharge data

In this section, the battery profile for 30 September 2019 is presented where Figure 48 displays the hourly maximum battery voltage and Figure 49 shows the hourly maximum battery current. An increase in the battery voltage can be observed from 6 am to 11 am from a starting voltage of 11.98 V to 13.94 V at 11 am in Figure 48. From then on, the battery voltage is observed to slowly decrease to a voltage of 12.29 V from 11 am, due to the decrease in charging current that is observed in Figure 49. The measurements show that the battery current increases from sunrise till midday, after which, it starts to decrease until sunset.

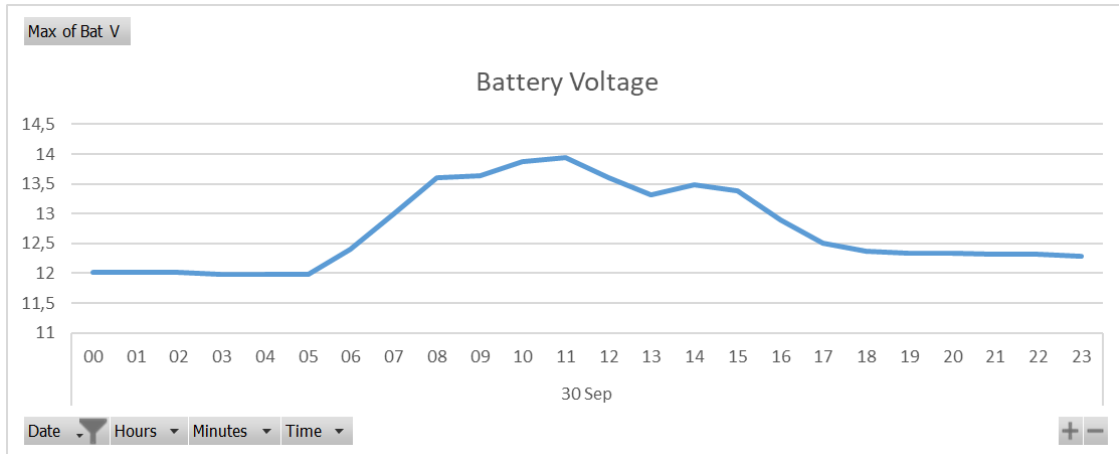


Figure 48: Hourly maximum battery voltage for 30 September 2019

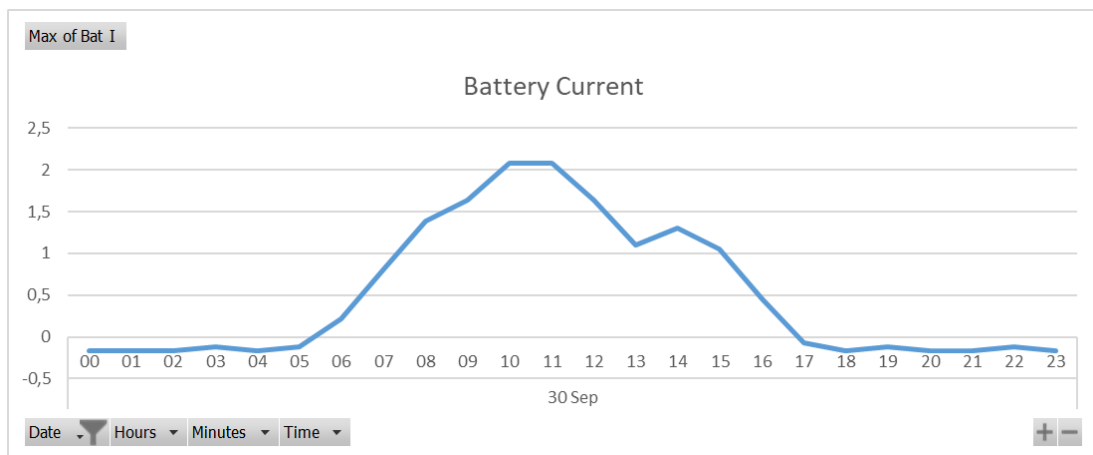


Figure 49: Hourly maximum battery current for 30 September 2019

4.3.4 PV module surface temperature verified by DMM

The measurements from the DHT11 sensor were verified using the Fluke 179 digital multimeter (DMM). The sensor measurement of 34 °C in Figure 50 was judged against the DMM reading of 33.8 °C seen in Figure 51, demonstrating how the DMM was used to verify temperature measurements. The percentage error was then calculated using equation 7 arriving at an error percentage of 0.59%, indicating that the measurements from the sensor are acceptable.

	D	F	H	I	J	K	L	M	N
1	Date	Time	PV V	Bat V	Load V	PV C	Bat C	Load C	Temp
419	27 Sep	12:55:41 PM	13.71	12.76	0.47	1.54	1.25	-0.17	41
420	27 Sep	12:57:21 PM	13.69	12.76	0.47	1.54	1.25	-0.17	41
421	27 Sep	01:00:42 PM	13.69	12.76	3.85	1.44	1.2	-0.12	38
422	27 Sep	01:02:23 PM	13.69	12.71	3.8	1.44	1.2	-0.12	38
423	27 Sep	01:04:03 PM	13.66	12.76	3.66	1.44	1.25	-0.12	37
424	27 Sep	01:05:44 PM	13.69	12.76	3.41	1.44	1.25	-0.12	37
425	27 Sep	01:07:24 PM	13.69	12.74	3.1	1.44	1.25	-0.17	37
426	27 Sep	01:09:05 PM	13.71	12.76	2.63	1.44	1.2	-0.12	35
427	27 Sep	01:10:46 PM	13.71	12.76	3.32	1.44	1.2	-0.17	34
428	27 Sep	01:12:26 PM	13.69	12.74	3.57	1.39	1.2	-0.17	34
429	27 Sep	01:14:07 PM	13.57	12.68	3.49	1.3	1.05	-0.17	34
430	27 Sep	01:17:28 PM	13.35	12.6	2.93	1.15	0.9	-0.12	33
431	27 Sep	01:19:08 PM	13.29	12.57	2.51	1.05	0.81	-0.12	34
432	27 Sep	01:20:49 PM	13.29	12.57	2.51	1.05	0.81	-0.12	34
433	27 Sep	01:22:29 PM	13.27	12.51	1.98	1	0.76	-0.12	33
434	27 Sep	01:24:10 PM	13.24	12.54	2.4	0.95	0.81	-0.12	32
435	27 Sep	01:25:50 PM	13.24	12.51	3.66	0.95	0.81	-0.12	32
436	27 Sep	01:27:31 PM	13.24	12.51	3.77	0.95	0.81	-0.17	32
437	27 Sep	01:29:11 PM	13.24	12.51	3.04	0.9	0.76	-0.07	32
438	27 Sep	01:30:52 PM	13.24	12.51	3.04	0.9	0.76	-0.07	32
439	27 Sep	01:32:32 PM	13.18	12.51	2.18	1	0.81	-0.07	32
440	27 Sep	01:34:13 PM	13.21	12.54	3.07	0.95	0.76	-0.17	32
441	27 Sep	01:35:53 PM	13.24	12.51	3.66	0.95	0.76	-0.12	32
442	27 Sep	01:39:14 PM	13.21	12.51	3.66	0.95	0.76	-0.12	32
443	27 Sep	01:40:55 PM	13.21	12.51	3.32	0.95	0.76	-0.12	32
444	27 Sep	01:45:56 PM	13.18	12.51	3.8	0.95	0.76	-0.12	32
445	27 Sep	01:47:37 PM	13.21	12.51	2.09	0.95	0.76	-0.12	32
446	27 Sep	01:50:58 PM	13.18	12.51	0.34	0.9	0.61	-0.07	31

PV Surface Temperature verified by DMM (33.8°C)

Figure 50: PV module surface temperature measurements verified by DMM



Figure 51: PV module surface temperature DMM reading

4.3.5 Practical setup measurement of PV surface temperature over 29 days

Figure 52 reflects hourly maximum PV surface temperature measurements for a cloudy day. The maximum surface temperature for 29 September 2019 is recorded as 39°C at 09:00 am. Figure 53 reflects hourly maximum PV surface temperature measurements for a sunny day. The maximum surface temperature for 27 September 2019 is recorded as 54°C at 12:00 pm.

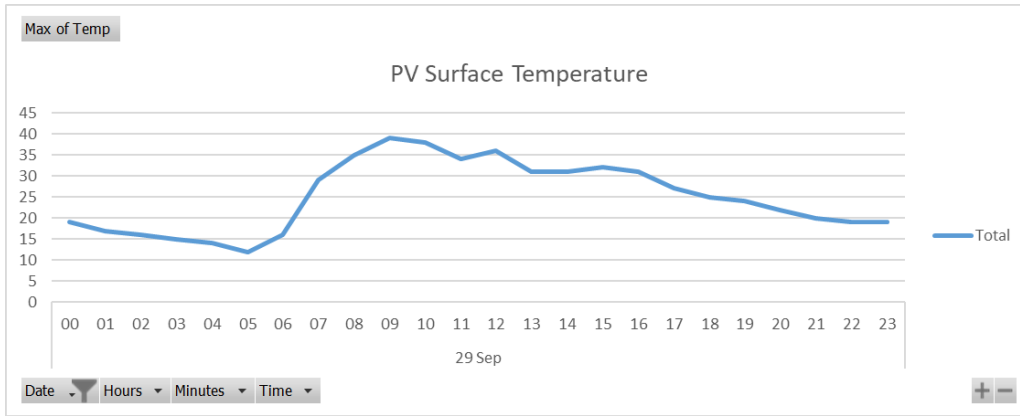


Figure 52: Hourly maximum of PV module surface temperature for 29 September 2019

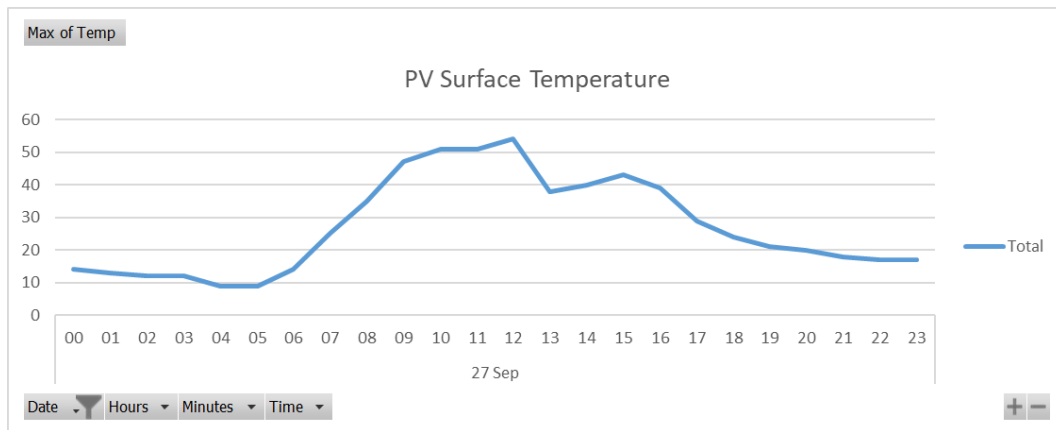


Figure 53: Hourly maximum of PV module surface temperature for 27 September 2019

Daily maximum and minimum PV surface temperature (T_{PV}) data from the DHT11 sensor is presented in Table 9, together with the daily maximum and minimum ambient temperature (T_a) data for Bloemfontein in South Africa, obtained from timeanddate.com (Time and Date, 2020). The T_a data available from the website is given in maximum and minimum for 00:00, 06:00, 12:00 and 18:00 for any required day. The available maximum and minimum T_a was then captured and processed, using pivot tables where daily maximum and minimum T_a were obtained. The T_{PV} data was sampled every 100 seconds from 19 July to 16 August 2019, where the highest surface temperature was recorded to be 55°C on 14 August. Pivot tables were used - due to the sheer quantity of data that had to be analysed - to determine the hourly maximum and

minimum T_{PV} values per day, and from those a daily maximum and minimum T_{PV} was derived.

Table 9: 29-day temperature data

Date	Max of T_{PV}	Max of T_a	Min of T_{PV}	Min of T_a
19 Jul	47	19	4	-2
20 Jul	48	12	3	0
21 Jul	39	15	3	-6
22 Jul	39	18	3	-4
23 Jul	38	22	4	0
24 Jul	48	12	4	-1
25 Jul	45	19	3	-5
26 Jul	48	23	4	-2
27 Jul	45	22	5	-1
28 Jul	51	22	6	-1
29 Jul	48	23	5	-1
30 Jul	45	22	5	-1
31 Jul	54	19	4	-1
1 Aug	40	22	4	-4
2 Aug	35	23	7	5
3 Aug	35	22	9	6
4 Aug	45	24	8	2
5 Aug	41	24	9	6
6 Aug	51	22	5	-2
7 Aug	45	28	6	-1
8 Aug	45	20	6	0
9 Aug	52	19	3	0
10 Aug	37	22	6	2
11 Aug	34	20	11	7
12 Aug	51	19	4	-1
13 Aug	49	23	5	-2
14 Aug	55	22	5	-1
15 Aug	48	24	7	0
16 Aug	52	26	7	2
Average	45	21	5	0

4.4 Water sprayer control

The water sprayer which is meant to lower the surface temperature of the PV module is also controlled by the user from the GUI. The “Sprayer Off” button indicates the next state of the sprayer when the button is clicked, in Figure 55. The text box then displays the command ‘N’ that was sent to the PV module transceiver to turn on the LED; Figure 54 shows the illuminating LED (representing the water sprayer). When the “Sprayer Off” button is clicked, the text of the button is then changed to “Sprayer On”, after

which the command “F” is displayed in the text box and sent to the PV module transceiver that then switches off the LED (Figure 54), indicating that the command to turn off the water sprayer has been executed.



Figure 54: LED is turned on and off representing the water sprayer

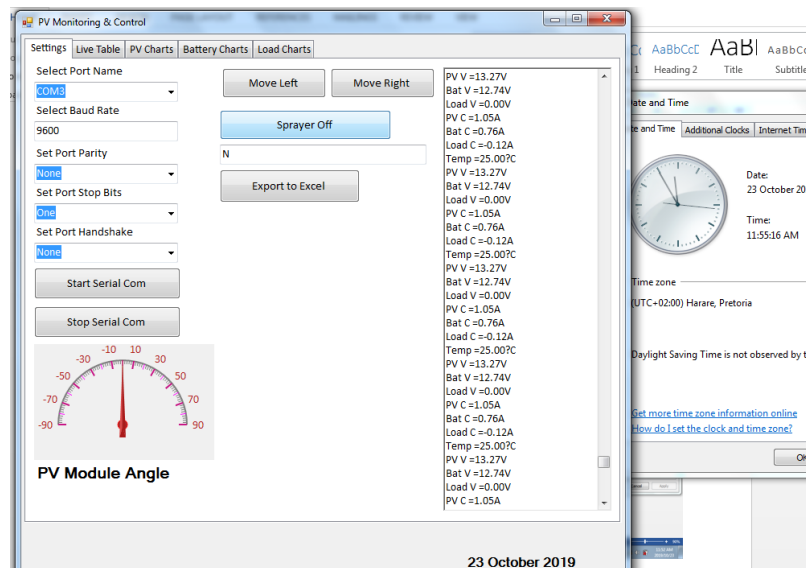


Figure 55: Sprayer on command to activate the water sprayer

4.5 PV Module orientation angle control

The orientation angle of the PV module would be controlled by an Eco link EL-12” Actuator that receives signals from the graphical user interface (GUI) via the RF link (Figure 57). As such, the control of the extension and retraction of the actuator is presented and not the measurement of the orientation angle itself. The mechanical structure and the measurement of the orientation angle does not form part of this research study. The initial position of the actuator is shown in Figure 56.



Figure 56: Actuator’s initial position

A single click of the “Move Left” button provides an extension of the actuator that would affect an adjustment of the orientation angle. A single click of the “Move Right” button however, results in the actuator being retracted to again achieve an adjustment of the orientation angle. The text box displays the command that is sent from the PC transceiver to the PV module transceiver, using the RF link to adjust the orientation angle back to the initial position of 90° ; the resulting action was the actuator being extended back to its initial position of 23 cm in Figure 56. In addition, the PV Module angle gauge displays the displacement of the orientation angle after executing either of the actuator commands. When either the “Move Left” or “Move Right” button is clicked, a command that is sent from the PC transceiver to the PV module transceiver using the RF link is displayed in the textbox of the GUI. In Figure 58, the actuator is observed to have retracted and extended by between three and four cm following the commands received from the GUI.

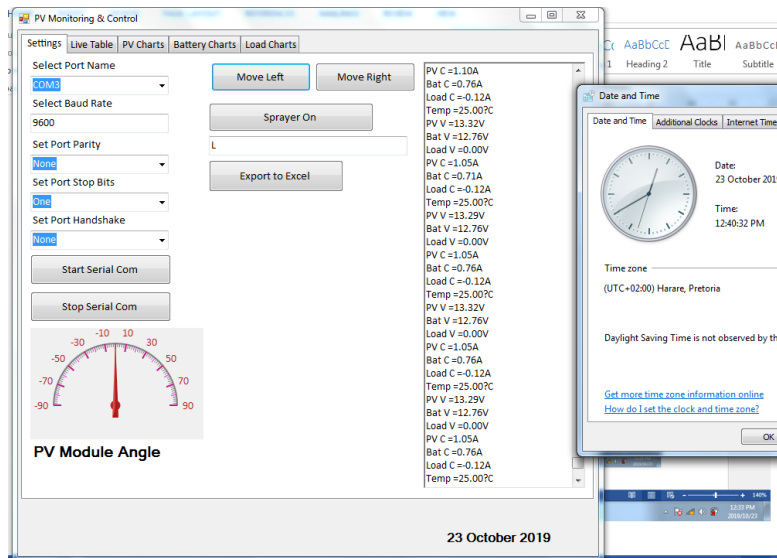


Figure 57: GUI: Move left command to get back to the initial position



Figure 58: Actuator retracted and extended to achieve 20 degrees

4.6 Summary

Data from measurements taken from the practical setup presented in Figure 17 of chapter 3 were shown in this chapter. The PV module voltage and current data were verified using the Fluke 115 DMM. The results showed a 4.9% error percentage for voltage measurements and a 3.9% error percentage for current measurements. Furthermore, a 29-day period of data for minimum and maximum T_{PV} were also presented and compared to the minimum and maximum T_a obtained from a weather website. T_{PV} was found to rise significantly higher than T_a during the day, indicating that there is considerable heating of the PV module when there is solar radiation. For low temperatures measured at night, T_{PV} and T_a are fairly similar. The relay of signals to control the orientation angle and the water sprayer were also presented, showing how

the actuator and the LED (representing the water sprayer) were controlled, using the RF link. The next chapter will present the conclusions drawn from the results, as well as possible recommendations.

Chapter 5 Conclusions and recommendations

5.1 Introduction

The previous chapter presented results of the practical setup. These results included voltage and current measurements of the PV module, battery and the load as well as the surface temperature measurements of the PV module. Evidence of the control of the water sprayer signals and the actuator was also offered. This chapter discusses how the research problem was solved and give conclusions drawn. Concise recommendations arising from the study is made.

5.2 Chapter overview

Chapter 1 gave the introduction of the research; it substantiated the research with a detailed background of the problem it aimed to resolve. It was proven that the operating temperature of a PV module must be kept within certain limits in order to obtain optimum electrical energy efficiency, depending on the model used. Measuring the instantaneous surface temperature, voltage and current of a PV module would enable the effective control of these parameters, in order to maintain a high output power. This chapter also presented six research objectives that had to be achieved and an overview of the dissertation. The success of this research could benefit the Telecommunications Industry as optimum operation of PV modules in remote locations may be maintained at all times without having personnel on site, contributing to a reduction in overall power consumption and maintenance costs associated with PV systems. The research, however, did not focus on the different types of PV modules, actuators or solenoid valves. The inclusion of an energy regulator and storage system also did not form part of the research. In addition, the incorporation of the mechanical mechanism to adjust the orientation angle was not considered. Lastly, only the relay of the signals for modifying the temperature and orientation angles of a PV module were considered, as their impact on the performance of a PV module have already been established.

Chapter 2 reviewed the literature available with regards to the research. It considered at length the effect of the surface temperature and the orientation angle of a PV module on its output power, and hence, its efficiency. A comparison of different methods of acquiring temperature and orientation angle measurements were investigated, along

with the use of radio frequency transceivers and microcontrollers for remote data acquisition.

Chapter 3 discussed the design and analysis of the practical setup. This part detailed what had to be measured, as well as how to interpret the measurements. Furthermore, voltage and current sensors were also employed to ensure effective monitoring of the output power. The PC transceiver of the system featured a CC1101 RF transceiver connected to the PC via an Arduino UNO using a USB cable. The PV transceiver featured an Arduino Mega 2560 connected to a CC1101 RF transceiver to make the slave transceiver board. Programming of the microcontroller also formed part of this chapter. The graphical user interface was developed for sending and receiving data between the PC transceiver and the PV transceiver.

Chapter 4 is where results were presented, analysed and interpreted. This mainly involved photographs of the operational system, as well as tables and graphs of the measured data. The method of verifying the measured data was shown arriving at the percentage error of 3.9% for current measurements and 4.9% for voltage measurements. The surface temperature measurements were also verified resulting in a percentage error of 0.59%.

5.3 Research objectives met

The primary objective of this research was to be able to remotely measure specific data, which could be used to make decisions regarding the cooling and orientation of a given PV module. This necessitated the following sub-objectives:

- Identifying a suitable microcontroller that will form the core of the data acquisition (DAQ) and control and the programming thereof.

Different microcontrollers for the processing and transfer of the obtained data were compared. The Arduino Uno R3 and Mega 2560 R3 were found to be ideal for the current application, the Uno for receiving measurements and sending controls at the PC transceiver and the Mega 2560 for data sensing and processing at the PV transceiver. The Arduino platform offered high modularity, guaranteeing a wide range of modules to interconnect with to meet many requirements for the data acquisition system. The

Mega 2560 boasts 54 I/O pins, which met the demand of the parameters to be detected. The two microcontrollers were the least expensive, and they also had extensive support on the internet, providing programming libraries and examples.

- Determining which temperature and orientation angle sensors will best suit the primary objective.

Semiconductor thermometers were identified as the most suitable sensors for this study, due to their linear nature that provides fast responses for real-time operations. The DHT11 digital temperature sensor was selected for detecting temperature for its ability to connect directly to the microcontroller with no need for complex circuitry, which contributed to the overall cost of the setup. Furthermore, a study done in South Africa showed PV module temperatures of around 50°C for a 200 W module (Ozemoya, Swart & Pienaar, 2014), which may readily be measured with this type of sensor. As such, for the PV surface temperature measurements, the DHT11 was used. The characteristics of the potentiometer, make it suitable for application to this study, given that the area of installation does not experience extreme temperatures and the orientation angles of interest would be limited to between 0° and 180°. These are also inexpensive and easy to use.

- Incorporating commands into the graphical user interface to control a 12 V actuator (controller) that could be used to vary the orientation angle for regulating the direct exposure of a PV module to the sun.

The control of the Eco Link EL 12” electric linear actuator that could be used to vary the orientation angle for regulating the direct exposure of a PV module to the sun, was successfully achieved by sending remote signals from the PC transceiver to the PV module transceiver that either extended or retracted the actuator using the GUI. A single click of the “Move Left” button provided an extension of three cm of the actuator. A single click of the “Move Right” button resulted in the actuator being retracted by four cm. These actuators added control of position and speed over stepper motors.

- Incorporating commands into the graphical user interface to control a 12 V water solenoid valve (controller), which could decrease the surface temperature of a PV module.

A water solenoid valve was not purchased. Instead remote signals from the PC transceiver were confirmed by switching on and off a LED at the PV module transceiver, which represented a solenoid valve that could be used to cool down the PV module should the need arise. This presented a method of controlling the surface temperature of the PV module.

- Developing a suitable data logging interface circuit for voltage conditioning between all sensors, controllers and the microcontroller.

Power measurements are equally important and different methods of obtaining them were explored. Voltage dividers were used to sense the voltage across the PV module, battery and load. They were used to reduce the sensed terminal voltage to a value low enough to be interfaced with the microcontroller that has a limited input voltage. This was a way to obtain higher voltage measurements that is non-complex and inexpensive, and is commonly used in PV data acquisition. ACS712 current sensors were used to obtain the current through the PV module, the battery and the load. These provided a precise voltage that is proportional to the sensed current. A data logging interface circuit was therefore designed and developed to successfully interface the PV module, battery and load with the microcontroller, as illustrated in section 3.2.2 of chapter 3. This circuit was named the slave transceiver board at the PV module transceiver and it harboured all the sensors and the RF transceiver itself.

- Establishing which RF transceiver will be used for wireless communication between the remote DAQ and the monitoring PC.

Specific features of the CC1101 highlighted in chapter 2 made these RF transceivers ideal tools of communication for the current research study. These include the open-air range of up to 500 m, coupled with high receiver sensitivity and high transmitter output power with minimal power consumption. The PV transceiver sent signals from the sensors through the CC1101 transceiver to the PC transceiver for processing and storage.

The synthesis of all these components has led to the development of an energy monitoring and control system where the output power and surface temperature of the PV module were monitored. Signals were relayed that would control the water solenoid

valve (if connected) and actuator, remotely using an RF link.

5.4 Solution to the problem statement

The problem statement, as laid out in the introduction chapter, reads as follows:

The output voltage, and subsequently output power, of a PV module reduce significantly with an increase in its surface temperature and with the misalignment of its orientation angle. Remotely measuring and controlling these two parameters in a cost-effective way proves challenging.

As such, the solution can be broken down into two major categories. First, remotely measuring the system parameters, in order to enable the decision-making process required to improve system performance. Secondly, remotely controlling the surface temperature and orientation angle of the PV module as a means to maintain the output power of the system.

5.4.1 Remotely measuring parameters

The terminal voltage of the PV module was successfully measured remotely, every 100 seconds uninterrupted for a period of seven days, as presented in section 4.3.2 of chapter 4. The daily maximum of this voltage was recorded to be between 12.76 V and 15.44 for the said period, thereby not exceeding the rated V_{mp} of 16.5 V for these PV modules. In addition, the PV current that was measured remotely for the same period, indicated more current for a sunny day (2.32 A) than a cloudy day (1.98 A), both which are less than the rated I_{mp} of 2.44 A. The highest power generated by this system was recorded as 28.81 W.

The battery charging cycle for one day was presented in section 4.3.3 and it made it evident that the battery started charging from sunrise with the increase in battery current until 11 am. From 12 pm the battery current was observed to decrease until sunset.

In section 4.3.4, measurements of T_{PV} also taken remotely, made it evident that the heating of the PV module occurred during the day, when there was solar radiation. T_{PV} was observed to be significantly higher than T_a during the day and more so around midday. An even wider gap was seen in the two parameters on a sunny day, compared

to a cloudy day, whereas at night, T_{PV} and T_a were evidently similar.

5.4.2 Remotely controlling parameters

Remotely controlling the two parameters that were proven to affect the output power of the PV module is another objective that was successfully achieved in section 4.4 and 4.5 by relaying control signals for the water sprayer and the actuator respectively. Signals were sent from the PC transceiver, using the GUI via the RF transceiver to the PV transceiver, to switch the LED on and off as means to show control of a water sprayer. The GUI was also used to send signals to extend and retract the actuator at the PV transceiver side via RF as a means to demonstrate control of the orientation angle.

5.5 Recommendations for future work

This research has unfolded possibilities of future studies that could contribute to the work of maintaining optimum power of PV modules. These may include, but are not limited to:

- Determining the power consumed by an actuator for a specific sized structure with a specific weight.
- Comparing the effect of cooling the PV module using the water sprayer in relation to a change in the orientation angle on the output power of the module.
- Modifying the GUI to form part of a smart city where the adjustment to the actuator and activation of the water sprayer could be automated.
- Incorporating cloud storage for monitoring of the output power and surface temperature from any location at any time.
- Adding automatic fault detection.

Bibliography

- Abinayaa, V., & Jayan, A. (2014). Case study on comparison of wireless technologies in industrial applications. *International Journal of Scientific and Research Publications*, 4(2), 2250-3153.
- Allegro Microsystems (2018). Jan 2018-last update. *Fully Integrated, Hall Effect-Based Linear Current Sensor with 2.1 kVRMS Voltage Isolation and a Low-Resistance Current Conductor*. Retrieved from <https://www.allegromicro.com/~media/files/datasheets/acs712-datasheet.ashx> [June 2019].
- Al-Sabounchi, A. (1998). Effect of ambient temperature on the demanded energy of solar cells at different inclinations. *Renewable Energy*, 14(1), 149-155.
- Andreoni Lopez, M., Galdeano Mantinan, F., & Molina, M. G. (2012). (2012). Implementation of wireless remote monitoring and control of solar photovoltaic (PV) system. Paper presented at the *Transmission and Distribution: Latin America Conference and Exposition (T&D-LA), 2012 Sixth IEEE/PES*, 1-6.
- Arduino (2018). 2018-last update. *Arduino Mega 2560 Rev3*. Retrieved from <https://store.arduino.cc/arduino-mega-2560-rev3> [June 2019].
- Asowata, O., Swart, A. J., & Pienaar, C. (2012a). Optimum tilt angles for photovoltaic panels during winter months in the Vaal Triangle, South Africa. *Smart Grid & Renewable Energy*, 3, 119-125.
- Asowata, O., Swart, J., & Pienaar, C. (2012b). (2012b). Optimum tilt and orientation angles for photovoltaic panels in the Vaal Triangle. Paper presented at the *Power and Energy Engineering Conference (APPEEC), 2012 Asia-Pacific*, 1-5.
- Asowata, O., Swart, J., & Pienaar, C. (2014). Evaluating the effect of orientation angles on the output power of a stationary photovoltaic panel. *Journal of Renewable and Sustainable Energy*, 6(4), 043114.

- Bai, A., Popp, J., Balogh, P., Gabnai, Z., Pályi, B., Farkas, I., . . . Zsiborács, H. (2016). Technical and economic effects of cooling of monocrystalline photovoltaic modules under Hungarian conditions. *Renewable and Sustainable Energy Reviews*, 60, 1086-1099.
- Baskerville, R., Baiyere, A., Gregor, S., Hevner, A., and Rossi, M. (2018). “Design Science Research Contributions: Finding a Balance between Artifact and Theory.” *Journal of the Association for Information Systems* 19(5): 358-376.
- Beagleboard. (2018). Sept 2019-last update. *Beaglebone Black*. Retrieved from <https://beagleboard.org/black> [Nov 2019].
- Belmili, H., Cheikh, S. M. A., Haddadi, M., & Larbes, C. (2010). Design and development of a data acquisition system for photovoltaic modules characterization. *Renewable Energy*, 35(7), 1484-1492.
- Benghanem, M. (2010). A low cost wireless data acquisition system for weather station monitoring. *Renewable Energy*, 35, 862-872.
- Benghanem, M., & Maafi, A. (1998). Data acquisition system for photovoltaic system performance monitoring. *IEEE Transactions on Instrumentation and Measurement*, 47
- Bhattacharya, T., Chakraborty, A. K., & Pal, K. (2014). Effects of ambient temperature and wind speed on performance of monocrystalline solar photovoltaic module in Tripura, India. *Journal of Solar Energy*, 2014
- Broadcom. (2018). 2018-last update. *ASSR-301C and ASSR-302C Datasheet*. Retrieved from <https://www.broadcom.com/products/optocouplers/industrial-plastic/other/solid-state-relay/assr-302c-002e> [2019, June 2019].
- Chhabra, N. (2013). Comparative Analysis of Different Wireless Technologies. *International Journal of Scientific Research in Network Security & Communication*, 1(5), 3-4.

- Chung, W., & Oh, S. (2006). Remote monitoring system with wireless sensors module for room environment. *Sensors and Actuators B*, 113, 64-70.
- Clini, C., Musu, I., & Gullino, M. L. (2008). *Sustainable development and environmental management* Springer.
- Dangerous Prototypes. (2012). Jan 2012-last update. Using a ACS712 hall-effect current sensor. Retrieved from <http://dangerousprototypes.com/blog/2012/01/27/interfacing-a-pic-microcontroller-with-the-ac712-hall-effect-current-sensor/> [June 2019].
- Digi International Inc..(2008). 2018-last update. XBee®/XBee-PRO OEM RF Modules. Retrieved from <https://docs-emea.rs-online.com/webdocs/1498/0900766b81498288.pdf> [June 2019].
- Dike, V., Chineke, T., Nwofor, O., & Okoro, U. (2012). Optimal angles for harvesting solar electricity in some African cities. *Renewable Energy*, 39(1), 433-439.
- Edimax Technology Co. Ltd. (2014). 2014-last update. AC600 Wi-Fi Dual-Band High Gain USB Adapter. Retrieved from <https://docs-emea.rs-online.com/webdocs/13a3/0900766b813a3e2f.pdf> [June 2019].
- Ehrlich, R. (2013). *Renewable Energy A First Course*. Boca Raton: Taylor & Francis Group.
- Elprocus. (2016). 2016-last update. Thermocouple operating principle. Retrieved from <https://www.elprocus.com/temperature-sensors-types-working-operation/> [March 18, 2016].
- Engineer on a Disk. (2016). 2016-last update. Potentiometer used for measuring angles. Retrieved from http://engineeronadisk.com/book_implementation/rotationsa5.html [March 11, 2016].

- Ertekin, C., & Yaldiz, O. (2000). Comparison of some existing models for estimating global solar radiation for Antalya (Turkey). *Energy Conversion and Management*, 41(4), 311-330.
- Forero, N., Hernandez, J., & Gordillo, G. (2006). Development of a monitoring system for a PV solar plant. *Energy Conversion and Management*, 47, 2329-2336.
- Fraden, J. (2010). *Handbook of Modern Sensors: Physics, Design and Application*. London: Springer.
- Fuchs, E. F., & Masoum, M. A. S. (2011). *Power Conversion of Renewable Energy System*. London: Springer Science+Business Media.
- Fuentes, M., Vivar, M., Burgos, J. M., Aguilera, J., & Vacas, J. A. (2014). Design of an accurate, low-cost autonomous data logger for PV system monitoring using Arduino that complies with OEC standards. *Solar Energy Materials & Solar Cells*, (130), 529.
- Gagliarducci, M., Lampasi, D., & Podesta, L. (2007). GSM based monitoring and control of photovoltaic power generation. *Measurement*, 40(3), 314-321.
- Inada, H., & Horio, H. (1992). (1992). A study on a home car support information system. Paper presented at the *7th World Congress on Medical Informatics*, 349.
- INTEL. (2017). 2017-last update. Intel® Galileo Gen 2 Development Board. Retrieved from https://www.rutronik.com/fileadmin/Micropages/Intel/intelgalileogen2prodbrief_330736_003.pdf [Oct 2018].
- Kaldellis, J., Kapsali, M., & Kavadias, K. (2014). Temperature and wind speed impact on the efficiency of PV installations. Experience obtained from outdoor measurements in Greece. *Renewable Energy*, 66, 612-624.
- Katu, U., Tola, M., Palle, S., & Hasanuddin, Z. (2016). Flood Early Warning System and Distribution of Information Communication Using Radio Link. *International Journal of Science and Research*, 5(12), 1044-1048.

- Koa Speer Electronics Inc.. (2017a). 2017-last update. Carbon Film Resistor. Retrieved from <https://www.mouser.co.za/Passive-Components/Resistors/Film-Resistors/Carbon-Film-Resistors-Through-Hole/ /N-7gz3y/> [Oct 2018].
- KOA SPEER ELECTRONICS INC.. (2017b). 2017-last update. General purpose metal film leaded resistor. Retrieved from <https://www.mouser.co.za/Passive-Components/Resistors/Film-Resistors/Metal-Film-Resistors-Through-Hole/Datasheets/ /N-7gz41/> [Oct 2018].
- Koutitas, G., & Demestichas, P. (2010). A review of energy efficiency in telecommunication networks. *Telfor Journal*, 2(1), 2-7.
- Koutroulis, E., & Kalaitzakis, K. (2003). Development of an intergrated data-acquisition system for renewable energy sources systems monitoring. *Renewable Energy*, 28, 139-152.
- Lalia, M., Dalila, A., & Ahmed, C. (2013). Solar Tracking with Photovoltaic Panel. *Energy Procedia*, 42, 103-112.
- Lange, C., Kosiankowski, D., Weidmann, R., & Gladisch, A. (2011). Energy consumption of telecommunication networks and related improvement options. *Selected Topics in Quantum Electronics, IEEE Journal Of*, 17(2), 285-295.
- Leite, V., & Chenlo, F. (2010). An improved electronic circuit for tracing the IV characteristics of photovoltaic modules and strings.
- Liu, J., Fang, W., Zhang, X., & Yang, C. (2015). An improved photovoltaic power forecasting model with the assistance of aerosol index data. *IEEE Transactions on Sustainable Energy*, 6(2), 434-442.
- Lubritto, C., Petraglia, A., Vetromile, C., Caterina, F., D'Onofrio, A., Logorelli, M., . . . Curcuruto, S. (2008). (2008). Telecommunication power systems: energy saving, renewable sources and environmental monitoring. Paper presented at the *Telecommunications Energy Conference, 2008. INTELEC 2008. IEEE 30th International*, 1-4.

- Mattei, M., Notton, G., Cristofari, C., Muselli, M., & Poggi, P. (2006). Calculation of the polycrystalline PV module temperature using a simple method of energy balance. *Renewable Energy*, 31(4), 553-567.
- Meco. (2018). 2018-last update. AC Voltage transducer. Retrieved from <https://www.mecoinst.com/meco-product-details/AC-Voltage-Transducer.aspx> [Oct 2019].
- Messenger, R. A., & Ventre, J. (2010). *Photovoltaic Systems Engineering* (3rd ed.). Florida: CRC Press.
- Microchip. (2018). 2018-last update. PIC18F24Q10. Retrieved from <http://ww1.microchip.com/downloads/en/DeviceDoc/PIC18F24-25Q10-Data-Sheet-DS40001945B.pdf> [Oct 2018].
- Moghavvemi, M., Ng, K. E., Soo, C. Y., & Tan, S. Y. (2005). A reliable and economically feasible remote sensing system for temperature and relative humidity measurement. *Sensors and Actuators B*, 117, 181-185.
- Morris, A. S., & Langari, R. (2012). *Measurement and Instrumentation: Theory and Application*. Waltham, MA: Elsevier Inc.
- Muhammad, B., Prasad, R., Nisi, M., Mennella, A., Gagliarde, G., Cianca, E., . . . Addabbo, P. (2017). (2017). Automating the maintenance of photovoltaic power plants. Paper presented at the *Wireless Summit (GWS), 2017 Global*, 6-11.
- Mukaro, R., & Carelse, X. (1999). A microcontroller-based data acquisition system for solar radiation and environmental monitoring. *IEEE Trans Instrum Measure*, 48, 6.
- NK Technologies. (2018). 2018-last update. Voltage transducers datasheet. Retrieved from http://www.thermocense.com/_www/_docs/nk_technologies_voltage_transducers.pdf [Oct 2018].

- Ozemoya, A., Swart, J., & Pienaar, H. (2014). (2014). Experimental assessment of PV module cooling strategies. Paper presented at the *SATNAC 2014. Boardwalk Conference Centre, Nelson Mandela Bay, Eastern Cape, South Africa*,
- Papadakis, K., Koutroulis, E., & Kalaitzakis, K. (2005). A server database system for remote monitoring and operational evaluation of renewable energy sources plants. *Renewable Energy*, *30*, 1649-1669.
- Papageorgas, P., Piromalis, D., Antonakoglou, K., Vokas, G., Tseles, D., & Arvanitis, K. (2013). Smart solar panels: in-situ monitoring of photovoltaic panels based on wired and wireless sensor networks. *Energy Procedia*, *36*, 535-545.
- Prashanthini, S., Adibah, M. I., Balbir, S., & Norani, M. M. (2011). Optimum Tilt Angle and Orientation of Stand-Alone Photovoltaic Electricity Generation Systems for Rural Electrification. *OAIster*,
- PV Education. (2018). 2018-last update. Short-circuit current. Retrieved from <https://www.pveducation.org/pvcdrom/solar-cell-operation/short-circuit-current> [Oct 2018].
- Ranhotigamage, C., & Mukhopadhyay, S. C. (2011). Field trials and performance monitoring of distributed solar panels using a low-cost wireless sensors network for domestic applications. *Sensors Journal, IEEE*, *11*(10), 2583-2590.
- Raspberry PI. (2018). 2018-last update. Raspberry Pi 3 model b+. Retrieved from <https://www.raspberrypi.org/products/raspberry-pi-3-model-b-plus/> [Oct 2018].
- Reddy, P. J. (2012). *Solar Power Generation Technology, New Concepts & Policy*. London, UK: Taylor & Francis Group.
- Rosiek, S., & Batlles, F. (2008). A microcontroller-based data acquisition system for meteorological station monitoring. *Energy Conversion and Management*, *49*, 3746-3754.

- Schwingshackl, C., Petitta, M., Wagner, J. E., Belluardo, G., Moser, D., Castelli, M., . . . Tetzlaff, A. (2013). Wind effect on PV module temperature: Analysis of different techniques for an accurate estimation. *Energy Procedia*, 40, 77-86.
- Semiconductor, D. (2007). DS18B20 data sheet. 2010-06-01].[Http://Www, Maxim-Ic, Com/Datasheet/Index.Mvp/Id/2812/T/Al](http://www.Maxim-Ic.Com/Datasheet/Index.Mvp/Id/2812/T/Al),
- Shariff, F., Rahim, N. A., & Hew, W. P. (2015). Zigbee-based data acquisition system for online monitoring of grid-connected photovoltaic system. *Expert Systems with Applications*, 42(3), 1730-1742.
- Sinclair, I. (2000). *Sensors and Transducers* (3rd ed.). Oxford: Newnes.
- Skoplaki, E., & Palyvos, J. (2009). On the temperature dependence of photovoltaic module electrical performance: A review of efficiency/power correlations. *Solar Energy*, 83(5), 614-624.
- Stackexchange. (2016). 2016-last update. How A Rotary Position Sensor Works. Retrieved from <https://electronics.stackexchange.com/questions/249074/how-a-rotary-position-sensor-works> [Sept 2016].
- Sun Calculator. (2018). 2018-last update. Sun Calculator. Retrieved from <https://www.suncalc.org/#/-29.0852,26.1596,12/2018.08.23/18:00/1/0> [Oct 2018].
- Suri, M., Cebecauer, T., Skoczek, A., & Betak, J. (2012). (2012). Solar electricity production from fixed-inclined and sun-tracking C-Si photovoltaic modules in South Africa. Paper presented at the
- Swapnil, D., Jatin Narotam, S., & Bharath, S. (2013). Temperature Dependent Photovoltaic (PV) Efficiency and Its Effect on PV Production in the World – A Review. *Energy Procedia*, 33, 311-321.
- Swart, A. J., Schoeman, R. M., & Pienaar, H. C. (2011). Assessing the effect of variable atmospheric conditions on the performance of photovoltaic panels: A case study from the Vaal Triangle. *Southern African Energy Efficiency Convention*, , 1-6.

- Telkom. (2014). 2014-last update. Integrated report for the year ended 31 March 2014 [Homepage of Telkom SA SOC Limited], [Online]. Retrieved from http://www.telkom-reports.co.za/reports/ar_2014/index.php [June 2015].
- Teo, H. G., Lee, P. S., & Hawlader, M. N. A. (2011). An active cooling system for photovoltaic modules. *Applied Energy*, 90, 309-315.
- Texas Instruments. (2018). 2018-last update. CC1101 Low-Power Sub-1 GHz RF Transceiver. Retrieved from <http://www.ti.com/lit/ds/symlink/cc1101.pdf> [Oct 2018].
- Time and Date. (2020). 2020-last update. July 2019 Weather in Bloemfontein - Graph. Retrieved from <https://www.timeanddate.com/weather/south-africa/bloemfontein/historic?month=7&year=2019> [March 2020].
- Tina, G. M., & Grasso, A. D. (2014). Remote monitoring system for stand-alone photovoltaic power plants: The case study of a PV-powered outdoor refrigerator. *Energy Conversion and Management*, 78, 862-871.
- TT electronics (2018). 2018-last update. Metal Film Resistor. Retrieved from https://www.mouser.co.za/Passive-Components/Resistors/Film-Resistors/Metal-Film-Resistors-Through-Hole/Datasheets/_/N-7gz41/ [Oct 2019].
- Vaishnavi, V., Kuechler, W., and Petter, S. (Eds.) (2004/19). “Design Science Research in Information Systems” January 20, 2004 (created in 2004 and updated until 2015 by Vaishnavi, V. and Kuechler, W.); last updated (by Vaishnavi, V. and Petter, S.), June 30, 2019. <http://www.desrist.org/design-research-in-information-systems/>.
- Virone, G., Noury, N., Thomesse, J., Rialle, V., & Demongeot, J. (2003). (2003). A home health information system based on the CAN fieldbus. Paper presented at the *Fieldbus Systems and their Applications*, 23.

- Vishay Day. (2016). 2016-last update. Carbon Metal Resistor. Retrieved from https://www.mouser.co.za/Passive-Components/Resistors/Film-Resistors/Carbon-Film-Resistors-Through-Hole/_/N-7gz3y/ [Oct 2018].
- Wenham, S. R., Green, M. A., Watt, M. E., Corkish, R., & Sproul, A. (2011). *Applied Photovoltaics* (3rd ed.). Abingdon, Oxon: Earthscan.
- Wikipedia. (2018). Opto-isolator. Retrieved from <https://en.wikipedia.org/wiki/Opto-isolator>
- Wikipedia. (2018). 2018-last update. Opto-isolator. Retrieved from <https://en.wikipedia.org/wiki/Opto-isolator> [Oct 2018].
- Yageo Corporation. (2019a). 2019-last update. Carbon Film Resistors. Retrieved from https://www.mouser.co.za/Passive-Components/Resistors/Film-Resistors/Carbon-Film-Resistors-Through-Hole/_/N-7gz3y/ [Sept 2019].
- Yageo Corporation. (2019b). 2019-last update. Metal Film Resistors. Retrieved from https://www.mouser.co.za/Passive-Components/Resistors/Film-Resistors/Metal-Film-Resistors-Through-Hole/Datasheets/_/N-7gz41/ [(Sept 2019)].
- Yuce, M. (2010). Implementation of wireless body are networks for healthcare system. *Sensors and Actuators A*, 162, 116-129.
- Zettlex. (2017). 2017-last update. A Guide to Position Sensors. Retrieved from <https://www.azosensors.com/article.aspx?ArticleID=743> [Oct 2019]
- Ziegler, S., Woodward, R. C., Iu, H. H., & Borle, L. J. (2009). Current sensing techniques: A review. *IEEE Sensors Journal*, 9(4), 354-376.

Annexure A: GUI Program

```
using System;
using System.Collections.Generic;
using System.ComponentModel;
using System.Data;
using System.Drawing;
using System.Linq;
using System.Text;
using System.Threading.Tasks;
using System.IO.Ports;
using System.Windows.Forms;
using System.Threading;
using System.Diagnostics;
using System.Windows.Forms.DataVisualization.Charting;
using System.Text.RegularExpressions;

namespace serial_Communication
{
    public partial class Form1 : Form
    {
        static bool _continue;
        static SerialPort _serialPort;
        public Thread readThread;
        delegate void TextChanger(string t);
        Dictionary<int, bool> DGV_saved =
            new Dictionary<int, bool>();
        List<string> PV_voltage = new List<string>();
        List<string> battery_voltage = new List<string>();
        List<string> Load_voltage = new List<string>();
        List<string> PV_current = new List<string>();
        List<string> batter_Current = new List<string>();
        List<string> Load_current = new List<string>();
        List<string> Temperature_ = new List<string>();
        List<string> time_ = new List<string>();
        string dataOut = "";
        public Form1()
        {
            InitializeComponent();
            foreach (string s in SerialPort.GetPortNames())
            {
                PortNameCBox.Items.Add(s);
            }
            textBoxBaudRate.Text = "9600";
            foreach (string s in Enum.GetNames(typeof(Parity)))
            {
                comboBoxSetPortParity.Items.Add(s);
            }

            foreach (string s in Enum.GetNames(typeof(StopBits)))
            {
                comboBoxSetPortStopBits.Items.Add(s);
            }
        }
    }
}
```



```
}
foreach (string s in Enum.GetNames(typeof(StopBits)))
{
    comboBoxSetPortStopBits.Items.Add(s);
}
foreach (string s in Enum.GetNames(typeof(Handshake)))
{
    comboBoxSetPortHandshake.Items.Add(s);
}
this.Width = 474; tabControl1.Width = 436;
labelDate.Text = DateTime.Now.ToLongDateString();
}
public void Read()
{
    //TextChanger dt = new TextChanger(txtEdit);
    while (_continue)
    {
        try
        {
            string message = _serialPort.ReadLine();

            Console.WriteLine(message);
            // Thread.Sleep(500); 23 Jan 2019
            if (richTextBoxLiveFeed.InvokeRequired)
            {
                richTextBoxLiveFeed.Invoke(new TextChanger(txtEdit),
                new object[] { message });
            }
        }
        catch { }
    }

    // }//dt(message);
    //richTextBoxLiveFeed.Text += "\n" + message;
    if (DGV_Table.Rows.Count % 100 == 0)
    {
        if (!DGV_saved.ContainsKey(DGV_Table.Rows.Count / 100))
        {
            ExportToExcel();
            DGV_saved.Add(DGV_Table.Rows.Count / 100, true);
            DGV_Table.DataSource = null;
            DGV_Table.Rows.Clear();
            DGV_Table.Refresh();
        }
    }
}
}
}
}
catch (TimeoutException) { Read(); }
}
}

public void txtEdit(string t) { richTextBoxLiveFeed.Text += t; }

private void buttonStartSrCom_Click(object sender, EventArgs e)
{
    readThread = new Thread(Read);
    readThread.IsBackground = true;
    // Create a new SerialPort object with default settings.
    _serialPort = new SerialPort();
    string parity = comboBoxSetPortParity.SelectedItem.ToString();
    string stopBits = comboBoxSetPortStopBits.SelectedItem.ToString();
    string handshake = comboBoxSetPortHandshake.SelectedItem.ToString();
}
```

```

        // Allow the user to set the appropriate properties.
        _serialPort.PortName = PortNameCBox.SelectedItem.ToString();
        _serialPort.BaudRate = int.Parse(textBoxBaudRate.Text);
        _serialPort.Parity = (Parity)Enum.Parse(typeof(Parity), parity,
true);
        _serialPort.StopBits = (StopBits)Enum.Parse(typeof(StopBits),
stopBits, true);
        _serialPort.Handshake = (Handshake)Enum.Parse(typeof(Handshake),
handshake, true);

```

```

        // Set the read/write timeouts
        _serialPort.ReadTimeout = 500;
        _serialPort.WriteTimeout = 500;

```

```

        _serialPort.Open();
        _continue = true;
        readThread.Start();
    }

```

```

// private void Form1_FormClosing(object sender, FormClosingEventArgs e)
//{
//    try
//    {
//        _continue = false;
//        readThread.Abort();
//        _serialPort.Close();
//    }
//    catch (ObjectDisposedException ex)
//    {
//        Console.WriteLine("Caught: {0}", ex.Message);
//    }
// }
private void richTextBoxLiveFeed_TextChanged(object sender, EventArgs
e)
{
    int totalLines = richTextBoxLiveFeed.Lines.Length;
    string [] lastLine = richTextBoxLiveFeed.Lines[totalLines -
2].Split('=');
    switch (lastLine[0])
    {
        case "PV V ":
            PV_voltage.Add(lastLine[1]);
addElement(CheckDGVRRowCount(PV_voltage), PV_voltage, 0);
            chartXY(PV_voltage, "PV Voltage", 0);
            time_.Add(DateTime.Now.ToLongTimeString());
addElement(CheckDGVRRowCount(time_), time_, 7); // changed ToLongTimeString
            break;
        case "Bat V ":
            battery_voltage.Add(lastLine[1]);
addElement(CheckDGVRRowCount(battery_voltage), battery_voltage, 1);
            chartXY(battery_voltage, "Battery Voltage", 2);
            break;
        case "Load V ":
            Load_voltage.Add(lastLine[1]);
addElement(CheckDGVRRowCount(Load_voltage), Load_voltage, 2);
            chartXY(Load_voltage, "Load Voltage", 4);
            break;
        case "PV C ":
            PV_current.Add(lastLine[1]);
addElement(CheckDGVRRowCount(PV_current), PV_current, 3);
            chartXY(PV_current, "PV Current", 1); powerChart(0);

```

```

        break;
        case "Bat C ":
            batter_Current.Add(lastLine[1]);
addElement(CheckDGVRowCount(batter_Current), batter_Current, 4);
            chartXY(batter_Current, "Battery Current", 3);
powerChart(1);
        break;
        case "Load C ":
            Load_current.Add(lastLine[1]);
addElement(CheckDGVRowCount(Load_current), Load_current, 5);
            chartXY(Load_current, "Load Current", 5); powerChart(2);
        break;
        case "Temp ":
            Temperature_.Add(lastLine[1]);
addElement(CheckDGVRowCount(Temperature_), Temperature_, 6);
            movingX(TemperatureChart);
            TemperatureChart.
                Series["Temperature"].
                Points.
                AddXY(
                    DateTime.Now.ToShortTimeString(),
                    Convert.ToDouble(Regex.Replace(lastLine[1], "[^0-
9.]", ""))
                );
        break;
    }
    labelDate.Text = DateTime.Now.ToLongDateString();
}

public void UpdatedGV()
{
    int count = PV_current.Count + battery_voltage.Count +
Load_current.Count + Load_voltage.Count +
    PV_voltage.Count + batter_Current.Count + Temperature_.Count;
    if (count % 7 == 0)
    {
        int n = DGV_Table.Rows.Add();
        DGV_Table.Rows[n].Cells[0].Value = PV_voltage[n-1];
        DGV_Table.Rows[n].Cells[1].Value = battery_voltage[n-1];
        DGV_Table.Rows[n].Cells[2].Value = Load_voltage[n-1];
        DGV_Table.Rows[n].Cells[3].Value = PV_current[n-1];
        DGV_Table.Rows[n].Cells[4].Value = batter_Current[n-1];
        DGV_Table.Rows[n].Cells[5].Value = Load_current[n-1];
        DGV_Table.Rows[n].Cells[6].Value = Temperature_[n-1];
    }
}

public bool CheckDGVRowCount (List<string> list){
    bool _checked = DGV_Table.Rows.Count < list.Count;
    return _checked;
}

public void addElement(bool test, List<string> list, int cell)
{
    if (list.Count <= DGV_Table.Rows.Count)
    {
        for(int i = 0; i < DGV_Table.Rows.Count && i < list.Count; i++)
        {
            DGV_Table.Rows[i].Cells[cell].Value = list[i];
        }
    }
    else
    {

```

```
int n = DGV_Table.Rows.Add();
for (int i = 0; i < DGV_Table.Rows.Count && i < list.Count;
i++)
{
    {
        DGV_Table.Rows[i].Cells[cell].Value = list[i];
    }
}
}
```

```
public void chartXY(List<string> list, string series, int chart)
{
    string temp = Regex.Replace(list[list.Count - 1], "[^0-9.]", "");
    string x;
    double num = 0;
    try
    {
        num = Convert.ToDouble(temp);
    }
    catch (Exception e)
    { Console.WriteLine(e.ToString()); }
    switch (chart)
    {
        case 0:
            movingX(chartPV_Voltage);
            x = DateTime.Now.ToShortTimeString();
            chartPV_Voltage.Series[series].Points.AddXY(x, num);
            break;
        case 1:
            movingX(chartPV_Curent);
            x = DateTime.Now.ToShortTimeString();
            chartPV_Curent.Series[series].Points.AddXY(x, num);
            break;
        case 2:
            movingX(chartBattery_Voltage);
            x = DateTime.Now.ToShortTimeString();
            chartBattery_Voltage.Series[series].Points.AddXY(x, num);
            break;
        case 3:
            movingX(chartBattery_Current);
            x = DateTime.Now.ToShortTimeString();
            chartBattery_Current.Series[series].Points.AddXY(x, num);
            break;
        case 4:
            movingX(chartLoad_Voltage);
            x = DateTime.Now.ToShortTimeString();
            chartLoad_Voltage.Series[series].Points.AddXY(x, num);
            break;
        case 5:
            movingX(chartLoad_Current);
            x = DateTime.Now.ToShortTimeString();
            chartLoad_Current.Series[series].Points.AddXY(x, num);
            break;
    }
}
```

```
private void tabPage1_Click(object sender, EventArgs e)
{
}
```

```
private void tabControl1_SelectedIndexChanged(object sender, EventArgs
e)
```

```

    {
}

private void ExportToExcel()
{
    // Creating a Excel object.
    Microsoft.Office.Interop.Excel._Application excel = new
Microsoft.Office.Interop.Excel.Application();
    Microsoft.Office.Interop.Excel._Workbook workbook =
excel.Workbooks.Add(Type.Missing);
    Microsoft.Office.Interop.Excel._Worksheet worksheet = null;

    try
    {
        worksheet = workbook.ActiveSheet;

        worksheet.Name = "ExportedFromDatGrid";

        int cellRowIndex = 1;
        int cellColumnIndex = 1;

        //Loop through each row and read value from each column.
        for (int i = 0; i < DGV_Table.Rows.Count - 1; i++)
        {
            for (int j = 0; j < DGV_Table.Columns.Count; j++)
            {
                // Excel index starts from 1,1. As first Row would have
the Column headers, adding a condition check.
                if (cellRowIndex == 1)
                {
                    worksheet.Cells[cellRowIndex, cellColumnIndex] =
DGV_Table.Columns[j].HeaderText;
                }
                else
                {
                    if (DGV_Table.Rows[i].Cells[j].Value != null)
                    {
                        worksheet.Cells[cellRowIndex, cellColumnIndex]
= DGV_Table.Rows[i].Cells[j].Value.ToString();
                    }
                }
                cellColumnIndex++;
            }
            cellColumnIndex = 1;
            cellRowIndex++;
        }

        //Getting the location and file name of the excel to save from
user.
        //SaveFileDialog saveDialog = new SaveFileDialog();
        //saveDialog.Filter = "Excel files (*.xlsx)|*.xlsx|All files
(*.*)|*.*";
        //saveDialog.FilterIndex = 2;
        string file = "C:\\PV Module Data\\" +
DateTime.Now.ToLongDateString() + "Data export_" + DateTime.Now.ToBinary() +
".xlsx";
        //if (saveDialog.ShowDialog() ==
System.Windows.Forms.DialogResult.OK)
        //{

```

```

        // workbook.SaveAs(saveDialog.FileName);
        // MessageBox.Show("Export Successful");
        //}
        workbook.SaveAs(file);
        Console.WriteLine("Export Successful");
        //MessageBox.Show("Export Successful");
    }
    catch (System.Exception ex)
    {
        Console.WriteLine(ex.Message);
    }
    finally
    {
        excel.Quit();
        workbook = null;
        excel = null;
    }
}

private void buttonExport_Click(object sender, EventArgs e)
{
    ExportToExcel();
}

public void movingX(Chart chart)
{
    Axis xaxis = chart.ChartAreas[0].AxisX;
    xaxis.Minimum = xaxis.Maximum - 50;
}

public void powerChart(int chartNum)
{
    double voltage = 0, current = 0; int lastPoint = 0;
    switch (chartNum)
    {
        case 0:
            movingX(PV_PowerChart);

            if (chartPV_Curent.Series["PV Current"].Points.Count > 0 &&
                chartPV_Voltage.Series["PV Voltage"].Points.Count > 0)
            {
                if (chartPV_Curent.Series["PV Current"].Points.Count <=
                    chartPV_Voltage.Series["PV Voltage"].Points.Count)
                {
                    lastPoint = chartPV_Curent.
                        Series["PV Current"].
                            Points.Count - 1;
                }
                else if (chartPV_Curent.Series["PV
Current"].Points.Count >=
                    chartPV_Voltage.Series["PV Voltage"].Points.Count)
                {
                    lastPoint = chartPV_Voltage.
                        Series["PV Voltage"].
                            Points.Count - 1;
                }
                voltage = yValueExt(chartPV_Voltage.
                    Series["PV Voltage"].
                        Points[lastPoint]);
                current = yValueExt(chartPV_Curent.

```

```

        Series["PV Current"].
        Points[lastPoint]);
        PV_PowerChart.
        Series["PV Power"].
        Points.
        AddXY(DateTime.Now.ToShortTimeString(), voltage *
current);
    }
    break;
    case 1:
        movingX(Battery_PowerChart);
        if (chartBattery_Current.Series["Battery
Current"].Points.Count > 0 &&
        chartBattery_Voltage.Series["Battery
Voltage"].Points.Count > 0)
        {
            if (chartBattery_Current.Series["Battery
Current"].Points.Count <=
            chartBattery_Voltage.Series["Battery
Voltage"].Points.Count)
            {
                lastPoint = chartBattery_Current.
                Series["Battery Current"].
                Points.Count - 1;
            }
            else if (chartBattery_Current.Series["Battery
Current"].Points.Count >=
            chartBattery_Voltage.Series["Battery
Voltage"].Points.Count)
            {
                lastPoint = chartBattery_Voltage.
                Series["Battery Voltage"].
                Points.Count - 1;
            }
            voltage = yValueExt(chartBattery_Voltage.
                Series["Battery Voltage"].
                Points[lastPoint]);
            current = yValueExt(chartBattery_Current.
                Series["Battery Current"].
                Points[lastPoint]);
            Battery_PowerChart.
            Series["Battery Power"].
            Points.
            AddXY(DateTime.Now.ToShortTimeString(), voltage *
current);
        }
        break;
    case 2:
        movingX(Load_PowerChart);
        if (chartLoad_Current.Series["Load Current"].Points.Count >
0 &&
        chartLoad_Voltage.Series["Load Voltage"].Points.Count >
0)
        {
            if (chartLoad_Current.Series["Load
Current"].Points.Count <=
            chartLoad_Voltage.Series["Load Voltage"].Points.Count)
            {
                lastPoint = chartLoad_Current.
                Series["Load Current"].
                Points.Count - 1;
            }

```

```

    }
    else if (chartLoad_Current.Series["Load
Current"].Points.Count >=
chartLoad_Voltage.Series["Load Voltage"].Points.Count)
    {
        lastPoint = chartLoad_Voltage.
            Series["Load Voltage"].
                Points.Count - 1;
    }
    voltage = yValueExt(chartLoad_Voltage.
        Series["Load Voltage"].
            Points[lastPoint]);
    current = yValueExt(chartLoad_Current.
        Series["Load Current"].
            Points[lastPoint]);
    Load_PowerChart.
        Series["Load Power"].
            Points.
                AddXY(DateTime.Now.ToShortTimeString(), voltage *
current);
    }
    break;
}
}
}

```

```

public double yValueExt(DataPoint p)
{
    return Convert.ToDouble(Regex.Replace(p.ToString(), "[^0-9.]",
    ""));
}

```

```

private void btnStopSerial_Click(object sender, EventArgs e)
{
    DialogResult result = MessageBox.Show("Do you really want to stop
communication?", "Serial Stop", MessageBoxButtons.YesNo);
    if (result == DialogResult.Yes)
    {
        _continue = false;
        readThread.Abort();
        _serialPort.Close();
        Environment.Exit(0); // 23 Jan 2019
    }
    else
    {
        _continue = true;
    }
}
}

```

```

}

```

```

private void timer1_Tick(object sender, EventArgs e)
{
    ExportToExcel();
}

```

```

private void label1_Click(object sender, EventArgs e)
{
}
}

```

```

private void ButtonSprayerOn_Click(object sender, EventArgs e)

```



```
{
    _continue = false;

    try
    {
        if (ButtonSprayerOn.Text == "Sprayer On")
        {
            dataOut = "N"; // 23 Jan 2019
        }
        else if (ButtonSprayerOn.Text == "Sprayer Off")
        {
            ButtonSprayerOn.Text = "Sprayer On";
            dataOut = "N";
        }
    }

    //_serialPort.Write("Sprayer state: ");
    _serialPort.WriteLine(dataOut);
    textBox1.Text = dataOut;
}

catch (TimeoutException) { }

    _continue = true;
}

private void flowLayoutPanel1_Paint(object sender, PaintEventArgs e)
{
}

private void textBox1_TextChanged(object sender, EventArgs e)
{
}

private void aGauge1_ValueInRangeChanged(object sender,
ValueInRangeChangedEventArgs e)
{
}

private void button1_Click(object sender, EventArgs e)
{
    _continue = false;
    // readThread.Suspend();

    try
    {
        dataOut = "L";
        aGauge1.Value -= 10;
        _serialPort.WriteLine(dataOut);

        textBox1.Text = dataOut;
    }

    catch (TimeoutException) { }
```

```
        _continue = true;
        //readThread.Resume();
    }

    private void button2_Click(object sender, EventArgs e)
    {
        _continue = false;
        // readThread.Suspend();

        try
        {
            dataOut = "R";
            aGauge1.Value += 10;
            _serialPort.WriteLine(dataOut);

            textBox1.Text = dataOut;
        }

        catch (TimeoutException) { }

        _continue = true;
        //readThread.Resume();
    }

    private void DGV_Table_CellContentClick(object sender,
DataGridViewCellEventArgs e)
    {
    }

    private void Form1_Load(object sender, EventArgs e)
    {
    }

    private void Form1_FormClosing(object sender, FormClosingEventArgs e)
    {
        if (e.CloseReason == CloseReason.UserClosing)
        {
            DialogResult result = MessageBox.Show("Do you really want to
exit?", "Close", MessageBoxButtons.YesNo);
            if (result == DialogResult.Yes)
            {
                Environment.Exit(0);
            }
            else
            {
                e.Cancel = true;
            }
        }
        else
        {
            e.Cancel = true;
        }
    }

    private void button1_Click_1(object sender, EventArgs e)
    {
        ExportToExcel();
    }
}
```

```
private void tabPage2_Click(object sender, EventArgs e)
{
}
}
```

Annexure B: PV Transceiver Program

```
#include <dht11.h>
#define DHT11PIN 16
dht11 DHT11;

const int PV_VPin = A0;
const int BT_VPin = A7;
const int LD_VPin = A2;
const int PV_IPin = A6;
const int BT_IPin = A4;
const int LD_IPin = A5;
int forwardPin = 5;
int backwardPin = 7;
int Spray_Pin = 9;
const int Angle_Pin = A10;

int LED = 13; //LED on Arduino board
byte rx_data = 0; //variable to store receive data
int data;

float Temp;
float PinRead;
float PV_Vin;
float BT_Vin;
float LD_Vin;
float PV_Iin;
float BT_Iin;
float LD_Iin;
```

```
void setup() {
  pinMode(LED, OUTPUT);
  pinMode(forwardPin, OUTPUT);
  pinMode(backwardPin, OUTPUT);
  pinMode(Spray_Pin, OUTPUT);
  Serial.begin(9600); //initialize UART for 9600bps
}

void loop(){

  //Voltage measurements
  PinRead = analogRead(PV_VPin);          //Read analog data
  PV_Vin = (((PinRead * 5.0) / 1023) / 0.175); //Convert to actual voltage
  delay(100);
  PinRead = analogRead(BT_VPin);          //Read analog data
  BT_Vin = (((PinRead * 5.0) / 1023) / 0.175); //Convert to actual voltage
  delay(100);
  PinRead = analogRead(LD_VPin);          //Read analog data
  LD_Vin = (((PinRead * 5.0) / 1023) / 0.175); //Convert to actual voltage
  delay(100);

  //Current measurements
  PinRead = analogRead(PV_IPin);          //Read analog value
  PV_Iin = (((PinRead / 1023.0) * 5000) - 2500) / 100; //Convert to actual current
  PinRead = analogRead(BT_IPin);          //Read analog value
  BT_Iin = (((PinRead / 1023.0) * 5000) - 2500) / 100; //Convert to actual current
  PinRead = analogRead(LD_IPin);          //Read analog value
  LD_Iin = (((PinRead / 1023.0) * 5000) - 2500) / 100; //Convert to actual current

  //Temperature measurements
  data = DHT11.read(DHT11PIN);
```

```
switch (data)
{
case DHTLIB_OK:
Temp = DHT11.temperature +2;
break;
case DHTLIB_ERROR_CHECKSUM:
Serial.println("Checksum error");
break;
case DHTLIB_ERROR_TIMEOUT:
Serial.println("Time out error");
break;
default:
Serial.println("Unknown error");
break;
}
```

```
Serial.print("PV V =");
Serial.print((float)PV_Vin);
Serial.println("V");//added 21Oct19
//Serial.print("\n");
Serial.print("Bat V =");
Serial.print((float)BT_Vin);
Serial.println("V");//added 21Oct19
//Serial.print("\n");
Serial.print("Load V =");
Serial.print((float)LD_Vin);
Serial.println("V");//added 21Oct19
//Serial.print("\n");

Serial.print("PV C =");
Serial.print((float)PV_Iin);
Serial.println("A");//added 21Oct19
//Serial.print("\n");
```

```
Serial.print("Bat C =");
Serial.print((float)BT_Iin);
Serial.println("A");//added 21Oct19
//Serial.print("\n");
Serial.print("Load C =");
Serial.print((float)LD_Iin);
Serial.println("A");//added 21Oct19
//Serial.print("\n");

Serial.print("Temp = " );
Serial.print(Temp);
//Serial.print("\n");
Serial.write(0xB0); //degree symbol 23 Jan 2019 //added 21Oct19
Serial.println('C'); //added 21Oct19
delay(100); // delay 23 Jan 2019

if(Serial.available()) // check if UART receive data
{
  rx_data = Serial.read(); //store data received
  if(rx_data==0x52) //turn right test for R
  {
    Serial.println("Right");
    digitalWrite(forwardPin, HIGH);
    delay(8100);
    digitalWrite(forwardPin, LOW);
  }
  else if(rx_data==0x4C) //turn left test for L
  {
    Serial.println("Left");
    digitalWrite(backwardPin, HIGH);
    delay(8100);
    digitalWrite(backwardPin, LOW);
  }
}
```

```
else if(rx_data==0x4E) //spray on test for N
{
  Serial.println("On");
  digitalWrite(Spray_Pin, HIGH);
  delay(10000);
  digitalWrite(Spray_Pin, LOW);
}
// else if(rx_data==0x46) // spray off
// {
//   Serial.println("Off");
//   digitalWrite(Spray_Pin, HIGH);
//   delay(5000);
//   digitalWrite(Spray_Pin, LOW);
// }
}
delay(1000); // 1 min delay 23 Jan 2019// removed 21Oct19 delay (100000)
}
```


Annexure C: PC Transceiver Program

```
#include <SoftwareSerial.h>
SoftwareSerial RFserial(5, 6); // RX, TX
const int CMD = 4;
int cycle,count, data;

void setup() {
  // Open serial communications and wait for port to open:
  pinMode(CMD, OUTPUT);
  digitalWrite(CMD, HIGH);
  Serial.begin(9600);
  while (!Serial) {
    ; // wait for serial port to connect. Needed for native USB port only
  }
  // set the data rate for the SoftwareSerial port
  RFserial.begin(9600);
  pinMode(13, OUTPUT);
  delay(1000);
}

void loop()
{ // run over and over
  Serial.println("Requesting Data");
  RFserial.flush();
  RFserial.print("D");
  count=0;
  while(count<100)
  {
```

```
if(RFserial.available())
{
  //data=RFserial.read(); // added 25 Oct 2018
  rcv();
  if(data==0x44)
  GetData();
  break;
}
delay(1);
count++;
}
if(Serial.available())
{
  data=Serial.read();
  if(data==0x52) //received 'R'
  {
    Serial.println("Turn Right");
    RFserial.print("R");
  }
  if(data==0x4C) //received 'L'
  {
    Serial.println("Turn Left");
    RFserial.print("L");
  }
  if(data==0x4E) //received 'O'
  {
    Serial.println("Spray On");
    RFserial.print("N");
  }
  if(data==0x46) //received 'F'
  {
    Serial.println("Spray Off");
    RFserial.print("F");
```

```
    }  
  }  
  delay(1000);  
}  
void rcv()  
{  
  count=0;  
  data=0x0F;  
  while(RFserial.available()<1 && count<10)  
  {  
    delay(1);  
    count++;  
  }  
  if(RFserial.available())  
    data=RFserial.read();  
}  
void rcv_data()  
{  
  rcv();  
  while(data!=0x0F)  
  {  
    Serial.write(data);  
    rcv();  
  }  
}  
  
void GetData()  
{  
  Serial.print("PV V = ");  
  Serial.write(data);  
  rcv_data();  
  Serial.println("V");  
  //TRXSerial.flush();
```

```
Serial.print("Bat V = ");
rcv_data();
Serial.println("V");
//TRXSerial.flush();
Serial.print("Load V = ");
rcv_data();
Serial.println("V");
//TRXSerial.flush();
Serial.print("PV C = ");
rcv_data();
Serial.println("A");
//TRXSerial.flush();
Serial.print("Bat C = ");
rcv_data();
Serial.println("A");
//TRXSerial.flush();
Serial.print("Load C = ");
rcv_data();
Serial.println("A");
//TRXSerial.flush();
Serial.print("Temp = ");
rcv_data();
Serial.println("C");
RFserial.flush();
}
```

Annexure D: T_{PV} 29 day data

Date	Time	Max T_a	Max T_{PV}	Min T_a	Min T_{PV}
19-Jul	00:00	3	10	-2	8
19-Jul	06:00	17	5	-2	4
19-Jul	12:00	19	47	15	37
19-Jul	18:00	15	16	11	14
20-Jul	00:00	11	11	2	9
20-Jul	06:00	11	5	2	5
20-Jul	12:00	12	48	6	45
20-Jul	18:00	6	11	0	9
21-Jul	00:00	0	3	-5	3
21-Jul	06:00	12	3	-6	3
21-Jul	12:00	15	38	10	33
21-Jul	18:00	10	13	0	11
22-Jul	00:00	-2	5	-4	4
22-Jul	06:00	15	3	-4	3
22-Jul	12:00	18	39	12	34
22-Jul	18:00	12	15	7	14
23-Jul	00:00	7	10	0	9
23-Jul	06:00	20	5	1	4
23-Jul	12:00	22	35	19	32
23-Jul	18:00	19	19	13	18
24-Jul	00:00	11	10	4	8
24-Jul	06:00	9	5	4	5
24-Jul	12:00	12	48	9	41
24-Jul	18:00	9	11	-1	10
25-Jul	00:00	-1	4	-4	4

25-Jul	06:00	17	3	-5	3
25-Jul	12:00	19	43	14	39
25-Jul	18:00	14	16	1	13
26-Jul	00:00	1	7	-2	6
26-Jul	06:00	21	5	-2	5
26-Jul	12:00	23	47	17	40
26-Jul	18:00	17	18	3	15
27-Jul	00:00	3	13	-1	12
27-Jul	06:00	19	6	-1	5
27-Jul	12:00	22	43	16	40
27-Jul	18:00	16	18	3	16
28-Jul	00:00	3	9	-1	8
28-Jul	06:00	19	6	-1	6
28-Jul	12:00	22	51	16	47
28-Jul	18:00	16	19	3	16
29-Jul	00:00	3	10	0	8
29-Jul	06:00	21	6	-1	5
29-Jul	12:00	23	48	16	39
29-Jul	18:00	16	18	4	17
30-Jul	00:00	4	11	0	9
30-Jul	06:00	19	6	-1	6
30-Jul	12:00	22	43	16	39
30-Jul	18:00	16	19	3	17
31-Jul	00:00	3	10	-1	8
31-Jul	06:00	15	5	-1	4
31-Jul	12:00	19	54	14	47
31-Jul	18:00	14	15	2	13
01-Aug	00:00	2	8	-3	6
01-Aug	06:00	19	4	-4	4
01-Aug	12:00	22	40	14	36
01-Aug	18:00	4	19	5	17
02-Aug	00:00	10	14	5	12

02-Aug	06:00	20	8	6	7
02-Aug	12:00	23	34	18	31
02-Aug	18:00	18	19	10	18
03-Aug	00:00	10	15	8	12
03-Aug	06:00	19	10	6	9
03-Aug	12:00	22	35	19	32
03-Aug	18:00	19	19	6	17
04-Aug	00:00	6	10	2	10
04-Aug	06:00	23	12	2	11
04-Aug	12:00	24	39	20	34
04-Aug	18:00	20	19	9	18
05-Aug	00:00	10	13	6	12
05-Aug	06:00	22	14	8	11
05-Aug	12:00	24	41	17	35
05-Aug	18:00	17	19	6	17
06-Aug	00:00	6	9	-2	8
06-Aug	06:00	19	6	-2	5
06-Aug	12:00	22	51	17	43
06-Aug	18:00	17	18	2	16
07-Aug	00:00	2	9	-1	8
07-Aug	06:00	25	6	-1	6
07-Aug	12:00	28	42	23	38
07-Aug	18:00	23	23	11	20
08-Aug	00:00	11	13	1	12
08-Aug	06:00	17	6	0	6
08-Aug	12:00	20	45	15	40
08-Aug	18:00	15	17	8	14
09-Aug	00:00	8	9	0	9
09-Aug	06:00	16	4	0	3
09-Aug	12:00	19	52	16	39
09-Aug	18:00	16	17	2	14
10-Aug	00:00	6	9	2	8

10-Aug	06:00	19	8	6	8
10-Aug	12:00	22	37	18	32
10-Aug	18:00	18	19	13	18
11-Aug	00:00	14	15	10	13
11-Aug	06:00	16	11	10	11
11-Aug	12:00	20	32	16	16
11-Aug	18:00	17	17	7	14
12-Aug	00:00	7	11	0	10
12-Aug	06:00	16	5	-1	4
12-Aug	12:00	19	48	15	45
12-Aug	18:00	15	17	2	14
13-Aug	00:00	2	7	-2	7
13-Aug	06:00	20	5	-2	5
13-Aug	12:00	23	47	18	40
13-Aug	18:00	18	19	4	16
14-Aug	00:00	4	11	-1	9
14-Aug	06:00	20	6	-1	5
14-Aug	12:00	22	55	17	47
14-Aug	18:00	17	19	3	16
15-Aug	00:00	3	11	0	9
15-Aug	06:00	21	9	2	9
15-Aug	12:00	24	48	20	42
15-Aug	18:00	20	21	5	19
16-Aug	00:00	5	12	2	10
16-Aug	06:00	24	8	2	7
16-Aug	12:00	26	51	22	45
16-Aug	18:00	22	24	7	22